Spring 5-15-2021

Synthetic Gene Circuits for Self-Regulating and Temporal Delivery of Anti-Inflammatory Biologic Drugs in Engineered Tissues

Lara Pferdehirt
Washington University in St. Louis

WASHINGTON UNIVERSITY IN ST. LOUIS

School of Engineering and Applied Science
Department of Biomedical Engineering

Dissertation Examination Committee:
Farshid Guilak, Chair
William Buchser
Erik Herzog
Nathaniel Huebsch
Jeffrey Millman

Synthetic Gene Circuits for Self-Regulating and Temporal Delivery of Anti-Inflammatory Biologic Drugs in Engineered Tissues

by

Lara Pferdehirt

A dissertation presented to
The Graduate School
of Washington University in
partial fulfillment of the
requirements for the degree
of Doctor of Philosophy

May 2021
St. Louis, Missouri

Table of Contents

List of Figures vii

List of Tables ix

Acknowledgments x

Abstract xiii

Chapter 1: Synthetic Biology and the Next Generation of Cell Therapies for Musculoskeletal Disease Treatment and Beyond 1

1.1 Genome engineering and cell therapies 1

1.2 Articular cartilage 1

1.2.1 Mechanobiologic response of articular cartilage 2

1.2.2 Articular cartilage circadian clock 3

1.3 Inflammation and articular cartilage 4

1.4 Current strategies for treatment of arthritis 5

1.5 Cartilage tissue engineering, gene therapy, and synthetic biology 6

1.6 Creation of the next generation of cell therapies for arthritis 7

1.6.1 Engineering of inflammation driven circuits 8

1.6.2 Engineering mechanically responsive circuits 8

1.6.3 Maintenance of cartilage homeostasis through clock-preserving circuits 9

1.7 Chronotherapy: the newest generation of controlled and prescribed cell therapies 9

1.8 Summary 11

Chapter 2: A Synthetic Gene Circuit for Self-Regulating Delivery of Biologic Drugs in Engineered Tissues 12

2.1 Abstract 12

2.2 Introduction 13

2.3 Materials and Methods 17

2.3.1 Overall Strategy 17

2.3.2 Vector Design 17

2.3.3 Lentivirus Production 18

2.3.4 Cell Culture and Differentiation 18

2.3.5 Lentiviral Transduction and Culture of PDiPSCs 19

2.3.6 Biomaterial-mediated Delivery 20

2.3.7 Inflammatory Challenge 21
2.3.8 Inflammation Activity Assay 21
2.3.9 Gene Expression 21
2.3.10 Enzyme-linked Immunosorbent Assays 22
2.3.11 Biochemical Analysis of Pellet Cultures 23
2.3.12 Histological Processing of Pellet Cultures 23
2.3.13 Statistical Analysis 23
2.4 Results 23
2.4.1 Responsiveness of the NF-κB synthetic promoter to IL-1α or TNF-α 23
2.4.3 Transduced NRE-IL1Ra iPSCs from tissue-engineered cartilage is protected from IL-1α 26
2.4.4 Biomaterial-mediated lentiviral delivery shows self-regulating production of IL-1Ra and attenuation of inflammation 28
2.5 Discussion 32
2.6 Supplemental Figures 37
2.7 Conclusions 39
Chapter 3: A Synthetic Mechanogenetic Gene Circuit for Autonomous Drug Delivery in Engineered Tissues 40
3.1 Abstract 40
3.2 Introduction 41
3.3 Materials and Methods 44
3.3.1 Tissue harvest, cell isolation, agarose gel casting, and culture 44
3.3.2 Chondrocyte mechanical and pharmacologic stimulation 45
3.3.3 Finite element modeling 48
3.3.4 Microarray collection and analysis 48
3.3.5 Mechanogenetic circuit design, development, viral development, and culture 49
3.3.6 Coculture studies 52
3.3.7 Statistical analysis 53
3.4 Results 53
3.4.1 The mechano-osmotic response of chondrocytes to loading is regulated by TRPV4 53
3.4.2 TRVP4 activation in chondrocytes induces transient anabolic and inflammatory signaling networks 57
3.4.3 Synthetic mechanogenetic circuits respond to TRVP4 activation to drive transgene expression 60

3.4.4 Mechanogenetic engineered cartilage activation protects cartilage tissues from IL-1α-induced inflammation-driven degradation 66
3.5 Discussion 69
3.6 Supplemental Figures 75
3.7 Conclusions 81
Chapter 4: Synthetic gene circuits for preventing disruption of the circadian clock due to inflammation 82
4.1 Abstract 82
4.2 Introduction 83
4.3 Materials and Methods 87
4.3.1 Cell culture and differentiation 87
4.3.2 Circadian reporter design 89
4.3.3 Development of inflammation resistant and self-regulating iPSCs 89
4.3.4 Lentivirus production and cell transduction 91
4.3.5 Circadian clock characterization through bioluminescence recordings and imaging 91
4.3.6 Inflammatory challenge and bioluminescence recordings and imaging 92
4.3.7 Histological and biochemical analysis of pellet cultures 93
4.3.8 Gene expression with quantitative real time polymerase chain reaction 94
4.3.9 Enzyme-linked immunosorbent assays 94
4.3.10 Statistical Analysis 94
4.4 Results 95
4.4.1 The circadian clock develops by chondrogenic stage of murine iPSC chondrogenesis 95
4.4.2 Inflammation disrupts the circadian clock in native and tissue engineered cartilage 98
4.4.3 IL-1 resistant engineered tissues are resistant to circadian disruption 103
4.5 Discussion 107
4.6 Conclusions 111
Chapter 5: A synthetic chronogenetic therapy gene circuit for temporal drug delivery 112
5.1 Abstract 112
5.2 Introduction 113
5.3 Materials and Methods 116
5.3.1 Murine induced pluripotent stem cell culture and differentiation 116
5.3.2 Cell-based chronotherapy circuit design 117

5.3.3 Lentivirus production and cell transduction 118
5.3.4 *In vitro* characterization of chronogenetic therapy circuits 119
5.3.5 Inflammatory challenge 121
5.3.6 *In vivo* characterization of chronogenetic therapy circuits 121
5.3.7 Statistical Analysis 122
5.4 Results 123
5.4.1 Characterization of chronogenetic reporter circuits and tissue engineered cartilage 123
5.4.2 Synthetic chronogenetic IL-1Ra circuit produces IL-1Ra in a circadian manner 124
5.4.3 Chronogenetic IL-1Ra therapy circuits are capable of delivering IL-1ra at different times of day and can entrain to the circadian clock of the host *in vivo* 127
5.5 Discussion 130
5.6 Conclusions 133
Chapter 6: Conclusions and Future Directions 134
Appendix: Genome Engineered Muscle Derived Stem Cells for Autoregulated Anti-Inflammatory and Anti-Fibrotic Activity 136
A.1 Abstract 136
A.2 Introduction 137
A.3 Materials and Methods 140
A.3.1 Isolation and Culture of MDSCs 140
A.3.2 Gene Array Analysis 140
A.3.3 Gene Editing of MDSCs 140
A.3.4 Luminescence Assay 141
A.3.5 Myogenic Differentiation Capacity 141
A.3.6 Decorin Gene Expression 141
A.3.7 Anti-Inflammatory and Anti-Fibrotic Activity of Engineered MDSCs 142
A.3.8 Statistical Analysis 142
A.4 Results 143
A.4.1 Signaling pathways activated by TGF-β1 stimulation in MDSCs 143
A.4.2 Myogenic differentiation and response of gene edited MDSCs to TGF-β1 145
A.4.3 Gene edited MDSC-Dec produce decorin in a dose-responsive and autoregulated manner 146
A.4.4 MDSC-Dec cells reduce inflammatory and fibrotic markers and eliminate fibrotic differentiation of MDSCs 147
A.5 Discussion 148

A.6 Conclusion 153
References 154
Curriculum Vitae 167

List of Figures

Figure 2.1 Overview of synthetic promoter design and experimental approach 32
Figure 2.2 Evaluation of cells after cytokine stimulation in monolayer to determine responsiveness of NRE-IL1Ra vector.....40
Figure 2.3 Assessment of engineered cartilage to determine if NRE-IL1Ra protects tissues from cytokine stimulation.....43
Figure 2.4 NF-κB activity of cells transduced via biomaterial-mediated lentiviral delivery 45
Figure 2.5 IL-1Ra production and gene expression in cells transduced via biomaterial-mediated lentiviral delivery.....46
Figure 2.6 Gene expression of cells transduced through biomaterial-mediated delivery and challenged with IL-1α.....47
Figure S2.1 IL-1Ra production in EF1α-IL1Ra group at different IL-1α doses over time 53
Figure S2.2 Relative gene expression of cells transduced through biomaterial-mediated delivery and challenged with IL-1α for the EF1α-IL1Ra group.....54

Figure 3.1 Mechanogenetic transduction and therapeutic drug delivery approach 60
Figure 3.2 Mechanical responsiveness of chondrocytes is mediated by dose-responsive hypo-osmotic stimulation of TRPV4 70
Figure 3.3 Transcriptomic profile induced by TRPV4 activation 74
Figure 3.4 Mechanogenetic constructs respond to TRPV4 activation.....78
Figure 3.5 Activation of TRPV4 via osmotic loading of mechanogenetic NFκBr constructs protects against IL-1α 82
Figure S3.1 Intracellular calcium signaling in chondrocytes in response to TRPV4 agonist GSK101 and TRPV4 antagonist GSK205 90
Figure S3.2 Chondrocytes respond mechanically to changes in external osmolarities 91
Figure S3.3 Finite element models of cellular loading conditions 92
Figure S3.4 Network schematic for intracellular pathways stimulated by TRPV4 activation 93
Figure S3.5 Daily IL-1Ra production from NFκBr-IL1Ra mechanogenetic cartilage exposed to pharmacologic TRPV4 activation.....93

Figure S3.6 PTGS2r-IL1Ra response to mechanical loading after 24 hours.....93
Figure S3.7 Dose-dependent response of NFκBr-IL1Ra cartilage to IL-1α.....94
Figure S3.8 NFκBr-IL1Ra mechanogenetic tissue response to IL-1α and deformational mechanical loading 94
Figure S3.9 Osmotically loaded PTGS2r-IL1Ra constructs in the presence of IL-1α 95

Figure 4.1 Inflammation resistant cell-based therapies and circadian measurements 102
Figure 4.2 Development of circadian clock in miPSC chondrogenesis.....112
Figure 4.3 Tissue engineered cartilage response to inflammatory cytokines 116
Figure 4.4 Cartilage circadian clock in response to inflammatory cytokines.....117
Figure 4.5 Engineered cell therapies in response to IL-1α 120

Figure 5.1 Cell-based chronogenetic therapy approach.....131
Figure 5.2 Characterization of chronogenetic reporter circuit and tissue engineered cartilage..139
Figure 5.3 *In vitro* characterization of Per2-IL1Ra-t2a-Luc circuit.....141
Figure 5.4 *In vivo* characterization of Per2-IL1Ra-t2a-Luc circuit 144

Figure A.1 Overview of design of CRISPR-Cas9 edited MDSCs.....154
Figure A.2 Genes activated by TGF-β1 stimulation in MDSCs.....159
Figure A.3 Characterization of MDSC response to TGF-β1 160
Figure A.4 Decorin gene expression in WT and MDSC-Dec cells given TGF-β1 162
Figure A.5 Assessment of MDSC-Dec cell's ability to reduce inflammation, fibrosis, and fibrotic differentiation.....163

List of Tables

Table 2.1 qRT-PCR primer pair sequences for inflammation and cartilage matrix genes, as well as transgene expression analysis. 38

Acknowledgments

Thank you to my mentor, Farshid Guilak, for his continuous support, guidance, and enthusiasm for my research and throughout my graduate school career. Thank you for your unending optimism about my projects and for giving me the independence to try different things. Additionally, thank you for mentoring me in other areas of my life outside of the lab, such as career development, and for supporting my participation in summer internships and other activities. Finally, thank you for introducing me to our favorite place, Pagan, and for never missing a chance to meet there.

Thank you to all the members of the Guilak Lab for their encouragement, advice, and friendship while setting a high bar for scientific achievement. I would like to thank Alison Ross for being my partner for part of the work in this dissertation and always being there for me with coffee when I needed it. Thank you to the entire mechanogenetics team and specifically to Robert Nims for being my partner in crime, always keeping things interesting with prank wars, and essentially being attached at the hip with me throughout the entire project. Thanks to Kristin Lenz who made all the *in vivo* work possible and saved me from having to handle mice. I would also like to thank Sara Oswald for checking up on me and giving me support and encouragement through many challenging days while writing. Thanks to Jim Maus and Nick Thompson for keeping the lab running smoothly and especially for getting me all the reagents I needed to finish my experiments during the COVID pandemic.

I would also like to thank Erik Herzog and Anna Damato for all of their guidance and help on the circadian components of this thesis detailed in Chapters 4 and 5. Thanks to Erik for your support, advice, and for helping us enter a new research field. Additionally, thank you for

introducing me to Anna. Thanks to Anna for all of your work and her friendship throughout the last two years of my PhD, these experiments would not have been possible without you.

Thank you to the research community at Washington University. Special thanks to the Center of Regenerative Medicine for their funding support (Philip and Sima Needleman Fellowship for Regenerative Medicine), the Institute of Clinical and Translational Sciences for their funding support (Just in Time Grant), and the Genome Engineering and iPSC Center. The work in this dissertation would not be possible without the additional funding support from the Nancy Taylor Foundation for Chronic Diseases, the Arthritis Foundation, the Shriners Hospitals for Children, and the National Institutes of Health (AR76665, AG46927, AG15768, AR072999, AR74270, AR73752, AR074992, AR073221, AG28716, AR072870). Thank you to my dissertation committee William Buchser, Erik Herzog, Nathaniel Huebsch, and Jeffrey Millman for your guidance and enthusiasm regarding my thesis.

Thank you to my friends and family for continuously supporting and encouraging me throughout my time in graduate school. Mom and dad, your love and support are unmatched, and I am forever grateful. Thank you for instilling in me the confidence to tackle any task. Thank you to my sister and brother-in-law, Melisa and Joseph, for always letting me know how proud you are, discussing science with me, and being there for me on both good and bad days. Lastly, thank you to Mandalina (Lina) Pferdehirt, for distracting me with cuddles and for being the best.

Lara Pferdehirt

Washington University in St. Louis

May 2021

Dedicated to my supportive parents and encouraging sister and brother-in-law.

And especially Mandalina (Lina) Pferdehirt

ABSTRACT OF THE DISSERTATION

Synthetic Gene Circuits for Self-Regulating and Temporal Delivery of Anti-Inflammatory Biologic Drugs in Engineered Tissues

by

Lara Pferdehirt

Doctor of Philosophy in Biomedical Engineering

Washington University in St. Louis, 2021

Professor Farshid Guilak, Chair

The recent advances in the fields of synthetic biology and genome engineering open up new possibilities for creating cell-based therapies. We combined these tools to target repair of articular cartilage, a tissue that lacks a natural ability to regenerate, in the presence of arthritic diseases. To this end, we developed cell-based therapies that harness disease pathways and the unique properties of articular cartilage for prescribed, localized, and controlled delivery of biologics, creating the next generation of cell therapies and new classes of synthetic circuits.

We created tissue engineered cartilage from murine induced pluripotent stem cells that had the ability to sense inflammatory stimuli to produce an anti-cytokine biologic to self-regulate and inhibit inflammation. To create this gene circuit, we developed a synthetic promoter activated by NF-κB signaling, a key inflammatory pathway activated within chondrocytes in arthritis. This lentiviral system was capable of producing an anti-cytokine therapeutic, IL-1Ra, and protecting tissue engineered cartilage from inflammation-mediated degradation.

Chondrocytes within articular cartilage respond to mechanobiologic signals through ion channels, such as the TRPV4 ion channel, involved in mechanotransduction. We developed synthetic cell-based therapies that could sense mechanical stimuli, such as activation of TRPV4,

and produce prescribed biologic drugs in response to mechanical stimuli. With this approach, we created two novel mechanogenetic circuits activated by TRPV4 that produced our therapeutic transgene with different drug release kinetics.

The cartilage circadian clock plays a key role in maintaining cartilage homeostasis and integrity. When the circadian clock is desynchronized, such as in the presence of inflammation, articular cartilage begins to degrade. Therefore, we created clock-preserving synthetic circuits that are capable of preserving circadian rhythms even in the presence of inflammation. In addition to creating these circuits, we also characterized the circadian clock throughout chondrogenic differentiation and uncovered interesting characteristics between circadian disruption and extracellular matrix (ECM) degradation that can be further examined to better understand the relationship between inflammation and circadian rhythm disruption.

Finally, we developed the newest generation of cell-based therapies by creating chronogenetic therapies. Expanding beyond preserving circadian rhythms, we developed synthetic chronogenetic circuits driven by the circadian clock for temporal delivery of biologic drugs at specific times of day. This approach was motivated by the field of chronotherapy and the increase in efficacy of drugs when administered at specific times of day. We developed the first cell-based chronotherapy capable of producing an anti-inflammatory biologic at a specific time to combat the peak of inflammatory flares exhibited by patients with chronic inflammation.

Overall, the work in this dissertation builds upon existing synthetic biology and genome engineering tools to create smart cell therapies that are activated by a prescribed input and can produce a therapeutic transgene in a controlled manner. These synthetic circuits provide novel strategies to target inflammation in an arthritic joint and can be expanded for other applications to create better and more effective therapeutics to treat disease.

Chapter 1: Synthetic Biology and the Next Generation of Cell Therapies for Musculoskeletal Disease Treatment and Beyond

1.1 Genome engineering and cell therapies

A biological revolution is currently occurring with the invention and discovery of synthetic biology and genome engineering tools. These tools, such as the development of synthetic gene circuits delivered through viruses and genome engineering tools such as CRISPR-Cas9, provide new approaches in developing cells programmed for specific cellular behavior in response to environmental signals. With the ability to engineer cells for controlled behaviors, the field of cell therapies is gaining popularity over the use of small molecule drugs and systemic delivery of biologics. This new era of therapeutics is driven by the need for a more targeted, controlled, and long-lasting effect that systemic oral delivery of drugs cannot provide. In this context, the use of personalized cell therapies and harnessing cells as drug delivery vehicles is increasing and will change the way diseases are treated. Therefore, we have decided to apply these revolutionary tools to our areas of interest: articular cartilage repair and the treatment of osteoarthritis (OA) and rheumatoid arthritis (RA).

1.2 Articular cartilage

Articular cartilage is the soft connective tissue that covers articulating bone surfaces in diarthrodial joints. It is a highly hydrated tissue with a dense extracellular matrix (ECM)

composed primarily of type II collagen and aggrecan. Type II collagen comprises 90-95% of the collagen in the ECM, with other collagens, such as types I, III, IV, V, VI, IX, and XI helping to form the type II collagen network, providing essential structure and organization (*1-3*). Proteoglycans are the second most abundant component in articular cartilage and consist predominantly of negatively charged sulfated glycosaminoglycan (sGAG) chains. Chondrocytes are the only resident cell type within articular cartilage and constitute only 1-2% of the total cartilage volume. Chondrocytes respond to a variety of stimuli, including mechanical loads, hydrostatic pressure, and growth factors to maintain the structure and function of articular cartilage. All these components come together to create the zonal structure of articular cartilage, contributing to its unique compressive, tensile, and viscoelastic properties that allow it to bear loads, dissipate energy, and provide joint lubrication (*3, 4*). Together, this structure allows for a near-frictionless and wear-resistant surface. Articular cartilage is avascular and aneural and is maintained through a balance between anabolic and catabolic activities; two important components of articular cartilage that maintain this balance are its mechanobiologic response and its circadian clock.

1.2.1 Mechanobiologic response of articular cartilage

As mentioned, articular cartilage contains unique mechanical properties, and chondrocytes respond to mechanical stimuli. Chondrocytes respond to mechanobiologic signals through specialized molecular components, such as mechanically sensitive ion channels and receptors that transduce specific stimuli from the physical environment (*5, 6*). In articular cartilage, the transient receptor potential vanilloid 4 (TRPV4) ion channel is activated by osmotic stress and plays an important role in the mechanosensitivity of chondrocytes (*7-11*). TRPV4 in articular cartilage has been shown to regulate the anabolic biosynthesis of chondrocytes in

response to physiologic mechanical strain (*12*). Therefore, the response of chondrocytes to TRPV4 mediated mechanical loading is an important characteristic of articular cartilage and is important in maintaining tissue homeostasis.

1.2.2 Articular cartilage circadian clock

In addition to mechanical loading, articular cartilage contains a tissue specific circadian clock that contributes to maintenance of tissue homeostasis. Circadian clocks are internal genetic timing mechanisms that exist in the brain and nearly all cells in peripheral tissues and operate on a roughly 24-hour period (*13-15*). These rhythms coordinate tissue-specific physiology with different cycles such as light and darkness, body temperature, and rest and activity (*13*). Core clock genes, comprised of transcriptional activators *Bmal1* and *Clock* and transcriptional repressors *Per1/2* and *Cry1/2* and output genes, such as *Rev-erbs, Dbp,* and *Nfil3,* create an auto-regulatory negative feedback loop that drives this oscillatory behavior of the clock (*14, 15*). These clocks genes drive expression of many other genes referred to as clock-controlled genes that are tissue-specific and play important roles in maintaining tissue homeostasis through their temporal expression (*16*). It has been shown that many anabolic and catabolic pathways in articular cartilage have different daily dynamics, driven by the cartilage circadian clock, to help maintain cartilage homeostasis (*16-22*). Pathways that have different activity at different times include metabolic, ECM remodeling, and catabolic pathways (*16, 21*). Serum levels of biomarkers related to cartilage metabolism that show day/night variations include aggrecan, collagen II, cartilage oligomeric matrix protein, hyaluronic acid, keratin sulfate, and transforming growth factor β (TGF-β) (*17, 20*). *Bmal1* has been implicated in controlling this cartilage homeostasis and integrity. In a *Bmal1* cartilage-specific knockout mouse model, the clock disruption showed dysregulation of TGF-β and NFATc2 pathways, which resulted in a

shift in homeostasis to an increased catabolic response (*19*). Therefore, preservation and synchrony of the cartilage circadian clock is also important in maintaining cartilage homeostasis.

1.3 Inflammation and articular cartilage

Inflammation plays an important role in wound healing and tissue repair; however, dysregulated and chronic inflammation is involved in the pathogenesis of any musculoskeletal diseases. Inflammation is a main regulator of the pression and severity of rheumatoid arthritis (RA), an auto-immune disorder affecting joints. In osteoarthritis (OA), inflammation directly contributes to the degradation of articular cartilage. Additionally, inflammation prevents stem cell chondrogenesis in engineered cartilage (*23-26*). OA is characterized by degradation of articular cartilage, subchondral bone thickening, and osteophyte formation, while both OA and RA are characterized by the modification of synovial fluid, leading to pain, inflammation, and stiffness, limiting mobility in affected individuals (*27, 28*).

Inflammatory signaling pathways are activated in chondrocytes by a variety of stimuli, such as traumatic injury through abnormal mechanical loading and biochemical mediators such as inflammatory cytokines, chemokines, and adipokines (*29*). In arthritis, pro-inflammatory cytokines from both the synovium and chondrocytes induce aberrant expression of catabolic and inflammation-related genes. The two primary pro-inflammatory cytokines present within an arthritic joint are tumor necrosis factor-α (TNFα) and interleukin-1 (IL-1) (*24*). These cytokines suppress synthesis of cartilage matrix components, such as type II collagen and aggrecan, and activate signaling pathways including nuclear factor kappa-light-chain-enhancer of activated B cells (NF-κB) and mitogen activated protein kinases (MAPK) that causes the expression of catabolic and degradative enzymes and inflammatory cytokines (*24, 26, 29-31*). Matrix metalloproteinases (MMPs) and disintegrin and metalloproteinase with thrombospondin motifs

(ADAMTS) family members are the main cartilage ECM degrading enzymes in OA and upregulated by TNFα and IL-1 (*32*). Additionally, these inflammatory cytokines, especially IL-1, induce expression of other inflammatory mediators such as IL-6, monocyte chemoattractant protein-1/C-C motif chemokine ligand 2 (MCP-1/CCL2), and nitric oxide (NO), and the upregulation of these inflammatory mediators creates a positive feedback loop that further amplifies and progresses cartilage degradation (*32*).

Additionally, inflammation has been shown to disrupt the circadian clock in cartilage (*33*). As previously mentioned, desynchronization of the circadian clock in articular cartilage led to a catabolic response and contributed to OA-like cartilage degradation (*19*). The addition of IL-1 to cartilage explants showed loss in circadian rhythms that was only rescued with the administration of dexamethasone, an anti-inflammatory agent (*33*). Therefore, the disruption of the circadian clock through stimuli such as inflammation, could be an important contributor to the pathogenesis of OA (*34*).

1.4 Current strategies for treatment of arthritis

For OA, where the degradation of articular cartilage is a primary characteristic, there are currently no disease modifying drugs available. Articular cartilage is avascular and aneural and lacks an intrinsic ability to repair itself (*23*). Additionally, the harsh inflammatory environment within an OA joint provides a challenging environment for cartilage repair. Non-steroidal anti-inflammatory drugs (NSAIDs), analgesic drugs, and local administration of corticosteroids are commonly prescribed for OA pain; however, these do not inhibit disease progression (*24, 35*). For patients with RA, NSAIDs as well as disease-modifying anti-rheumatic drugs are prescribed and have shown some efficacy in alleviating symptoms of RA.

A number of therapies targeting IL-1 and TNFα have been explored, including delivery of anti-cytokines. IL-1 receptor antagonist (IL-1Ra, anakinra), a competitive antagonist of IL-1, has been shown to alleviate symptoms of RA and post-traumatic OA (*36-38*). TNFα targeting therapies include monoclonal antibodies (infliximab, adalimumab, golimumab) and the soluble TNF receptor-2-IgG-Fc fusion protein (sTNFR1, etanercept). These drugs have some efficacy in patients with RA and have been shown to relieve pain and reduce synovitis (*39, 40*). Clinical trials of IL-1Ra therapy to patients with established OA have not shown efficacy, suggesting that controlled long-term delivery in a localized manner may be necessary for disease modification (*38, 41, 42*). Additionally, anti-cytokine therapies are often delivered at high doses, which may have significant off-target effects, including an increased susceptibility to infection and certain autoimmune diseases (*43*) as well as increased resistance to anti-cytokine therapies in RA patients, reducing the effect of the drug (*44*).

Gene therapy, a technique that includes the delivery or modification of a gene for the treatment or prevention of disease, has been used to delivery IL-1Ra to the joints of patients with RA and OA (*25, 45, 46*). However, despite the therapeutic potential of anti-cytokine drugs and gene therapy approaches, there are currently no effective disease-modifying treatments to address both the symptoms and structural changes of OA (*45-47*).

1.5 Cartilage tissue engineering, gene therapy, and synthetic biology

To address these limitations, tissue engineering and gene therapy approaches can be combined to create a cartilaginous tissue that is capable of replacing damaged tissue while delivering therapeutic drugs to diseased joints (*48*). Murine induced pluripotent stem cells (miPSCs) are an attractive option for tissue engineering because they are a source of large

numbers of precisely defined, patient-matched cells and are capable of chondrogenic differentiation and disease modeling (*49, 50*). Additionally, by using both gene therapy and synthetic biology, cells can be transduced *ex vivo* with expression vectors designed to produce a desired gene through specific stimuli (*51, 52*). Furthermore, by using genome engineering techniques, cells can be generated to be resistant to specific stimuli (*53*). The creation and implantation of tissue-engineered constructs allows for localized delivery of biologic drugs to specific sites in the body. Applying synthetic biology approaches allows for the engineering of new biological systems that do not exist in nature. Previously, miPSCs were edited using CRISPR-Cas9 to lack a functional IL-1 receptor 1 (IL1R1). These IL1R1 knock-out cells were then grown into tissue engineered cartilage that was protected from IL-1 induced degradation (*53*). While this and other gene therapy approaches to target inflammation (*54-58*) are significant advances, there are still limitations in methods to have localized and prescribed delivery of effective biologic therapeutics.

1.6 Creation of the next generation of cell therapies for arthritis

We sought to create cell therapies that were able to deliver biologic therapeutics to target inflammation in OA and RA in a localized and prescribed manner (*59*). To this end, we have focused on creating the next generation of cell therapies for arthritis applications. This involves using genome engineering, gene therapy, and synthetic biology tools to create cells capable of sensing specific stimuli and producing a prescribed therapeutic in an auto-regulating manner.

1.6.1 Engineering of inflammation driven circuits

Due to the tremendous role inflammation plays in both OA and RA, we first sought to create cell therapies capable of sensing inflammatory stimuli and producing an anti-inflammatory biologic. To this end, CRSIPR-Cas9 gene editing was used to incorporate sTNFR1, the TNFα inhibitor, or IL-1Ra, the IL-1 inhibitor, downstream of the *Ccl2* promoter, a promoter activated by inflammatory cytokines, in miPSCs (*60*). These cells were grown into tissue-engineered cartilage, and this cell therapy was able to autonomously produce anti-inflammatory mediators in the presence of inflammatory stimuli, protecting tissue engineered cartilage from degradation and mitigating the effects of RA in an *in vivo* model (*57, 61*). However, transgene production is limited to the level of endogenous promoter activation.

Therefore, we sought to expand further in creating self-regulating systems to sense and inhibit inflammation and developed a lentiviral gene therapy approach by creating a synthetic promoter activated by NF-κB signaling to drive production of a prescribed therapeutic transgene, in this case IL-1Ra (*62*). This system is explained in detail in Chapter 2 of this dissertation. Briefly, this lentiviral system was capable of sensing and responding to inflammatory stimuli by producing therapeutic levels of IL-1Ra capable of protecting tissue-engineered cartilage (*62*). Additionally, the synthetic promoter can be modified to change the sensitivity of the system, and the transgene can be easily replaced with another therapeutic drug.

1.6.2 Engineering mechanically responsive circuits

Inflammation, however, is not the only important stimuli that articular cartilage experiences. As mentioned earlier, mechanical input is a key component of chondrocytes. Therefore, we sought to create gene circuits capable of sensing mechanobiologic stimuli and using mechanical input to drive production of a prescribed transgene. To this end, we created

two mechanogenetic lentiviral gene circuits that respond to TRPV4 activation, which are described in detail in Chapter 3 (*63*). The first circuit was our NF-κB responsive synthetic promoter driving IL-1Ra (*62*), as we found that NF-κB is activated in response to mechanical loading and subsequent TRPV4 activation. The second circuit was driven by prostaglandin-endoperoxide synthase 2 (PTGS2) to produce IL-1Ra. Both mechanogenetic circuits were able to produce our therapeutic drug in response to mechanical, osmotic, and pharmacologic activation of TRPV4 (*63*).

1.6.3 Maintenance of cartilage homeostasis through clock-preserving circuits

As mentioned earlier, preservation of the circadian clock is important to mitigate loss in cartilage homeostasis and cartilage degradation. However, inflammation disrupts the circadian clock. Therefore, we sought to create clock-preserving cell therapies to maintain circadian clock synchrony. These circuits are detailed in Chapter 4. Through the use of cells non-responsive or resistant to inflammation (*53, 60, 62*) we have created clock-preserving cell therapies as a novel approach to establish new therapeutics and enhance tissue repair.

1.7 Chronotherapy: the newest generation of controlled and prescribed cell therapies

Chronotherapy is based on the idea that the time of day when a drug is taken is important to its efficacy. If the drug targets a clock-controlled gene that is only expressed at certain times of the day, the drug will only be effective when the target is highly expressed. This finding is important, as a recent study showed that over half (56) of the top 100 selling drugs in the United States target the product of a circadian gene (*64*). To this end, there are research and clinical trials looking into timed delivery of drugs and increasing their efficacy (*16, 17, 20, 64-68*). For

example, taking low dose aspirin for heart disease is more effective if taken at night since aspirin has a half-life of 6 hours and its target, Cox1, is upregulated at night (*64*). The timing of drugs can be applied not only to heart disease, but also to many other diseases like metabolic diseases and even brain cancers and the timing of chemotherapy (*16, 17, 20, 64-69*).

In musculoskeletal diseases such as OA and RA, there are daily inflammatory flares normally in the early morning. Cytokines present in both OA and RA knee patients exhibited diurnal expression patterns, with inflammatory cytokines peaking in the early hours of the morning (*16, 17, 66, 67*). Patients with RA who took glucocorticoids at night instead of in the morning reported reduced joint pain and inflammation, showing the importance of chronotherapy in arthritis (*68*). Expanding beyond just cartilage and arthritis, cyclic delivery of parathyroid hormone (PTH) has shown improved bone growth, whereas continuous delivery of PTH showed enhanced bone resorption (*70*). Therefore, there are plenty of targets and instances where intermittent or delivery of biologics at specific times of day are required for the drug to be effective.

Unfortunately, this process can be difficult to maintain since it can require constant daily injections or delivery of drugs at inconvenient times, such as the case of arthritis where delivery of the drug in the early morning immediately before the inflammatory flare would be best. To this end, we have created the first cell therapy using the cell's own biologic circadian clock to provide gene-based delivery of biologic drugs at prescribed times and frequencies. This cell therapy is detailed in Chapter 5, but briefly the core clock gene *Per2* was used to drive production of a therapeutic transgene IL-1Ra in an oscillatory and timed way. This approach is the very first creation of a cell-based therapy for chronotherapy.

1.8 Summary

Taking all of this together, we worked to build upon synthetic biology, gene therapy, and gene editing tools and applied these systems to musculoskeletal diseases in a way that is controlled, prescribed, and localized. Taking into consideration the important drivers of arthritis, we developed a synthetic system that can sense and attenuate inflammation, as detailed in Chapter 2 (*62*). Basing the ability of chondrocytes to respond to mechanical stimuli, we created mechanogenetic synthetic circuits that produce a biologic drug in response to loading, as detailed in Chapter 3 (*63*), creating a new class of synthetic circuits. We then built systems based on preserving an important and usually overlooked part of tissues, the circadian clock, for maintaining tissue homeostasis and integrity, as detailed in Chapter 4. Finally, we developed the first-of-its-kind cell-based chronogenetic therapy that delivers a therapeutic drug in a temporal manner, as detailed in Chapter 5.

Chapter 2: A Synthetic Gene Circuit for Self-Regulating Delivery of Biologic Drugs in Engineered Tissues

Partially adapted from: Pferdehirt, L.*, Ross, A. K.*, Brunger, J. M., & Guilak, F. (2019). A synthetic gene circuit for self-regulating delivery of biologic drugs in engineered tissues. *Tissue Engineering Part A*, 25(9-10), 809-820.

2.1 Abstract

Transient, resolving inflammation plays a critical role in tissue repair and regeneration. In the context of joint disease, however, chronic inflammation following injury or with osteoarthritis can lead to irreversible articular cartilage degradation and joint pain. Developing tissue engineering strategies for the regeneration of articular cartilage remains challenging due to the harsh inflammatory environment of an injured or arthritic joint, which can promote degradation of engineered tissues as well as native articular cartilage. Here, we developed an artificial gene circuit for controlled, cell-based delivery of biologic drugs, based on a nuclear factor kappa-light-chain enhancer of activated B cells (NF-κB)-responsive synthetic promoter. Using lentivirus-based gene therapy, we engineered murine induced pluripotent stem cells (iPSCs) capable of attenuating inflammation through controlled release of an anti-inflammatory drug, interleukin-1 receptor antagonist (IL-1Ra), subsequently inhibiting gene circuit activation in a self-regulating manner. Murine iPSCs were transduced with the synthetic gene circuit either in monolayer or through biomaterial-mediated transduction. Cells were maintained in monolayer or differentiated into cartilage constructs and stimulated with different doses of interleukin 1 alpha (IL-1α) to determine the ability of this synthetic NF-κB responsive system to inhibit

inflammation and protect tissue-engineered constructs. In response to IL-1α, cells produced high levels of IL-1Ra, which inhibited inflammatory signaling and protected tissue-engineered cartilage from proteoglycan degradation. Our results show that the combination of gene therapy and tissue engineering can be used to successfully create iPSCs capable of producing biologic drugs in a controlled manner. This self-regulating system provides a tool for cell-based drug delivery as the basis for a novel therapeutic approach for a variety of diseases.

2.2 Introduction

Osteoarthritis (OA) is a debilitating joint disease that causes severe pain and loss of joint function, affecting over 32 million adults in the United States alone (*71*). OA is characterized by the degeneration of articular cartilage, the hyaline cartilage that covers the articulating surfaces of bones in diarthrodial joints. Because articular cartilage is avascular, aneural, and alymphatic, it lacks an intrinsic ability to repair (*23*). While there are many risk factors for OA—including injury, aging, metabolic disorders, obesity, and genetics—a common pathway for the pathogenesis and progression of joint degeneration and pain involves the proinflammatory activity of several cytokines, particularly the interleukin-1 (IL-1) family of cytokines, including IL-1α and IL-1β, and tumor necrosis factor-α (TNF-α) (*24*). These cytokines primarily signal via the nuclear factor kappa-light-chain enhancer of activated B cells (NF-κB) to induce extracellular matrix (ECM) degradation through the inhibition of anabolic activities and enhanced production of degradative enzymes and catabolic cytokines, particularly in articular chondrocytes (*25, 30*). Furthermore, inflammation can significantly inhibit repair of cartilage and other joint tissues, as several studies have shown high sensitivity of stem cells and engineered cartilage to cytokines such as IL-1 and TNF-α (*26, 56, 72, 73*).

IL-1 receptor antagonist (IL-1Ra, anakinra), a competitive antagonist of IL-1, has been shown to alleviate symptoms of rheumatoid arthritis (RA) and post-traumatic OA (*36-38*). Furthermore, several gene therapy approaches to deliver IL-1Ra to the joints of patients with RA and OA are in progress or pending (*25, 45, 46*). However, despite the potential for success of anti-cytokine drugs and gene therapy approaches, there are currently no effective disease-modifying treatments to address both the symptoms and structural change of OA (*45, 47, 74*). Additionally, the inability of these approaches to accomplish a sustained delivery of biologic drugs in a dynamically and spatially controlled manner is an important limitation. Anti-cytokine therapies are often delivered at high doses, which may have significant off-target effects, including an increased susceptibility to infection and certain autoimmune diseases (*43*), as well as limited tissue regeneration and repair (*75-77*). Therefore, the long-term success of stem cell–based therapies for cartilage repair or OA may require engagement of intrinsic cellular abilities to regulate the inflammatory environment of the joint.

To address these limitations, tissue engineering and gene therapy approaches can be combined to create a cartilaginous tissue that is capable of replacing damaged tissue while delivering therapeutic drugs to diseased joints (*48*). Additionally, by using both gene delivery and synthetic biology, cells can be transduced ex vivo with expression vectors designed to produce a desired gene through specific inputs (*51, 52*). Furthermore, the implantation of tissue-engineered constructs allows for localized delivery of biologic drugs to specific sites in the body.

The overall goal of this study was to create self-regulating (i.e., feedback-controlled) stem cells capable of attenuating inflammation in a prescribed manner for a controlled release of anti-inflammatory molecules. We engineered a synthetic transcriptional regulator system capable of producing a therapeutic drug and packaged it into a lentiviral vector to allow for transduction

into various cell types and through different transduction strategies. Specifically, we developed an NF-κB-inducible synthetic promoter that controls the release of a biologic drug, IL-1Ra, to maintain tissue homeostasis in response to the activation of NF-κB in a long-term and sustained manner (Figure 2.1). We utilized this lentiviral vector to create murine induced pluripotent stem cells (iPSCs) capable of sensing and responding to inflammation. Additionally, we show the proof-of-concept for site-specific, scaffold-mediated delivery (*57, 78*) of this lentivirus to iPSCs. The transduced iPSCs were chondrogenically differentiated into articular cartilage tissue to determine the efficacy of this vector in protecting engineered tissue against cytokine-induced degradation. We hypothesized that this NF-κB-inducible biologic drug delivery system will allow for controlled, self-regulating production of anti-inflammatory molecules in direct response to dynamic changes in inflammatory stimuli. This type of cell-based approach could provide an effective method to treat OA and chronic inflammatory diseases while overcoming limitations of current drug delivery techniques.

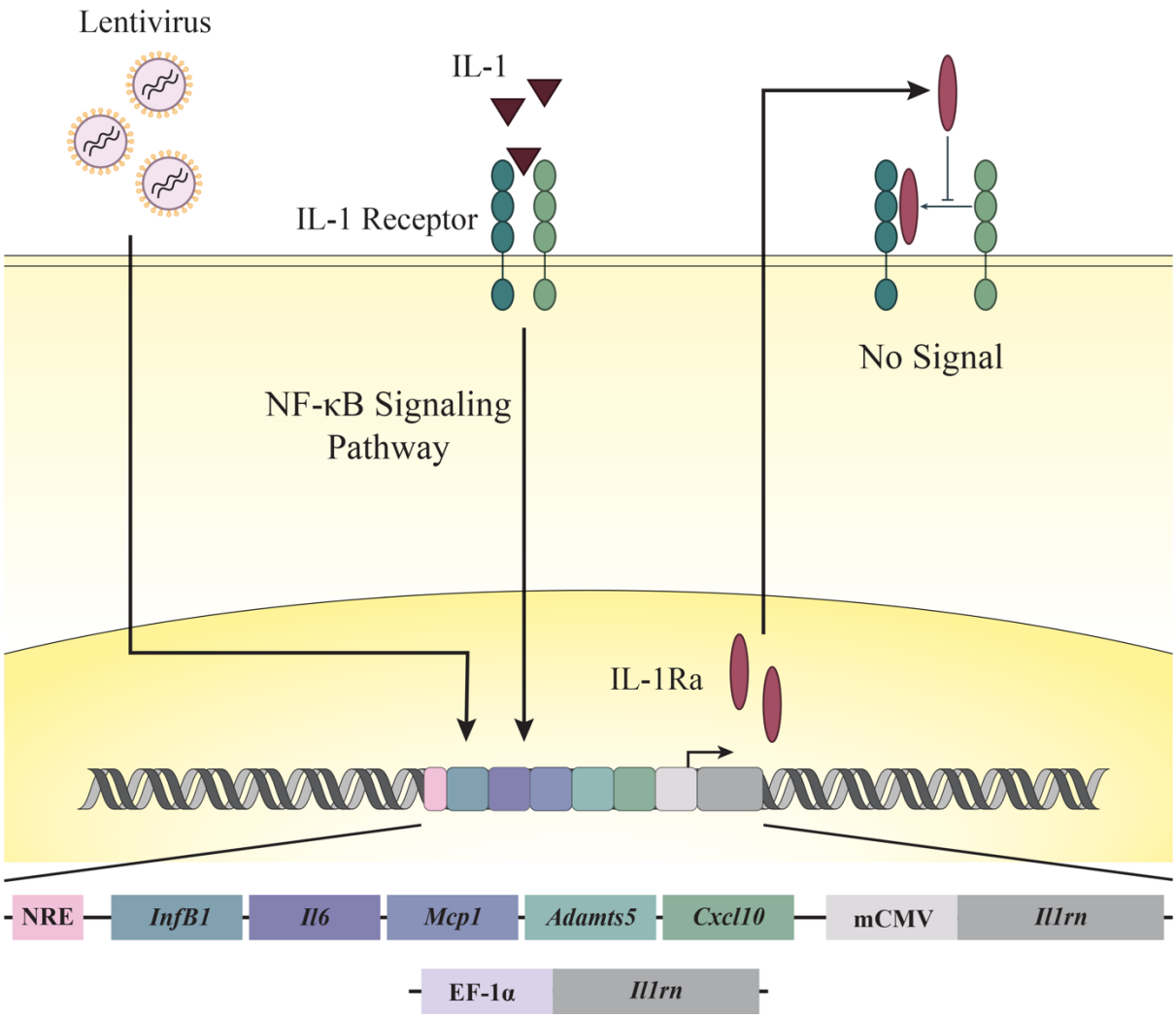

Figure 2.1 Overview of synthetic promoter design and experimental approach. A synthetic promoter was designed with five NF-κB recognition motifs upstream of IL-1Ra to create an NF-κB inducible promoter. The EF1α constitutive promoter was used to drive continuous expression of IL-1Ra. iPSCs were transduced with lentivirus containing an NF-κB inducible promoter that drives expression of IL-1Ra. In the presence of IL-1α, the synthetic promoter is activated and produces IL-1Ra, preventing IL-1α from binding to the IL-1 receptor and inhibiting activation of inflammatory cascades within the cell.

2.3 Materials and Methods

2.3.1 Overall Strategy

The overall strategy for this work was to create a synthetic transcription system that is activated by inflammatory cytokines and, when incorporated into a lentiviral vector, can be readily delivered to different types of cells for applications in cell therapy or tissue engineering. Cells transduced by the lentiviral vectors were programmed to express anti-inflammatory biologic drugs downstream of the synthetic promoter, providing a negative feedback system that blocks the action of an inflammatory cytokine (Figure 2.1). Here, we specifically tested the ability of our synthetic transcription system to protect engineered cartilage from its intrinsic response to inflammatory cytokines through three different methods: in monolayer, in tissue-engineered cartilage, and with biomaterial-mediated delivery of vectors.

2.3.2 Vector Design

A synthetic NF-κB-inducible promoter was designed to incorporate multiple NF-κB response elements that drive a target gene of interest (*60*). Briefly, a synthetic promoter was developed containing five consensus sequences approximating the NF-κB canonical recognition motif based on genes that are upregulated by inflammatory challenge: *InfB1*, *Il6*, *Mcp1*, *Adamts5*, and *Cxcl10* (*60, 79*). Murine *Il1rn* or firefly luciferase from the pGL3 basic plasmid (Promega) was cloned downstream of this synthetic promoter; a TATA box derived from the minimal CMV promoter was cloned between the synthetic promoter and downstream target genes; and an NF-κB-negative regulatory element (NRE-5'-AATTCCTCTGA-3') (*80*) was cloned upstream of the promoter to reduce background signal (Figure 2.1). This engineered NRE-IL1Ra cassette results in transgene expression when the promoter is activated in response

to NF-κB-based inflammatory stimuli, resulting in a ‘‘self-regulating’’ system. A constitutive control vector was also tested using murine *Il1rn* cloned into the lentiviral transfer vector (No. 12250; Addgene) downstream of the EF1α promoter sequence (*81*) (EF1α-IL1Ra) using Gibson Assembly (*82*). A nuclear-targeted green fluorescent protein (GFP) (*83*) (No. 11680; Addgene) was cloned into a constitutive, lentiviral vector (*84*) (No. 11645; Addgene) and was used as a transduction control (GFP).

2.3.3 Lentivirus Production

HEK293T cells were co-transfected with an expression transfer vector, second-generation packaging plasmid psPAX2 (No. 12260; Addgene), and an envelope plasmid pMD2.G (No. 12259; Addgene) by calcium phosphate precipitation to make vesicular stomatitis virus glycoprotein pseudotyped lentivirus (*85*). The expression transfer vectors include the NRE-IL1Ra, NRE- Luc, EF1α-IL1Ra, and GFP plasmids. The lentivirus was stored at -80°C until further use. The functional titer of each virus group was determined via quantitative real-time polymerase chain reaction to determine the number of lentiviral DNA copies integrated into the genome of transduced HeLa cells (*85*).

2.3.4 Cell Culture and Differentiation

Murine iPSCs, generated from tail fibroblasts from adult C57BL/6 mice and validated for pluripotency as described by Diekman et al. (*49, 86*), were maintained on mitomycin C-treated mouse embryonic fibroblasts (Millipore). To track inflammatory activity in cells, an iPSC reporter cell line was created via the CRISPR-Cas9 genome editing system to incorporate firefly luciferase downstream of the *Ccl2* locus (Ccl2-Luc) (*60*). In this cell line, proinflammatory signaling activates *Ccl2* promoter activity, resulting in the transcription of luciferase (*87*).

Unedited and Ccl2-Luc cells were then differentiated toward a mesenchymal state using a high-density micromass culture. Differentiation medium contained Dulbecco's modified Eagle's medium high glucose (DMEM-HG); 1% culture medium supplement containing recombinant human insulin, human transferrin, and sodium selenite (ITS+); minimum essential medium (MEM) nonessential amino acids; 55 μM 2-mercaptoethanol; 24 ng/mL gentamicin; 50 mg/mL L-ascorbic acid; and 40 mg/mL L-proline. On days 3–5, this medium was supplemented with 100nM dexamethasone and 50ng/mL bone morphogenetic protein 4 (BMP-4; R&D Systems) (*49*). After 15 days of culture, the micromasses were dissociated with pronase and collagenase type II and the predifferentiated iPSCs (PDiPSCs) were plated on gelatin-coated dishes in expansion medium containing DMEM-HG, 10% fetal bovine serum, 1% ITS+, MEM nonessential amino acids, 55 μM 2-mercaptoethanol, 1% penicillin/streptomycin, 50 mg/mL L-ascorbic acid, 40 mg/mL L-proline, and 4 ng/mL of basic fibroblast growth factor (bFGF; R&D Systems). These cells were then expanded, transduced, and either used for monolayer experiments or in pellet cultures to produce engineered cartilage to evaluate the ability of these cells to protect against inflammation.

2.3.5 Lentiviral Transduction and Culture of PDiPSCs

For initial characterization, PDiPSCs were transduced with the NRE-Luc virus. For all other monolayer experiments, passage 4 PDiPSCs and Ccl2-Luc cells were transduced with NRE-IL1Ra and EF1α-IL1Ra virus, and non-transduced (NT) cells were used as control.

In pellet experiments, PDiPSCs were transduced at passage 1 with NRE-IL1Ra, EF1α-IL1Ra, or GFP virus. Passage 1 cells were trypsinized, and pellet cultures were created by centrifuging 250k cells at 200xg for 5 min. The pellets were cultured in chondrogenic media containing DMEM-HG, 1% ITS+, MEM nonessential amino acids, 55 μM 2-mercaptoethanol,

1% penicillin-streptomycin, 50 mg/mL L-ascorbic acid, 40 mg/mL L-proline, 100 nM dexamethasone, and 10 ng/mL transforming growth factor-β3 (TGF-β3) for 21 days (*49*).

For all monolayer and pellet studies, transduction media consisted of expansion medium supplemented with 4 mg/mL polybrene (Sigma-Aldrich) and the desired number of viral particles to achieve a multiplicity of infection = 3. Transduction media were exchanged with expansion medium after 24 hours of transduction.

2.3.6 Biomaterial-mediated Delivery

Biomaterial-mediated lentiviral transduction was tested using a model system based on poly(ε-caprolactone) (PCL; molecular weight 70,000–90,000; Sigma-Aldrich), a scaffold material commonly used for cartilage tissue engineering (*88, 89*). PCL was dissolved in glacial acetic acid at a 10% wt/vol ratio. Tissue culture-treated plates were coated wit the dissolved PCL, and the acid was evaporated overnight. The acid was quenched with 1N NaOH, washed with phosphate buffered saline (PBS), and sterilized with an ethanol gradient. Plates were then incubated in 0.002% poly-L-lysine (PLL) solution (Sigma-Aldrich). PLL was aspirated, and two groups of lentivirus (NRE-IL1Ra and EF1α-IL1Ra) or PBS for NT controls were added to the plates and allowed to incubate for 4 hours at 37°C (*57, 88*). After virus immobilization, viral supernatant was aspirated, wells were washed with PBS, and passage 4 PDiPSCs and Ccl2-Luc control cells were plated in the wells. After an additional 3 days of culture, the ability of these cells to respond to and attenuate inflammation was evaluated through a luminescence activity assay, protein production, and gene expression analysis.

2.3.7 Inflammatory Challenge

To evaluate the response of the synthetic promoter to inflammatory cytokines, unedited PDiPSCs transduced with NRE-Luc were challenged with 1 ng/mL IL-1α or 20 ng/mL TNF-α and evaluated at 72 hours after challenge.

To determine the sensitivity and kinetics of the synthetic promoter, all groups of Ccl2-Luc and unedited PDiPSCs (NT, NRE-IL1Ra, and EF1α-IL1Ra) were evaluated at 0, 4, 12, 24, and 72 hours post supplementation of media with 0.05, 0.1, 0.5, or 1 ng/mL IL-1α and removal of bFGF. Control cells were cultured in the absence of IL-1α.

For characterizing the pellets' response to inflammation, after 21 days of chondrogenic culture, pellets were challenged with 0.5 or 1 ng/mL IL-1α and removal of TGF-β and dexamethasone for 72 hours. Control pellets were cultured in the absence of IL-1α.

2.3.8 Inflammation Activity Assay

Luciferase activity from NRE-Luc transduced cells and Ccl2-Luc cells in all monolayer experiments was measured using the BrightGlo Luminescence kit (Promega) and a Cytation5 plate reader (Biotek). Luciferase activity is reported as a fold change of IL-1α-stimulated cells over control cells cultured without IL-1α (n = 4–6).

2.3.9 Gene Expression

Unedited PDiPSCs from monolayer studies and pellets were harvested for quantitative, reverse transcription polymerase chain reaction (qRT-PCR) after inflammatory challenge (n=4). Monolayer cells were rinsed in PBS, lysed in Buffer RL (total RNA purification; Norgen Biotek), and stored at -80°C until RNA isolation. Pellets of engineered cartilage tissue were rinsed in PBS and stored at -80°C until RNA isolation. Pellets were homogenized using a

miniature bead beater. RNA isolation was carried out following the manufacturer's protocol (Norgen Biotek). Reverse transcription was performed using Superscript VILO complementary DNA (cDNA) master mix (Invitrogen). qRT-PCR was performed using Fast SyBR Green master mix (Applied Biosystems) following the manufacturer's protocol. Primer pairs (Table 2.1) were synthesized by Integrated DNA Technologies, Inc. Fold changes were calculated using the $\Delta\Delta C_T$ method and are shown relative to the 0 hour no cytokine, NT control samples for monolayer experiments, or GFP pellets without cytokines. For samples with no amplification, C_T threshold was set to the cycle limit.

Table 2.1 qRT-PCR primer pair sequences for inflammation and cartilage matrix genes, as well as transgene expression analysis.

TARGET	FORWARD PRIMER	REVERSE PRIMER
R18S	5'-CGGCTACCACATCCAAGGAA-3'	5'-GGGCCTCGAAAGAGTCCTGT-3'
CCL2	5'-GGCTCAGCCAGATGCAGTTAA-3'	5'-CCTACTCATTGGGATCATCTTGCT-3'
IL6	5'-AAGTGCATCATCGTTGTTCATACA-3'	5'-CGAACTTCGACACTGACAAGAAGT-3'
COL2A1	5'-TCCAGATGACTTTCCTCCGTCTA-3'	5'-AGGTAGGCGATGCTGTTCTTACA-3'
ACAN	5'-GCATGAGAGAGGCGAATGGA-3'	5'-CTGATCTCGTAGCGATCTTTCTTCT-3'
IL1RN	5'-GTCCAGGATGGTTCCTCTGC-3'	5'-TCTTCCGGTGTGTTGGTGAG-3'

2.3.10 Enzyme-linked Immunosorbent Assays

Culture media were collected from all unedited PDiPSC monolayer and pellet samples after inflammation challenge and stored at -20°C. IL-1Ra concentration was measured with DuoSet enzyme-linked immunosorbent assay (ELISA) specific to mouse IL-1Ra/IL-1F3 (n=4; R&D Systems). Each sample was measured in technical duplicates. Absorbance was measured at 450 and 540 nm.

2.3.11 Biochemical Analysis of Pellet Cultures

After 72 hours of inflammatory challenge, pellets were washed with PBS and stored at -20°C until processing. Pellets were digested overnight in 125 mg/mL papain at 65°C for biochemical analysis. DNA content was measured with PicoGreen assay (Thermo Fisher), and total sulfated glycosaminoglycan (sGAG) content was measured using a 1,9-dimethylmethylene blue assay at 525 nm wavelength (*90*) (n=4).

2.3.12 Histological Processing of Pellet Cultures

After 72 hours of cytokine challenge, pellets were washed with PBS and fixed in 10% neutral buffered formalin for 24 hours, paraffin-embedded, and sectioned at 8 mm thickness. Slides were stained for Safranin-O/hematoxylin/fast green using a standard protocol (*91*).

2.3.13 Statistical Analysis

Statistical analysis was performed with the JMP Pro soft- ware package. Luminescence data and biomaterial-mediated delivery qRT-PCR data were analyzed using analysis of variance (ANOVA) with Dunnett's post hoc test using NT as the control ($\alpha = 0.05$). A two-way ANOVA with Tukey's HSD post hoc test was used to analyze all ELISA data, pellet biochemistry, and pellet qRT-PCR data ($\alpha = 0.05$).

2.4 Results

2.4.1 Responsiveness of the NF-κB synthetic promoter to IL-1α or TNF-α

Pre-differentiated iPSCs (PDiPSCs) receiving the NRE-Luc vector responded to 1 ng/mL IL-1α and 20 ng/mL TNF-α with a 10.17–0.54- and 8.40–0.32-fold increase in luminescence after 72 hours of cytokine stimulation, respectively (Figure 2.2A).

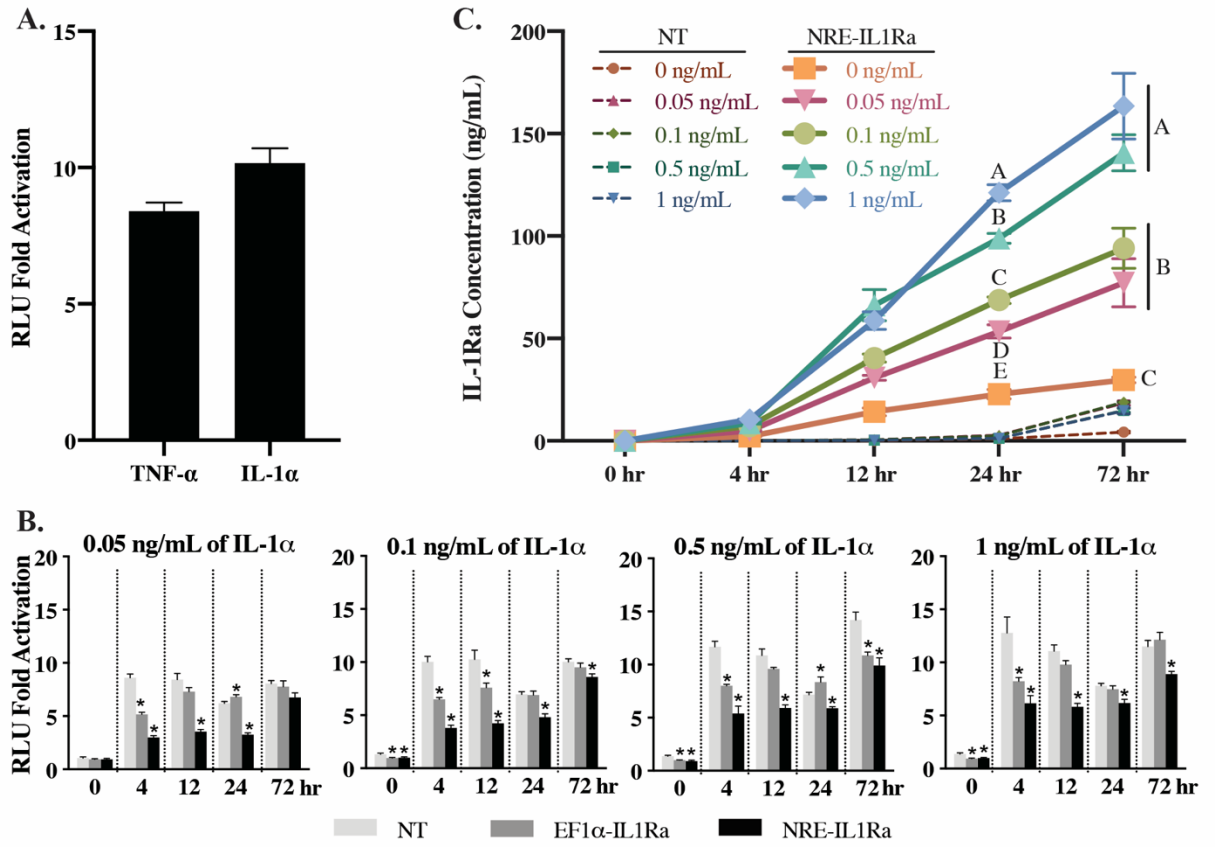

Figure 2.2 Evaluation of cells after cytokine stimulation in monolayer to determine responsiveness of NRE-IL1Ra vector. (**A**) NRE-Luc cells were stimulated with 20 ng/mL TNF-α or 1 ng/mL IL-1α and luminescence was measured after 72 hours. Bars represent the mean relative luminescence units (RLU) ± SEM (n=4). (**B**) Fold change of NF-κB activity measured by luminescence signal from Ccl2-Luc cells. Bars represent the mean fold change in RLU ± SEM (n=6). Asterisks represent significance ($p < 0.05$) compared to NT control. (**C**) NT and NRE-IL1Ra cells were treated with IL-1α and an ELISA was performed on samples to determine IL-1Ra protein production. Values represent mean ± SEM (n=4). Groups not sharing same letter are statistically significant ($p < 0.05$).

2.4.2 Self-Regulating attenuation of inflammation by iPSCs

Attenuation of inflammatory signaling was tested in Ccl2-Luc reporter cells that produce luciferase in response to inflammatory stimuli. After transduction, cells transduced with either

the NRE-IL1Ra or EF1α-IL1Ra lentivirus and NT control cells were treated with IL-1α at a range of doses from physiologic (0.1 ng/mL) to supraphysiologic (1 ng/ mL) (*73*) and compared with cells without cytokine. In all doses of IL-1α, by 4 hours there was significantly less luminescence output in both NRE-IL1Ra and EF1α-IL1Ra groups compared with NT control. This trend was sustained up to 24 hours in all doses in the NRE-IL1Ra groups and up to 72 hours in all doses except 0.05 ng/mL of IL-1α (Figure 2.2B) ($p < 0.01$). This decrease in luminescence shows that there was attenuation of IL-1 signaling with the NRE-IL1Ra group and that this system is responsive at a range of cytokine concentrations.

To evaluate the ability of these vectors to produce therapeutic levels of IL-1Ra, unedited PDiPSCs were lentivirally transduced with the NRE-IL1Ra or EF1α-IL1Ra vectors, and IL-1Ra protein production was measured. The transduced cells and NT control cells were administered with IL-1α and compared with cells without cytokine. Culture media were collected at 0, 4, 12, 24, and 72 hours to measure the production of IL-1Ra in response to an inflammatory challenge. NRE-IL1Ra groups had an increase in IL-1Ra production over time and exhibited higher IL-1Ra production with increased doses of IL-1α. There was a significant increase in IL-1Ra production in the NRE-IL1Ra groups challenged with IL-1α compared with the NRE- IL1Ra cells without cytokine at 24 and 72 hours ($p < 0.0001$) with 140.64–8.78 and 163.41–16.04 ng/mL IL-1Ra produced with 0.5 and 1 ng/mL IL-1α stimulation at 72 hours, respectively. Additionally, there was an increase in IL-1Ra in NRE-IL1Ra groups compared with the NT and EF1α-IL1Ra groups (Figure 2.2C and Figure S2.1A) ($p < 0.0001$). These results taken together show that this iPSC-based NRE- IL1Ra system responds to an inflammation challenge by producing increased levels of the biologic drug.

2.4.3 Transduced NRE-IL1Ra iPSCs from tissue-engineered cartilage is protected from IL-1α

Following lentiviral delivery to iPSCs and 21 days of chondrogenic differentiation, pellets were administered 0.5 or 1 ng/mL IL-1α for 72 hours and were compared with pellets that did not receive cytokine. GFP control pellets showed rich Safranin-O staining for sGAG, one of the primary components of cartilage ECM. Pellets treated with 0.5 ng/ mL or 1 ng/mL IL-1α for 72 hours displayed reduced Safranin-O staining (Figure 2.3A). Pellets made from NRE-IL1Ra PDiPSCs produced 72.90–2.42 and 92.24–2.31 ng/mL IL-1Ra in response to 0.5 and 1 ng/mL IL-1α, respectively, which was significantly higher than both GFP and EF1α-IL1Ra pellets ($p < 0.0001$). EF1α-IL1Ra pellets produced significantly higher levels of IL-1Ra compared with GFP control pellets (Figure 2.3B) ($p < 0.001$). NRE-IL1Ra pellets showed protection against IL-1α-mediated matrix degradation, as indicated by robust Safranin-O staining and quantitative biochemical analysis. NRE-IL1Ra pellets that received IL-1α had significantly higher amounts of sGAG when normalized to the concentration of DNA in each pellet (normalized to pellets that did not receive IL-1α) compared with EF1α-IL1Ra and GFP control pellets (Figure 2.3C) ($p = 0.0322$ and 0.0005, respectively). Despite the increased levels of IL-1Ra production, the EF1α-IL1Ra pellets showed little or no inhibition of IL-1α-mediated sGAG loss, as indicated by the loss of Safranin-O staining and sGAG/DNA content (Figure 2.3C).

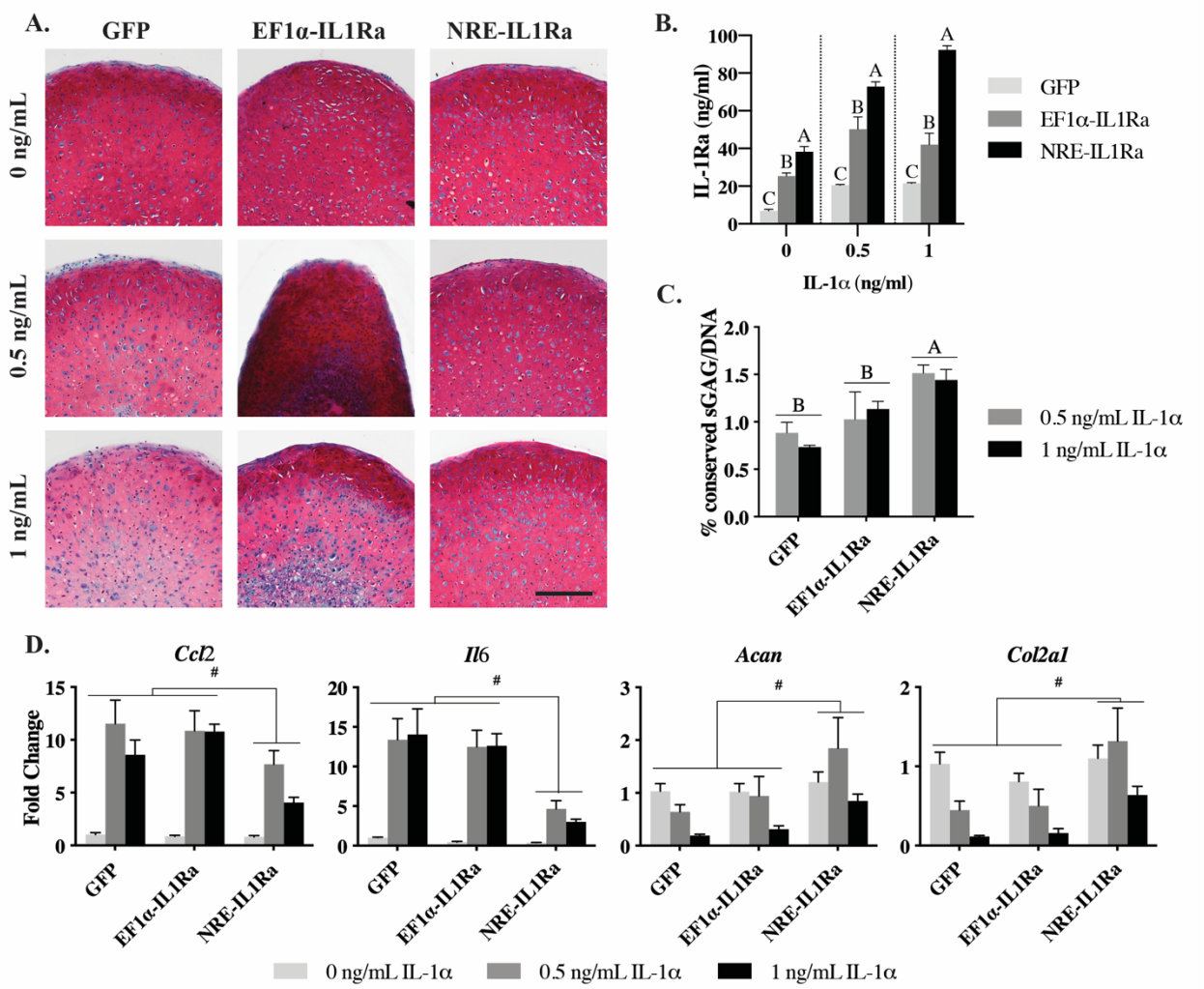

Figure 2.3 Assessment of engineered cartilage to determine if NRE-IL1Ra protects tissues from cytokine stimulation. (**A**) Safranin-O/fast green/hematoxylin stained tissue sections of engineered cartilage (scale bar = 200μm). (**B**) IL-1Ra production collected from media samples after IL-1α stimulation (n=4). Groups not sharing same letter are statistically significant ($p < 0.05$). (**C**) % conserved sGAG/DNA in pellets after addition of IL-1α (n=4). Groups not sharing same letter are statistically significant ($p < 0.05$). (**D**) Relative gene expression compared to 0 hour control measured by qRT-PCR (n=4). Hash represents significance ($p < 0.05$).

Gene expression analysis of the pellets showed a significantly decreased expression of inflammation-related genes, *Ccl2* and *Il6*, in pellets engineered with the NRE-IL1Ra vector compared with GFP control ($p = 0.0164$ and 0.0004, respectively) and EF1α-IL1Ra ($p=0.0054$ and 0.0008, respectively) pellets. Furthermore, NRE-IL1Ra pellets had significantly higher levels of expression of cartilage matrix- related genes, *Col2a1* and *Acan*, compared with GFP

control ($p = 0.0088$ and 0.0090, respectively) and EF1α-IL1Ra pellets (Figure 2.3D) ($p = 0.0044$ and 0.041, respectively).

2.4.4 Biomaterial-mediated lentiviral delivery shows self-regulating production of IL-1Ra and attenuation of inflammation

Ccl2-Luc reporter cells were seeded on a PCL film and were transduced through biomaterial-mediated delivery of either NRE-IL1Ra or EF1α-IL1Ra vectors. Cell were also seeded on PCL without virus as a NT control. Cells were then administered with IL-1α. For all doses of IL-1α, the NRE-IL1Ra group had significantly less luminescence out-put compared with NT controls by 24 hours ($p < 0.001$) (Figure 2.4). At 72 hours post stimulation, NRE-IL1Ra and EF1α- IL1Ra cells had decreased luminescent output compared with NT controls in all doses, showing attenuation of inflammation ($p < 0.0001$).

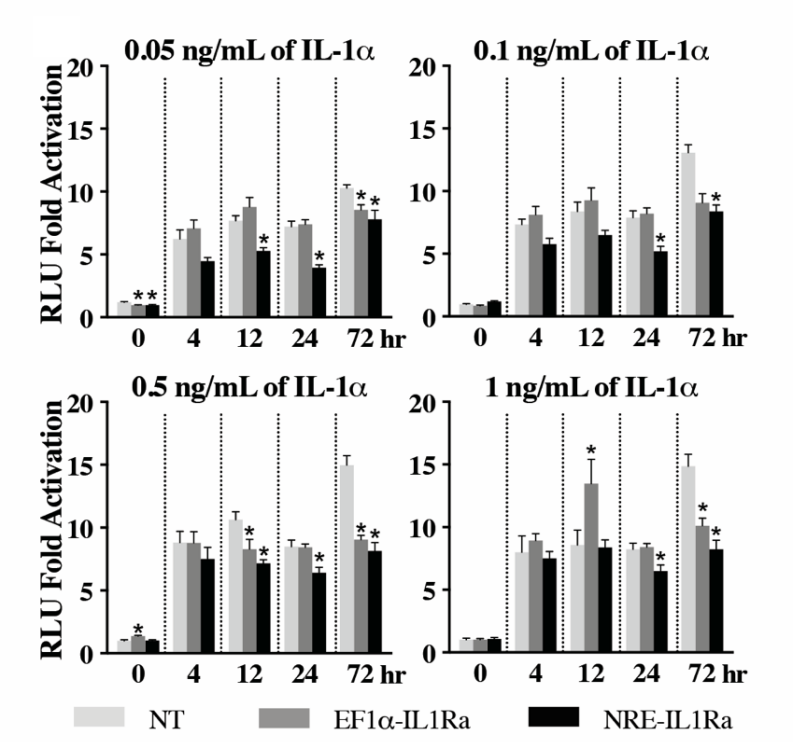

Figure 2.4 NF-κB activity of cells transduced via biomaterial-mediated lentiviral delivery. Reported as fold change measured by luminescence signal from Ccl2-Luc cells. Bars represent the mean fold change in RLU ± SEM of cells treated with IL-1α compared with controls cultured with no cytokine (n=6). Asterisks represent significance ($p < 0.05$) compared to NT control.

Culture media were collected at 0, 4, 12, 24, and 72 hours to measure IL-1Ra production from cells transduced via biomaterial-mediated transduction. The NRE-IL1Ra group exhibited a time- and dose-dependent response of IL-1Ra production. IL-1Ra protein production was significantly increased at higher doses of IL-1α, with 139.31–19.6 and 165.91–15.83 ng/mL IL-1Ra being produced when stimulated with 0.5 and 1 ng/mL IL-1α, respectively, at 72 hours ($p < 0.001$). Additionally, IL-1Ra production was increased in the NRE-IL1Ra group compared with NT and EF1α-IL1Ra groups (Figure 2.5A and Figure S2.1B) ($p < 0.0001$). There was an increase

in *Il1rn* gene expression in all cells that received the NRE-IL1Ra vector at 24 hours (Figure 2.5B), and in EF1α-IL1Ra cells at 0, 12, and 24 hours (Figure S2.2C). By 72 hours, NT and NRE-IL1Ra groups were not significantly different from each other, indicating that a decreased inflammatory signaling led to an autoregulated decrease in *Il1rn* gene expression due to IL-1Ra-mediated inhibition of inflammation and subsequent gene circuit activation.

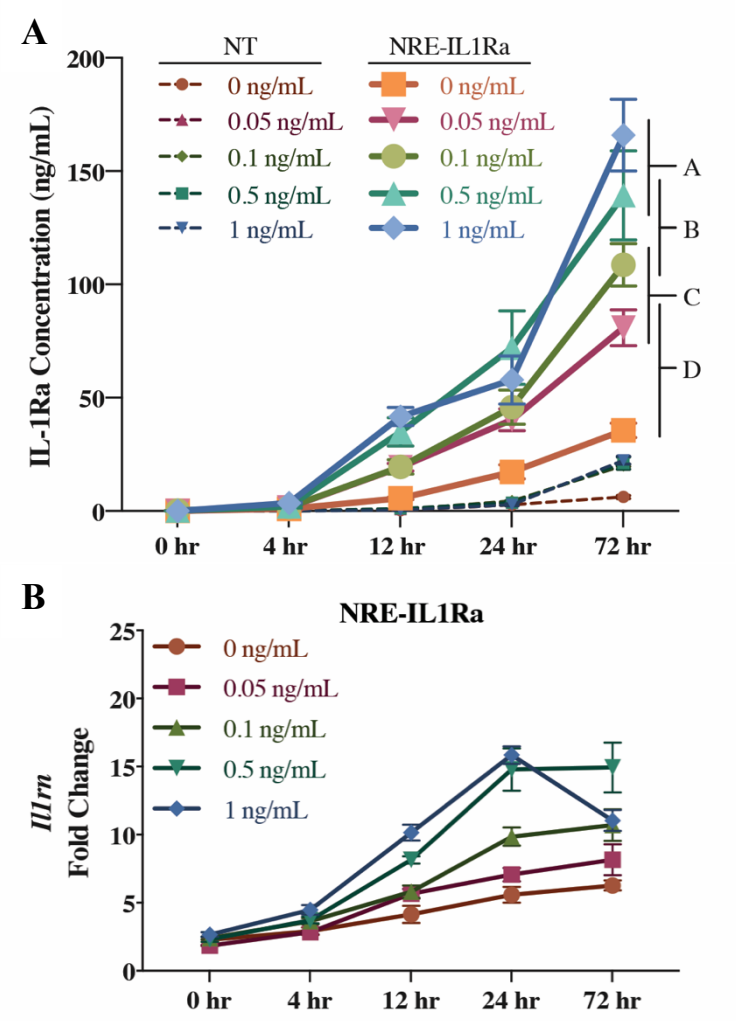

Figure 2.5 Transgene induction in cells transduced via biomaterial-mediated lentiviral delivery. (**A**) NT and NRE-IL1Ra cells were treated with IL-1α and an ELISA was performed on samples to determine IL-1Ra protein production. Values represent mean ± SEM (n=4). Groups not sharing same letter are statistically significant ($p < 0.05$). (**B**) *Il1rn* gene expression. Fold changes were determined relative to 0 hour NT cells without cytokine. Error bars represent means of fold change ± SEM (n=6).

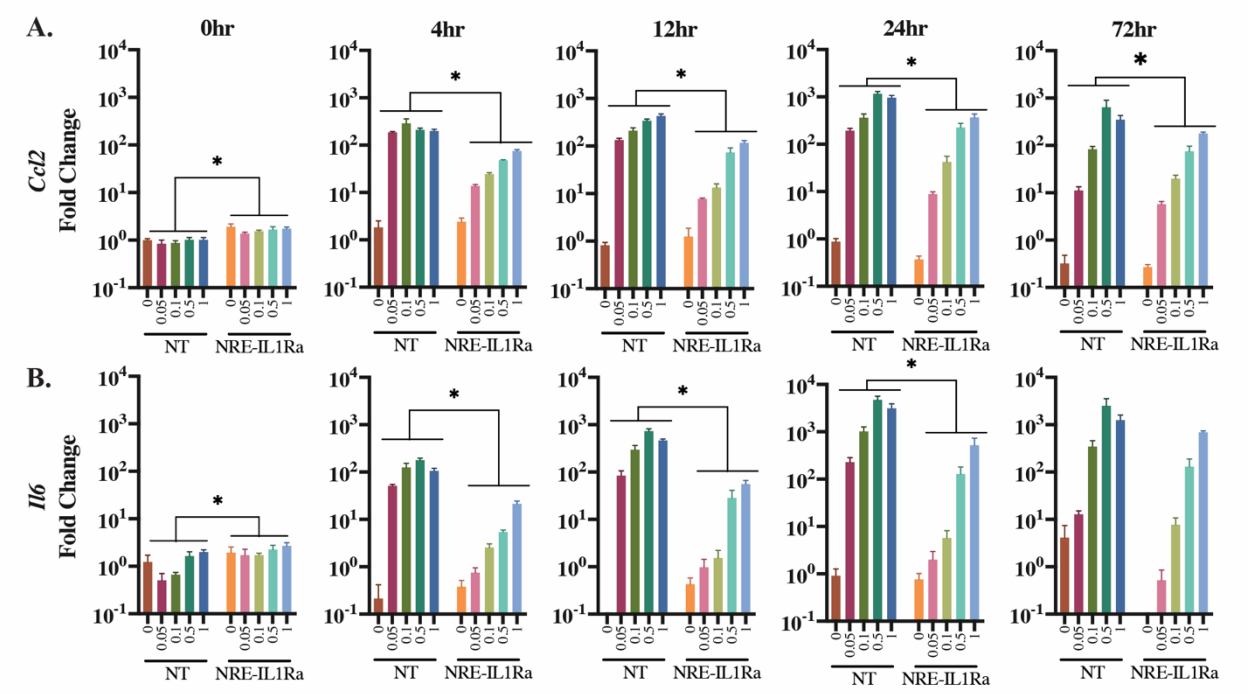

Figure 2.6 Gene expression of cells transduced through biomaterial-mediated delivery and challenged with IL-1α. Fold changes were determined relative to 0 hour NT cells without cytokine. Error bars represent means of fold change ± SEM (n=6). Asterisks represent significance relative to NT control group ($p < 0.05$). (**A**) *Ccl2* gene expression. (**B**) *Il6* gene expression.

Gene expression analysis showed a dose-dependent increase in inflammation-related genes, *Ccl2* and *Il6*, as early as 4 hours following the delivery of inflammatory cytokines to all groups of cells, which persisted through 72 hours. However, the biomaterial-mediated delivery of the self-regulating NRE-IL1Ra compared with NT controls significantly decreased the expression of *Ccl2* starting at 4 hours and was maintained through 72 hours (Figure 2.6A) ($p < 0.01$). *Ccl2* was also decreased in EF1α-IL1Ra cells compared with NT controls at 24 and 72 hours (Figure S2.2A). *Il6* was significantly decreased in NRE-IL1Ra cells from 4 hours through 24 hours (Figure 2.6B) ($p < 0.0001$) and was significantly decreased in EF1α-IL1Ra cells at 24 hours (Figure S2.2B). Together, these results show that this system responds to inflammatory stimulus and suggests that the therapeutic levels produced could inhibit inflammation. Additionally, these findings show a successful proof-of-concept experiment for the delivery of

either our transduced cells for implantation into the joint (*56-58*) or of our gene therapy vectors for transduction of endogenous cells *in vivo.*

2.5 Discussion

A significant challenge in the field of regenerative medicine has been the ability to tissue-engineer cartilage that is capable of withstanding the harsh inflammatory environment of an injured or arthritic joint. We developed an iPSC-based lentiviral system in which cells sense and respond to inflammatory stimuli by producing anti-inflammatory mediators. Using a combination of regenerative medicine, synthetic biology, and gene therapy, we developed self-regulating iPSCs that are capable of forming engineered cartilage for the replacement of diseased tissue and mitigating the inflammatory effects of IL-1α (*49*). Additionally, the versatility of both the iPSCs and the lentiviral system allows for translation to various cell types or tissues. Lastly, by leveraging the flexibility of lentiviral transduction in tissue engineering applications, we demonstrated proof-of-concept of a targeted delivery method allowing for spatial control of therapy via biomaterial-mediated lentiviral transduction.

Using lentivirus-based gene therapy, we engineered iPSCs with the NRE-IL1Ra vector, creating a system that can dynamically respond to and attenuate NF-κB signaling. Cells receiving the NRE-IL1Ra vector responded rapidly to IL-1α as all groups had reduced inflammatory signaling by 4 hours after stimulation. Importantly, NRE-IL1Ra cells responded to both physiologic and supraphysiologic doses of IL-1α, and this response was sustained throughout 72 hours for all doses, except 0.05 ng/mL IL-1α. In addition, all doses of IL-1α activated the synthetic promoter to produce therapeutic levels of IL-1Ra by 24 and 72 hours and in a dose-dependent manner. This dose response provides a controlled production of the therapeutic drug

in response to different levels of inflammation. Cells that received the EF1α-IL1Ra vector produced IL-1Ra, however, at a significantly lower amount than the NRE-IL1Ra vector. This could be due to the low production of the transgene from the constitutive promoter, which has previously been reported in lentiviral systems with constitutive reporters (*92*).

An important advance of this work is the application of our lentiviral system in iPSCs. iPSCs are attractive for tissue engineering and regenerative medicine because they can be expanded, patient-matched, and differentiated into a variety of different cell types to treat multiple tissues, overcoming the limitations of other common cell sources (*49, 50*). Here, we show that the NRE-IL1Ra vector can be delivered to PDiPSCs, and these cells can form cartilaginous tissues, and that in the presence of 0.05 or 1 ng/mL IL-1α, engineered cartilage pellets produced high levels of IL-1Ra. This indicates the potential use of this system for the repair of diseased articular cartilage and mitigation of inflammation through a soluble release of IL-1Ra into the joint. We observed less IL-1Ra production from tissue-engineered cartilage than cells in monolayer. This difference can be attributed to the different differentiation states of the cells, as well as their accessibility to the culture media. In pellets, cells are embedded within a dense ECM, which may bind or hinder the transport of IL-1Ra and/or IL-1α (*93*). Despite these transport limitations, NRE-IL1Ra pellets were protected from IL-1α-mediated degradation, as evidenced by rich Safranin-O staining and significantly higher levels of sGAG/ DNA. Furthermore, NRE-IL1Ra pellets had decreased expression of inflammation-related genes, while cartilage matrix-related genes were sustained, showing the attenuation of inflammatory pathways and protection of the matrix.

In previous approaches, gene therapy for the treatment of OA has been performed with plasmid DNA (*94*), retrovirus (*95*), lentivirus (*96-98*), and most commonly non-integrating viral

vectors such as adeno-associated virus (*88, 99-102*). Lentiviral delivery is advantageous for this system due to its ability to stably integrate into the genome of dividing and non-dividing cells for long-term gene expression, its larger packaging capacity, low immunogenicity, and low cytotoxicity (*103, 104*). The vector used in this study is self-inactivating and, therefore, replication-defective, overcoming safety concerns previously associated with viral gene therapy (*105-107*). Additionally, our group and others have shown that viral vectors can be immobilized to biomaterial surfaces or scaffolds for the delivery of therapeutic vectors to cells (*56-58, 78, 108*). Our study showed that biomaterial-mediated delivery of NRE-IL1Ra from PCL provided efficient transduction and effectively decreased inflammatory signaling. Specifically, biomaterial-mediated transduction of NRE-IL1Ra significantly decreased the expression of inflammation-related genes, *Ccl2* and *Il6*, and stimulated high levels of IL-1Ra production in a dose-dependent manner. These results indicate that this approach provides an effective method for delivering therapeutic vectors and can be applied for broader tissue engineering applications. This strategy could address limitations of existing gene therapy approaches such as the loss of therapeutic transgene expression over time when using non-integrating delivery methods, lack of spatial control of transduction when using systemic injections of vectors, and lack of controllable or inducible production of transgenes when using constitutive expression vectors.

Previously, investigators have developed various systems for inflammation-inducible expression of pro-regenerative or anti-inflammatory transgenes. Rachakonda et al. created a self-limiting promoter construct that was based on truncated promoter sequences of cyclooxygenase-2 upstream of IL-4 to express IL-4 only in the presence of inflammation (*54*). Others have also created expression systems based on NF- κB binding sequences for luciferase reporting vectors (*109, 110*) or inducible systems driving the expression of anti-inflammatory mediators in adeno-

associated viral vectors (*111, 112*). Previous work in our lab utilized CRISPR-Cas9 technology to genome-engineer stem cells capable of using the endogenous systems within the cells to sense inflammation and produce therapeutic transgenes (*60*). While this system has specific advantages in terms of the precision of CRISPR-based gene editing, by packaging our NRE-IL1Ra system into a lentiviral expression cassette, we expand the vector's applicability to transduce different cell types and tissues, such as mesenchymal stem cells, adipose-derived stem cells, or primary cells such as articular chondrocytes or synovial cells, all of which are commonly used in tissue engineering or targeted for gene therapy but are more challenging to edit with CRISPR-Cas9. The sensitivity of the synthetic promoter can be tuned dependent on the sequence, number of tandem repeats, and neighboring regulatory elements, as well as through gene editing (*53*) or epigenetic modification (*113*) of the cells' receptors. Additionally, other inflammatory cytokines, such as TNF-α, or intracellular signaling components can be targeted for specific or broad inhibition of inflammation.

Our synthetic lentiviral system can create self-regulating cells capable of sensing and responding to inflammation with a therapeutic level of biologic drug. The continued development of designer circuits through gene switches (*114-116*), microRNA classifiers (*117, 118*), and synthetic transcription systems (*119-121*) provides a toolkit to engineer more complex circuits with specialized control. This work adds to our long-term goals of developing a molecular toolbox (*122, 123*) of biological building blocks for novel synthetic applications in mammalian cells for ameliorating chronic diseases.

The autoregulatory capabilities of this system allow applications for regenerative medicine or for use as a preventative approach to inflammatory disease. Applying this methodology not only allows for protection against inflammation to aid in cartilage repair, but

also provides protection of any tissue-engineered constructs inserted to help repair an osteoarthritic joint or biomaterial-mediated lentiviral transduction of any infiltrating cells through localized transduction. The customization aspect of this system and its functionality in monolayer, an engineered tissue replacement, and through scaffold-mediated delivery gives innovative opportunities for effective treatments that are applicable in a variety of diseases.

2.6 Supplemental Figures

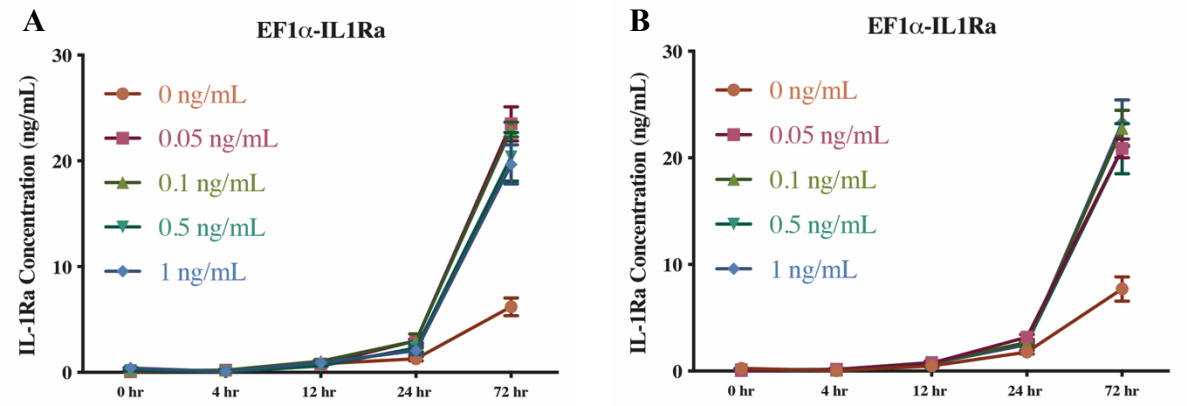

Figure S2.1 IL-1Ra protein production in EF1α-IL1Ra group at different IL-1α doses over time in **(A)** monolayer cells and **(B)** in monolayer cells transduced through biomaterial-mediated delivery. Values represent mean ± SEM (n=4).

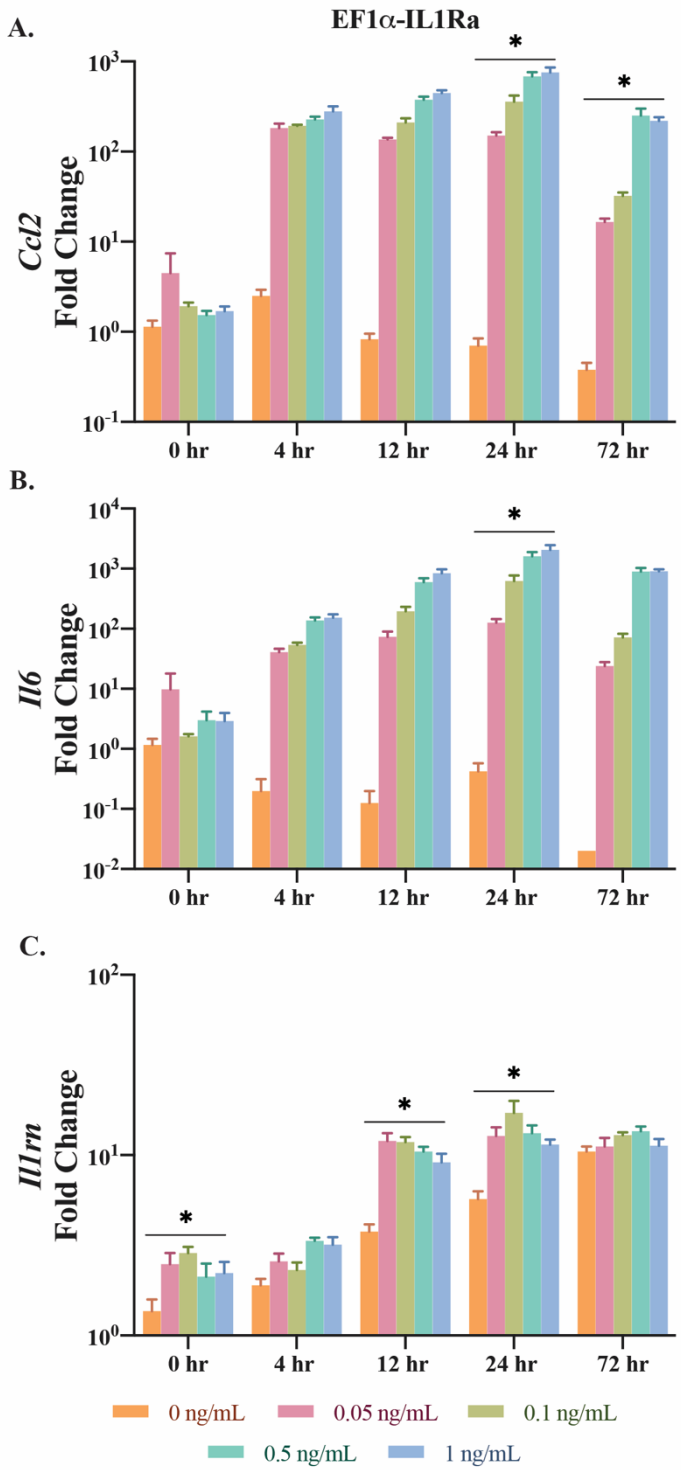

Figure S2.2 Relative gene expression of cells transduced through biomaterial-mediated delivery and challenged with IL-1α for the EF1α-IL1Ra group. Fold changes were determined relative to 0 hour controls. Error bars represent means of fold change ± SEM (n=6). Asterisks represent significant relative to NT control group ($p < 0.05$). (**A**) *Ccl2* gene expression. (**B**) *Il6* gene expression. (**C**) *Il1rn* gene expression.

2.7 Conclusions

We engineered a synthetic transcription system based on NF-κB signaling that can attenuate the effects of the inflammatory cytokine IL-1α in a self-regulating manner. This system responds in a time- and dose-dependent manner to rapidly produce therapeutic levels of IL-1Ra. The use of lentiviral gene therapy allows this system to be utilized through different transduction methods and in different cell types for a variety of applications. Broadly, this approach may be applicable in developing autoregulated biologic systems for tissue engineering and drug delivery in a range of disease applications.

Chapter 3: A Synthetic Mechanogenetic Gene Circuit for Autonomous Drug Delivery in Engineered Tissues

Partially adapted from: Nims, R. J.*, Pferdehirt, L.*, Ho, N. B., Savadipour, A., Lorentz, J., Sohi, A., Kassab, J., Ross, A. K., O'Conor, C. J., Leidtke, W. B., Zhang, B., McNulty, A. L., & Guilak, F. (2021). A synthetic mechanogenetic gene circuit for autonomous drug delivery in engineered tissues. *Science Advances*, 7, eabd9858.

3.1 Abstract

Mechanobiologic signals regulate cellular responses under physiologic and pathologic conditions. Using synthetic biology and tissue engineering, we developed a mechanically responsive bioartificial tissue that responds to mechanical loading to produce a preprogrammed therapeutic biologic drug. By deconstructing the signaling networks induced by activation of the mechanically sensitive ion channel transient receptor potential vanilloid 4 (TRPV4), we created synthetic TRPV4 responsive genetic circuits in chondrocytes. We engineered these cells into living tissues that respond to mechanical loading by producing the anti-inflammatory biologic drug, interleukin-1 receptor antagonist. Chondrocyte TRPV4 is activated by osmotic loading and not by direct cellular deformation, suggesting that tissue loading is transduced into an osmotic signal that activates TRPV4. Either osmotic or mechanical loading of tissues transduced with TRPV4 responsive circuits protected constructs from inflammatory degradation by interleukin-1α. This synthetic mechanobiology approach was used to develop a mechanogenetic system to enable long-term, autonomously regulated drug delivery driven by physiologically relevant loading.

3.2 Introduction

Smart biomaterials or bioartificial tissues that autonomously respond to biologic cues and drive a therapeutic or restorative response are promising technologies for treating both chronic and acute diseases (*124*). Mechanotherapeutics, in particular, are a rapidly growing class of smart biomaterials that use mechanical signals or mechanical changes within diseased tissues to elicit a therapeutic response (*125-127*) and ameliorate the defective cellular mechanical environment (*128-131*). Current mechanotherapeutic technologies rely on exogenous protein drug delivery or ultrasound stimulation, or on synthetic polymer implants that offer a finite lifespan for drug delivery (*132-134*). Creating systems with cellular-scale resolution of mechanical forces that offer long-term, feedback-controlled synthesis of biologic drugs could provide a completely new approach for therapeutic delivery.

In contrast to synthetic polymers, biological tissues grow, adapt, and respond to mechanobiologic signals through the use of specialized molecular components, such as mechanically sensitive ion channels and receptors that transduce specific stimuli from the physical environment (*5, 6*). In particular, mechanosensitive ion channels are sensitive to both context and deformation mode, making them uniquely suited as mechanotherapeutic sensors (*135-137*). The transient receptor potential (TRP) family is a class of selective ion channels including some mechanically sensitive members, such as TRPA1, TRP vanilloid 1 (TRPV1), and TRPV4 (*138, 139*). TRPV4 is activated by osmotic stress and plays an important role in the mechanosensitivity of various tissues such as articular cartilage, uterus, and skin (*7, 9-11, 140*). In cartilage, TRPV4 has been shown to regulate the anabolic biosynthesis of chondrocytes in response to physiologic mechanical strain (*141*).

Osteoarthritis is a chronic joint disease for which there are no available disease modifying drugs, ultimately leading to a total joint replacement once the diseased and degraded cartilage and surrounding joint tissues incapacitate a patient from pain and a loss of joint function (*142*). Cartilage tissue engineering is a promising strategy to resurface damaged and diseased articular cartilage with an engineered cartilage tissue construct as a means to reduce the need for, or prolong the time before, a total joint replacement (*56, 143*). An ongoing challenge in the field, however, is developing engineered cartilage constructs that withstand both the high mechanical loads present within the articular joint and the chronic inflammation present within an osteoarthritic joint (*72, 144*). For example, the knee cartilage of healthy individuals can experience compressive strains of ~5 to 10% during moderate exercise, while individuals with a history of joint injury or high body mass index, populations at risk for developing osteoarthritis, can experience higher magnitudes of cartilage compression under similar loading (*145-147*). In this regard, a bioartificial tissue that can synthesize biologic drugs in response to inflammation or mechanical loading, either independently or concurrently, could greatly enhance the therapeutic potential of an engineered tissue replacement.

In this study, we engineered a mechanically responsive bioartificial tissue construct for therapeutic drug delivery by using the signaling pathways downstream of the mechano/osmosensitive ion channel TRPV4 to drive synthetic mechanogenetic gene circuits (Figure 3.1). To do this, we first establish that mechanical loading of tissue engineered cartilage activates TRPV4 through fluctuations in the local osmotic environment and not direct mechanical deformation of chondrocytes. We next deconstructed the gene regulatory networks (GRNs) and signaling pathways evoked by TRPV4 activation and revealed the transient activation of several mechanosensitive transcription factors. We engineered synthetic gene

circuits to respond to mechanical TRPV4 activation for driving transgene production of an anti-inflammatory molecule, interleukin-1 receptor antagonist (IL-1Ra). While IL-1Ra (drug name anakinra) is approved as a therapy for rheumatoid arthritis and has successfully attenuated osteoarthritis progression in preclinical models, clinical trials of IL-1Ra therapy patients with established osteoarthritis have not shown efficacy, suggesting that controlled long-term delivery may be necessary for disease modification (*38, 41, 42*). Here, we show that mechanical or osmotic loading of implantable engineered cartilage tissue constructs induces an autonomous mechanogenetic response and protects tissue constructs from inflammatory insult, suggesting a modality for long-term *in vivo* drug delivery.

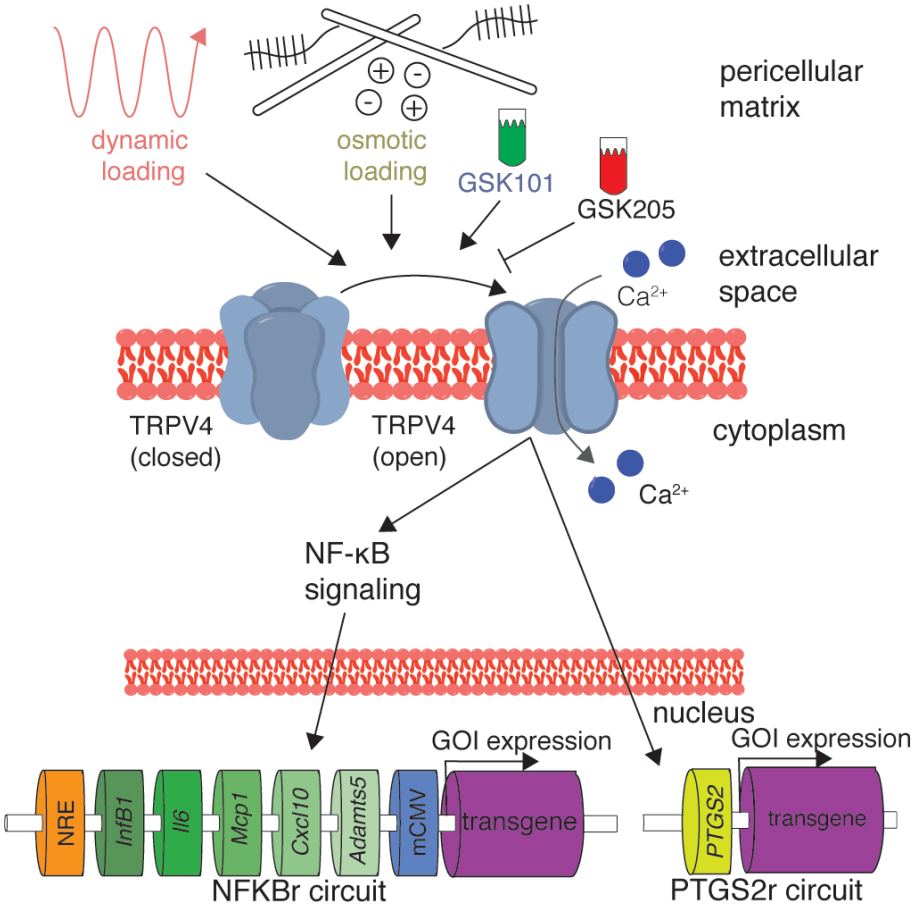

Figure 3.1 Mechanogenetic transduction and therapeutic drug delivery approach. TRPV4 is an osmotically sensitive cation channel in the cell membrane of chondrocytes, which can be activated by mechanical loading secondary to mechano-osmotic coupling through the extracellular matrix or pharmacologically with the agonist GSK101. TRPV4 can also be inhibited with the antagonist GSK205. Upon TRPV4 activation, chondrocytes respond with intracellular calcium signaling that initiates NF-κB signaling and upregulation of the *PTGS2* gene. By lentivirally transducing synthetic mechanogenetic circuits that respond to either NF-κB activation or *PTGS2* upregulation into chondrocytes within an engineered cartilage tissue, mechanically activated TRPV4 signaling was used to drive transgene production of either a luciferase reporter or the therapeutic anti-inflammatory biologic IL-1Ra. GOI, gene of interest.

3.3 Materials and Methods

3.3.1 Tissue harvest, cell isolation, agarose gel casting, and culture

Full-thickness porcine articular chondrocytes were enzymatically isolated using collagenase (Sigma-Aldrich) from the femurs of pigs obtained from a local abattoir (~30 kg; 12

to 16 weeks old) postmortem in accordance with an exemption protocol by the Institutional Animal Care and Use Committee. Filtered cells were mixed 1:1 with 4% molten type VII agarose (Sigma-Aldrich) and the cell-agarose mixture was injected into a gel apparatus and allowed to set at room temperature. Chondrocyte-laden disks were punched out yielding engineered cartilage at a final concentration of 2% agarose and 15 to 20 million cells/mL. All constructs were given 2 to 3 days to equilibrate, and media were changed three times per week during chondrogenic culture using a base medium that consisted of Dulbecco's modified Eagle's medium (DMEM) High Glucose (Gibco) supplemented with 10% fetal bovine serum (FBS) (Atlas), 0.1 mM nonessential amino acids (Gibco), 15 mM Hepes (Gibco), 40 μg/mL proline (Sigma-Aldrich), 1x penicillin/streptomycin, and fungizone (Gibco), and fresh 50 μg/mL ascorbyl-2-phosphate (Sigma-Aldrich) and maintained at 37°C and 5% CO_2 (*12*).

3.3.2 Chondrocyte mechanical and pharmacologic stimulation

Confocal imaging of mechanical compression

A custom mechanical compression device was used to compress agarose constructs while simultaneously performing intracellular calcium imaging on a confocal microscope (Zeiss LSM880) using fluo-4 AM and fura-red AM (ThermoFisher Scientific) based on the manufacturer's protocols. Opposing platens were controlled with stepper motors to apply 60 rounds of compressive loading (10%) after a 2% tare strain. Ratiometric calcium imaging (Calcium Ratio = $Intensity_{fluo\text{-}4}/Intensity_{fura\text{-}red}$) was analyzed within each sample with ImageJ for 2.5 min before and for 2.5 min after the mechanical loading.

High-throughput mechanical compression

A custom mechanical compression device was used for sinusoidal compression of 24-individual tissue constructs simultaneously using a closed loop displacement-feedback system (*12*). This system allows for compression at 37º C and 5% CO_2.

Osmotic stimulation

For calcium imaging studies, osmotic loading media were prepared using Hanks' balanced salt solution medium (Gibco). For mechanogenetic tissue culture studies, osmotic loading media were prepared using DMEM supplemented with 1% culture medium supplement containing recombinant human insulin, human transferrin, and sodium selenite (ITS+). These media were titrated to hypoosmotic media by adding distilled water and measured with a freezing-point osmometer (Osmette 2007; Precision Systems). For osmotic stimulation of mechanogenetic samples, standard culture medium (containing 10% FBS) was replaced with iso-osmotic (380 mOsm) ITS+ base medium, containing 1% ITS+ premix (Corning), 0.1 mM nonessential amino acids, 15 mM Hepes, and 1x penicillin/streptomycin, 3 days before osmotic loading to acclimate tissues.

Micropipette aspiration

Detailed methods for micropipette aspiration are described previously (*148*). Briefly, glass micropipettes were drawn to a diameter of ~10 μm and coated with Sigmacote (Sigma-Aldrich) to prevent cell binding to the glass micropipette. The micropipette was brought in contact with a cell, and a tare pressure of 10 Pa was applied for a period of 3 min. Increasing step pressures were then applied in increments of 100 Pa for 3 min each until the cell was fully aspirated. Laser scanning microscopy was used to measure cell deformation (DIC channel) and $[Ca^{2+}]_i$ throughout the experiment. Ratiometric calcium imaging, as described above, was

performed to assess the mechanoresponse of chondrocytes to micropipette aspiration; however, we found that the application of step increases in pressure to the cell surface using a micropipette rarely initiated a Ca^{2+} transient.

Atomic force microscopy

Freshly isolated chondrocytes were plated on glass coverslips and incubated for 2 to 3 days. Before atomic force AFM compression, cells were incubated with 10 μM GSK205 or DMSO (vehicle) and stained with intracellular calcium dye Fura-2 AM (Molecular Probes) according to the manufacturer's protocols. Cells were loaded to 400 nN using an AFM (Asylum Research MFP-3D) with tipless cantilevers (k=6.2 N/m; MikroMasch) while simultaneously recording intracellular calcium levels with an Olympus microscope and cycled with 340- and 380-nm light to produce a ratiometric output (Calcium Ratio = $\text{Intensity}_{\text{Fura-2 @ 380 nm}}$ / $\text{Intensity}_{\text{Fura-2 @ 340 nm}}$) for intracellular calcium levels which were analyzed with ImageJ (*149*).

Pharmacologic TRVP4 modulation

GSK1016790A (GSK101, Millipore-Sigma) was resuspended at final concentrations (1 to 10 nM) and matched with a DMSO (vehicle) control. GSK205 (manufactured at the Duke Small Molecule Synthesis Facility) was used as a TRPV4-specific inhibitor and preincubated with samples before analysis to allow diffusion within three-dimensional tissues and used at a final concentration of 10 μM with appropriate DMSO (vehicle) controls.

FLIPR assay

After digestion and isolation, filtered chondrocytes were plated in a 96-well plate at 10,000 cells per well and left for 24 hours before stimulation on a fluorescent imaging plate reader (FLIPR) by which individual wells were stimulated with either osmotic or GSK101-containing medium. Cellular response in each well was measured via fluo-4 intracellular calcium

dye using the Fluo-4 No-Wash Calcium Assay Kit (Molecular Probes) according to the manufacturer's directions. GSK205 was preincubated and added alongside stimulated and unstimulated chondrocytes to directly assess the TRPV4-dependent response of osmotic and pharmacologic stimulation.

3.3.3 Finite element modeling

Finite element models of cellular deformation were performed using the FEBio (www.febio.org) finite element software package (version 2.6.4). Models were run using a neo-Hookean elastic material for the cell and membrane compartments of the cell (*150*). All model geometries use axisymmetry boundary conditions to reduce the model size. Osmotic loading was assessed using a Donnan osmotic loading material with parameters taken from the van't Hoff relation for chondrocytes under osmotic loading and loading chondrocytes with a -60 mOsm osmotic medium shift. Models for micropipette aspiration were run assuming a cell modulus of 1 kPa and Poisson's ratio of 0.4 while imposing a pressure of -200 Pa to the cell (*148*). Models of single-cell direct deformational loading (AFM) were performed by simulating an elastic sphere being compressed to 13% of its original height. FEBio testing suites were used to validate the shell, contact, and neo-Hookean code features, and the Donnan model was validated against the van't Hoff equation.

3.3.4 Microarray collection and analysis

After a 14-day preculture, engineered cartilage constructs (∅4 mm × 2.25 mm) were stimulated under 10% compressive loading or 1 nM GSK101 for 3 hours/day for 3 days. An unstimulated control (free swelling) was cultured under identical conditions. Immediately after stimulation, constructs were washed and then fed with culture medium. Constructs were snap

frozen in liquid N_2 at 0, 3, 6, 12, 20, 24, and 72 hours after initial stimulation. Total RNA was extracted from the constructs using a pestle homogenizer and the Norgen Biotek RNA/protein purification plus kit. RNA quantity and quality were assessed with NanoDrop (Thermo Fisher Scientific) and the Agilent Bioanalyzer. Total RNA was processed using the Ambion WT expression labeling kit and the Porcine Gene 1.0 ST Array (Affymetrix). The raw signal of arrays was induced into R environment and quantile-normalized by using "affy" and "oligo" package. The significant DEGs were identified and analyzed by using one regression model in R with package "genefilter", "limma", "RUV", "splines", "gplots" and "plotly" at an adjusted p-value cutoff of 0.05. Then, the DEGs were imported into Ingenuity Pathway Analysis (IPA) to perform the pathway enrichment analysis. The DEG heatmap was plotted by using "gplots" in R. The microarray data generated and analyzed are publicly available (GEO Accession: GSE165027).

3.3.5 Mechanogenetic circuit design, development, viral development, and culture

We developed two lentiviral systems consisting of an NF-κB inducible promoter upstream of either IL-1Ra (NFKBr-IL1Ra) or luciferase (NFKBr-Luc). Therefore, upon NF-κB signaling, either IL-1Ra (NFKBr -IL1Ra) or luciferase (NFKBr -Luc) is expressed as a measure of mechanogenetic circuit activation. In addition, we developed two lentiviral systems consisting of a synthetic human *PTGS2* promoter upstream of either IL-1Ra (PTGS2r-IL1Ra) or luciferase (PTGS2r-Luc). Therefore, when *PTGS2* is activated either IL-1Ra or luciferase is expressed.

NFκBr circuit design

A synthetic NF-κB inducible promoter was designed to incorporate multiple NF-κB response elements as previously described (*62*). A synthetic promoter was developed containing

five consensus sequences approximating the NF-κB canonical recognition motif based on genes upregulated through inflammatory challenge: *InfB1, Il6, Mcp1, Adamts5,* and *Cxcl10*. A TATA box derived from the minimal CMV promoter was cloned between the synthetic promoter and downstream target genes, either murine *Il1rn* or firefly luciferase from the pGL3 basic plasmid (Promega), and an NF-κB-negative regulatory element (NRE-5'-AATTCCTCTGA-3') was cloned upstream of the promoter to reduce background signal (*62, 79, 151*).

PTGS2r circuit design

A synthetic human *PTGS2* promoter was obtained from SwitchGear Genomics and cloned into the NFKBr-IL1Ra or NFKBr-Luc lentiviral transfer vectors in place of the NF-κB inducible promoter. The NF-κB inducible promoter was excised using Eco RI and Psp XI restriction enzymes and the *PTGS2* promoter was inserted in its place using the Gibson Assembly method to create the PTGS2r-IL1Ra and PTGS2r-Luc circuits (*82*).

Lentivirus production and chondrocyte transduction

Human embryonic kidney (HEK) 293T cells were co-transfected with second-generation packaging plasmid psPAX2 (No. 12260; Addgene), the envelope plasmid pMD2.G (No. 12259; Addgene), and the expression transfer vector by calcium phosphate precipitation to make vesicular stomatitis virus glycoprotein pseudotyped lentivirus (*85*). The lentivirus was harvested at 24- and 48-hours post-transfection and stored at -80℃ until use. The expression transfer vectors include the NFKBr-IL1Ra, NFKBr-Luc, PTGS2r-IL1Ra, and PTGS2r-Luc plasmids. The functional titer of the virus was determined with quantitative real-time polymerase chain reaction to determine the number of lentiviral DNA copies integrated into the genome of transduced HeLa cells (*85*). For chondrocyte transductions, freshly isolated chondrocytes were plated in monolayer at a density of 62,000 cells/cm^2 and incubated overnight in standard 10% FBS

medium. The following day, virus was thawed on ice and diluted in 10% FBS medium to obtain the desired number of viral particles to achieve a multiplicity of infection of 3 (*62*). Polybrene was added to a concentration of 4 μg/mL to aid in transduction. The conditioned medium of the chondrocytes was aspirated and replaced with the virus-containing medium, and cells were incubated for an additional 24 hours before aspirating the viral medium and replacing with standard 10% FBS medium. Five days later, cells were trypsinized, counted, and cast in agarose as described above to prepare mechanogenetic constructs at 15 million cells/mL in 2% agarose gel. Constructs were cultured as described above until testing. Viral titers measured by qPCR revealed that ~95% of chondrocytes were transduced with this method.

Mechanogenetic circuit testing outcome measures

Assessing mechanogenetic tissue construct activation in IL-1Ra producing constructs was measured with an enzyme linked immunosorbent assay (ELISA) for mouse IL-1Ra (R&D Systems) according to the manufacturer's protocols. Data are reported as the amount of IL-1Ra produced per construct (in nanogram) normalized by the tissue wet weight mass of the construct (in grams). Luciferase-based mechanogenetic protection was assessed using a bioluminescent imaging reader (Cytation5, BioTek) at 37 °C and 5% CO2 and cultured in phenol-red free high-glucose DMEM supplemented with 1% ITS+, 2 mM GlutaMAX, 1 mM sodium pyruvate, 15 mM Hepes, 40 μg/mL proline, 1x-penicillin/streptomycin, and 1 μM luciferin. Before stimulation, samples were imaged under free swelling conditions for ~1 day to get a baseline bioluminescent level (F_o). For mechanical loading studies, constructs were then mechanically loaded or similarly transferred for a free swelling control and then returned to the bioluminescent imaging. For GSK101 pharmacologic studies, the bioluminescent medium (above) was supplemented with GSK101 or DMSO (vehicle control) to the appropriate dose (1 to 10 nM) and

simultaneously imaged for 3 hours, before washing and replacing with standard bioluminescent medium. Pre-stimulation baseline was normalized from post-stimulation bioluminescent readings (F) to yield F/F_o as the outcome measure.

3.3.6 Coculture studies

To assess mechanogenetic anti-inflammatory protection, NFKBr-IL1Ra constructs were cultured with a porcine cartilage explant for 72 hours in the presence of 0 or 0.1 ng/mL porcine IL-1α. Porcine cartilage explants (3 mm diameter) were cored from condyle cartilage and the subchondral bone was removed, leaving a cartilage explant ~1-2 mm thick including the superficial, middle, and deep zones and cultured in iso-osmotic ITS+ medium (380 mOsm, formulation listed above) base medium until experimentation. Mechanical loading was applied daily with hypo-osmotic loading (3 hours/day) (180 mOsm) before returning to the iso-osmotic medium (380 mOsm) containing the explant and IL-1α. Iso-osmotic controls were moved similarly to an iso-osmotic medium (380 mOsm). Control, non anti-inflammatory mechanogenetic tissue constructs, consisted of NFKBr-Luc tissues. Tissue S-GAG content in the engineered tissue construct and medium were assessed with the 1,9-dimethylmethylene blue assay (*90*). Tissue samples were digested with papain overnight (65 °C) to measure tissue S-GAG using the DMB assay. Bulk S-GAG amount was normalized to tissue wet weight. Constructs were fixed in neutral buffered formalin overnight before embedding in paraffin and sectioning to 7 μm. Histological slices were stained with safranin-O to examine S-GAG distribution and abundance.

3.3.7 Statistical analysis

Data were analyzed with one-way analysis of variance (ANOVA) or two-way ANOVA (α=0.05) where appropriate using R software (www.r-project.org). For two-way ANOVAs, individual groups were compared using a Tukey post-hoc analysis when the interaction of factors was also significant. Correlation trends of strain magnitude to IL-1Ra production was analyzed in R using linear model analysis. Temporal bioluminescent data were analyzed using a two-tailed t-test comparison between the groups at each analyzed time point.

3.4 Results

3.4.1 The mechano-osmotic response of chondrocytes to loading is regulated by TRPV4

To deconstruct the mechanotransduction pathways through which chondrocytes perceive mechanical loading, we encapsulated freshly isolated primary porcine chondrocytes within an agarose hydrogel scaffold to engineer cartilage tissue constructs. Constructs were cultured for 3 weeks to allow extracellular matrix deposition before applying compressive loading and simultaneously imaging the intracellular calcium levels of the chondrocytes. This engineered cartilage system allows mechanical signals to be transduced to chondrocytes through de novo synthesized extracellular matrix in a manner similar to in vivo mechanotransduction (*57, 152, 153*). Chondrocytes express an array of mechanically-sensitive ion channels and receptors, including TRPV4, PIEZO1 and PIEZO2, integrins, and primary cilia (*154*), so we investigated the mechanism by which physiologic magnitudes of dynamic mechanical loading are transduced by chondrocytes. Dynamic mechanical loading of engineered cartilage constructs immediately provoked a 108% increase of intracellular calcium response compared with unloaded tissues (Figure 3.2A) (p=0.022). Inhibiting TRPV4 activity using the TRPV4 antagonist GSK205

suppressed calcium signaling ($p=0.03$, GSK205 supplementation reduced signaling by ~47%), implicating TRPV4 as a critical component in transducing compressive loading in chondrocytes.

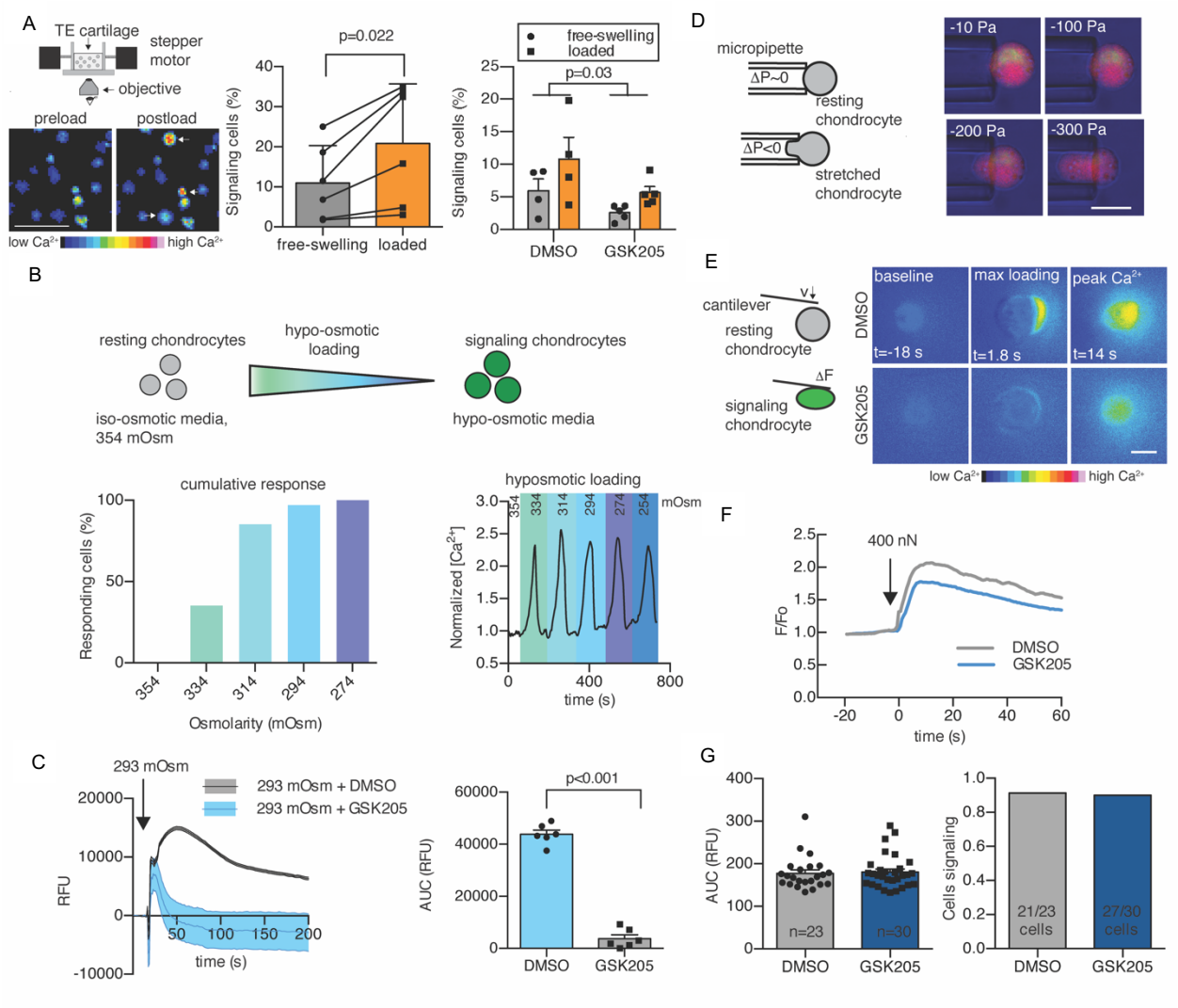

Figure 3.2 Mechanical responsiveness of chondrocytes is mediated by hypo-osmotic stimulation of TRPV4. (**A**) Set up of real-time cellular imaging of mechanical loading. Loading chondrocytes within engineered cartilage increases intracellular calcium compared to free swelling. Arrows indicate immediately responsive cells. Scale bar, 50 µm. The number of cells exhibiting intracellular calcium signaling increased by 108% after loading, and GSK205 suppressed cellular calcium signaling (n=4-5 constructs per treatment). TE, tissue engineered. (**B**) Isolated chondrocytes are sensitive to osmotic perturbations and exhibit intracellular calcium increases in response to hypo-osmotic stimulation (n=15-20 cells per group, calcium response is normalized to calcium levels at 354 mOsm). (**C**) Chondrocyte responsiveness to hypo-osmotic stimulation is inhibited with GSK205 (n=6 per treatment). (**D**) Chondrocytes are not sensitive to direct membrane stretch applied under iso-osmotic, iso-volumetric conditions with micropipette aspiration (n=38, scale bar, 10 µm). RFU, relative fluorescence units. (**E**) Direct cellular compression under a 400 nN load with an AFM induces intracellular calcium signaling. Scale bar, 10 µm. (**F**) GSK205 does not modulate calcium response of chondrocytes to AFM loading. (**G**) TRPV4 inhibition alters neither the intensity of calcium responsiveness nor the population response to AFM compression (n=23-30 cells per group). Data are presented as mean ± SEM.

While the molecular structure of TRPV4 has recently been reported (*155*), the mechanisms underlying TRPV4 activation are complex and may involve direct mechanical activation or osmotic activation secondary to mechanical loading of the charged and hydrated extracellular matrix (*9, 138, 156, 157*). To determine the physical mechanisms responsible for TRPV4 activation secondary to tissue compression, we subjected freshly isolated chondrocytes to osmotic loading, direct membrane stretch, and direct single-cell mechanical compression (Figure 3.2B, 3.2D, 3.2E). To better understand the biophysical mechanisms underlying TRPV4 activation, we determined the mechanical state of the chondrocyte membrane in each of these cases using finite element modeling (FEBio; www.febio.org) (*158*). Chondrocytes rapidly responded to physiologically relevant changes in medium osmolarity through intracellular calcium signals (Figure 3.2B). Calcium signaling was highly sensitive to modest changes in osmolarity, with an osmolarity shift of -20 mOsm inducing intracellular signaling in 35% of chondrocytes and -80 mOsm inducing activation of 100% of chondrocytes. Inhibition of TRPV4 with GSK205 suppressed calcium signaling caused by hypo-osmotic loading (Figure 3.2C) or by the TRPV4 agonist GSK1016790A (GSK101) (Figure S3.1). Chondrocyte volumetric analysis and finite element modeling of hypo-osmotic stress showed that a change of -60 mOsm, sufficient to induce signaling in nearly all chondrocytes, increased cellular volume by 13% and induced an apparent first principle strain of 0.04 homogeneously throughout the membrane (Figure S3.2 and S3.3). To investigate the role of direct membrane stretch in TRPV4 activation in the absence of osmotic fluctuations, we used micropipette aspiration of individual chondrocytes to apply controlled deformation of the cell membrane (Figure 3.2D). Unexpectedly, micropipette aspiration did not provoke any calcium signaling response in chondrocytes, with only 1 of 38 tested cells responding with increased intracellular calcium,

indicating that membrane deformation *per se* was not the primary signal responsible for mechanical activation. Finite element simulations of the micropipette experiment showed the presence of heterogenous apparent membrane strains in aspirated chondrocytes, with a first principle strain reaching 0.31 around the micropipette mouth and ~0.04 within the micropipette under an applied pressure of 100 Pa (Figure S3.3E to S3.3H). To test whether calcium signaling in response to direct mechanical compression of chondrocytes is mediated by TRPV4, we loaded isolated chondrocytes with an atomic force microscope (AFM) to 400 nN (*149*). Only at high, pathologic levels of mechanical compression did direct chondrocyte compression provoke intracellular calcium signaling, but this response was not inhibited by GSK205 (Figure 3.2E to 3.2G). Finite element modeling predicted high membrane strains with an ultimate apparent first principle membrane strain of 2.27 around the cell at the peak cell deformations necessary to elicit intracellular calcium signaling (Figure S3.3I to 3.3L). Together, these findings suggest that activation of TRPV4 in chondrocytes *in situ* may not result directly from cellular strain but rather from osmotic fluctuations induced from the deformation of a chondrocyte's osmotically active environment. Because of the complex relationship between deformational compressive loading of engineered cartilage and osmotic loading, we will hereafter refer to deformational compressive loading (concomitant with the secondary osmotic effects) as mechanical loading and direct changes in the medium osmolarity as osmotic loading.

3.4.2 TRVP4 activation in chondrocytes induces transient anabolic and inflammatory signaling networks

We next sought to understand the time course of specific downstream signaling pathways and GRNs regulated by mechanical activation of TRPV4 using microarray analysis. Because TRPV4 is a multimodal channel, downstream signaling is likely dependent on the activation

mode, as well as cell and tissue type. For these studies, primary porcine chondrocytes were cast in agarose to create engineered cartilage constructs, and subjected to either compressive mechanical loading [10% sinusoidal peak-to-peak strain at 1 Hz for 3 h as described in (*12*)] or pharmacologic stimulation with the TRPV4 agonist GSK101 (1 nM for 3 hours), or left unloaded (free-swelling controls), and measured the transcriptional activity at 0, 3, 12, and 20 hours following an initial round of stimulation and then at 24 and 72 hours after additional daily bouts of mechanical loading or GSK101 (n=3 per condition per time point) (Figure 3.3A). In the first 20 hours following initial stimulation there were 43 transcripts upregulated under both mechanical loading and pharmacologic stimulation (Figure 3.3B) compared to unloaded controls. Up-regulation of these targets was immediate and subsided quickly, with transcript levels returning to baseline 12 to 20 hours after activation. In particular, the adenosine 3',5'-monophosphate (cAMP)/Ca^{2+}-responsive transcription factors *C-JUN*, *FOS*, *NR4A2*, and *EGR2* (Figure 3.3C) were all up-regulated in response to TRPV4-mediated calcium signaling.

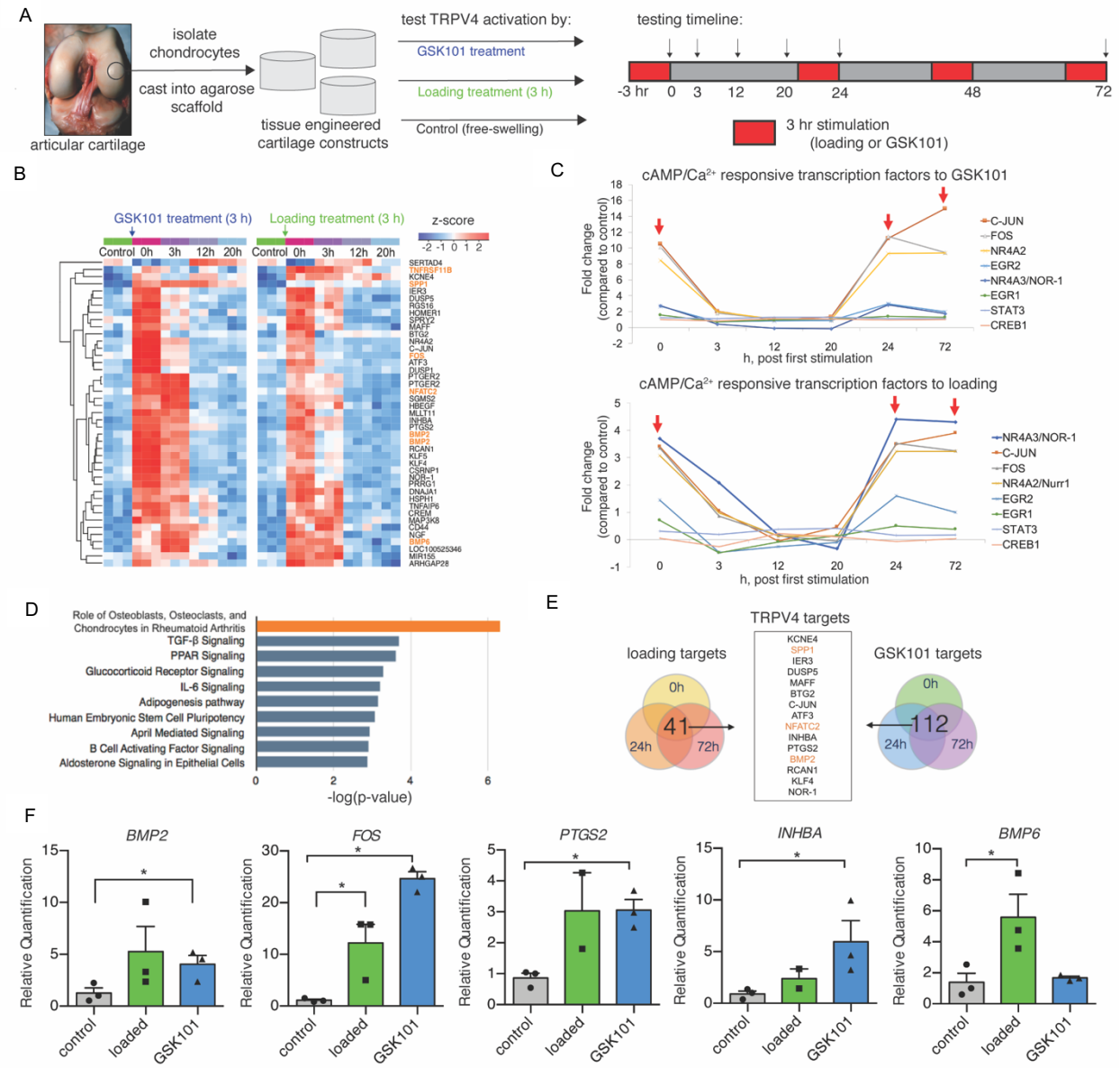

Figure 3.3 Transcriptomic profile induced by TRPV4 activation. (**A**) Engineered cartilage tissue constructs were made from isolated primary porcine chondrocytes cast into agarose hydrogels. Tissue constructs were subjected to deformational mechanical loading or GSK101 pharmacologic stimulation (red, 3 hours/round) following the indicated time course and cartilage construct harvest (arrows). (**B**) 41 genes were differentially upregulated in response to TRPV4 activation and levels returned back to baseline after 12-20 hours post loading (n=3/treatment/timepoint). (**C**) cAMP and calcium-responsive transcription factors were immediately and highly regulated by both mechanical loading and GSK101 stimulation (red arrows indicate loading removal). (**D**) Pathway analysis based on transcription activity suggests that both inflammatory and anabolic pathways are strongly regulated by TRPV4 activation. (**E**) Analysis of gene target response after all bouts of mechanical loading and of GSK101 stimulation produces a list of distinctly TRPV4 sensitive genes. (**F**) TRPV4 responsive targets from the microarray analysis were confirmed by qPCR (n=2-3), and a one-tailed t-test was used to test whether loaded or GSK101 groups were significantly upregulated with treatment.

We then used Ingenuity Pathway Analysis to identify candidate targets for a synthetic gene circuit that would be responsive to TRPV4 activation. The most enhanced pathway was "the role of osteoblasts, osteoclasts, and chondrocytes in rheumatoid arthritis," with members including transcription factors (*FOS* and *NFATC2*), extracellular matrix synthesis gene (*SPP1*), growth factors (*BMP2* and *BMP6*), and *TNFSF11*, the decoy ligand for RANKL, all of which were upregulated by TRPV4 activation (Figure 3.3D). The inflammatory pathways "IL-6 signaling" and "B cell activating factor signaling" were also up-regulated by TRPV4 activation, as were the established chondrocyte anabolic pathways "TGF-β signaling" and "glucocorticoid signaling." Because of the rapid response times of nearly all of the differentially expressed genes (DEGs), we further analyzed which genes responded to repeated bouts of TRPV4 stimulation at all three time points (0, 24, and 72 hours). There were 41 transcripts repeatedly responsive to mechanical loading and 112 transcripts repeatedly responsive to GSK101 supplementation. Of these targets, 15 genes were commonly responsive to both mechanical loading and pharmacologic activation of TRPV4 (Figure 3.3E) and include both pathways associated with inflammation (*PTGS2*, *SPP1,* and *ATF3*) and cartilage development and homeostasis (*BMP2*, *DUSP5*, *NFATC2*, and *INHBA*). The most robustly regulated and cartilage-relevant genes were confirmed by quantitative polymerase chain reaction (qPCR) (Figure 3.3F). Together, these data suggest that the TRPV4 mechanotransduction pathway involves activation of a rapidly resolving inflammatory pathway as part of the broad anabolic response to physiologic mechanical loading.

3.4.3 Synthetic mechanogenetic circuits respond to TRVP4 activation to drive transgene expression

TRPV4 activation in response to mechanical loading upregulates a diverse group of targeted genes. On the basis of the TRPV4-activated signaling pathway (Figure S3.4), we

identified activation of the nuclear factor kappa-light-chain enhancer of activated B cells (NF-κB) pathway and upregulation of the prostaglandin-endoperoxide synthase 2 (*PTGS2*) gene as two distinct avenues to construct TRPV4-responsive synthetic mechanogenetic gene circuits. Targeting the NF-κB signaling pathway and regulation of the *PTGS2* promoter (Figure 3.1), we developed two lentiviral systems that would either (i) respond to NF-κB activity by linking five synthetic NF-κB binding motifs and a NF-κB negative regulatory element (*62*) with the cytomegalovirus (CMV) enhancer to drive transgene expression of either the therapeutic anti-inflammatory biologic IL-1Ra or a luciferase reporter (henceforth referred to as NFKBr-IL1Ra and NFKBr-Luc, respectively) or (ii) respond to *PTGS2* regulation by using a synthetic human *PTGS2* promoter to drive either IL-1Ra or luciferase expression (henceforth referred to as PTGS2r-IL1Ra and PTGS2r-Luc, respectively). We then created mechanogenetically sensitive engineered cartilage tissue constructs by lentivirally transducing primary porcine chondrocytes with a mechanogenetic circuit and seeding these cells into an agarose hydrogel to produce synthetically programmed cartilage constructs (Figure 3.4A).

To test whether mechanogenetic tissues actively respond to mechanical stimulation for transgene production, we first applied compressive mechanical loading to NFKBr-IL1Ra transduced mechanogenetic cartilage constructs, which showed a 38% increase in IL-1Ra production ($p=0.006$) with mechanical loading (Figure 3.4B) compared to free swelling controls. To establish whether this response was dependent on TRPV4, we antagonized TRPV4 with GSK205 and observed a significant attenuation of NFKBr-IL1Ra circuit activity (Figure 3.4B), demonstrating that the mechanogenetic circuit responded to both mechanical loading ($p<0.001$) and TRPV4 antagonism ($p<0.001$). GSK205 also reduced circuit activation in unloaded tissues, suggesting TRPV4 activation in chondrocytes may not be entirely dependent on mechanical

loading. To further assess the specificity of TRPV4 regulation in mechanogenetic cartilage constructs, we applied direct hypo-osmotic loading and pharmacologic GSK101 stimulation to NFKBr-IL1Ra tissues. A step change to hypo-osmotic medium (-200 mOsm change) activated the NFKBr-IL1Ra mechanogenetic circuit (Figure 3.4C) ($p=0.019$) compared with an iso-osmotic medium change (0 mOsm change). In addition, daily pharmacologic activation of TRPV4 with 1 nM GSK101 for 3 hours/day over the course of 5 days activated the NFKBr-IL1Ra circuit compared to dimethyl sulfoxide (DMSO) controls (Figure 3.4D) ($p<0.001$). Engineered cartilage constructs responded repeatedly and reproducibly to the daily GSK101 stimulation (Figure S3.5), demonstrating the role of TRPV4 in activating the mechanogenetic NFKBr circuits and confirming that a cell-based mechanotherapy can offer prolonged and unabating biologic drug delivery. Testing of conditioned medium from constructs seeded with either non-transduced chondrocytes or chondrocytes transduced with a green fluorescent protein (GFP) expression cassette found that only cells transduced with a mechanogenetic IL-1Ra producing circuits were capable of synthesizing detectable levels of IL-1Ra.

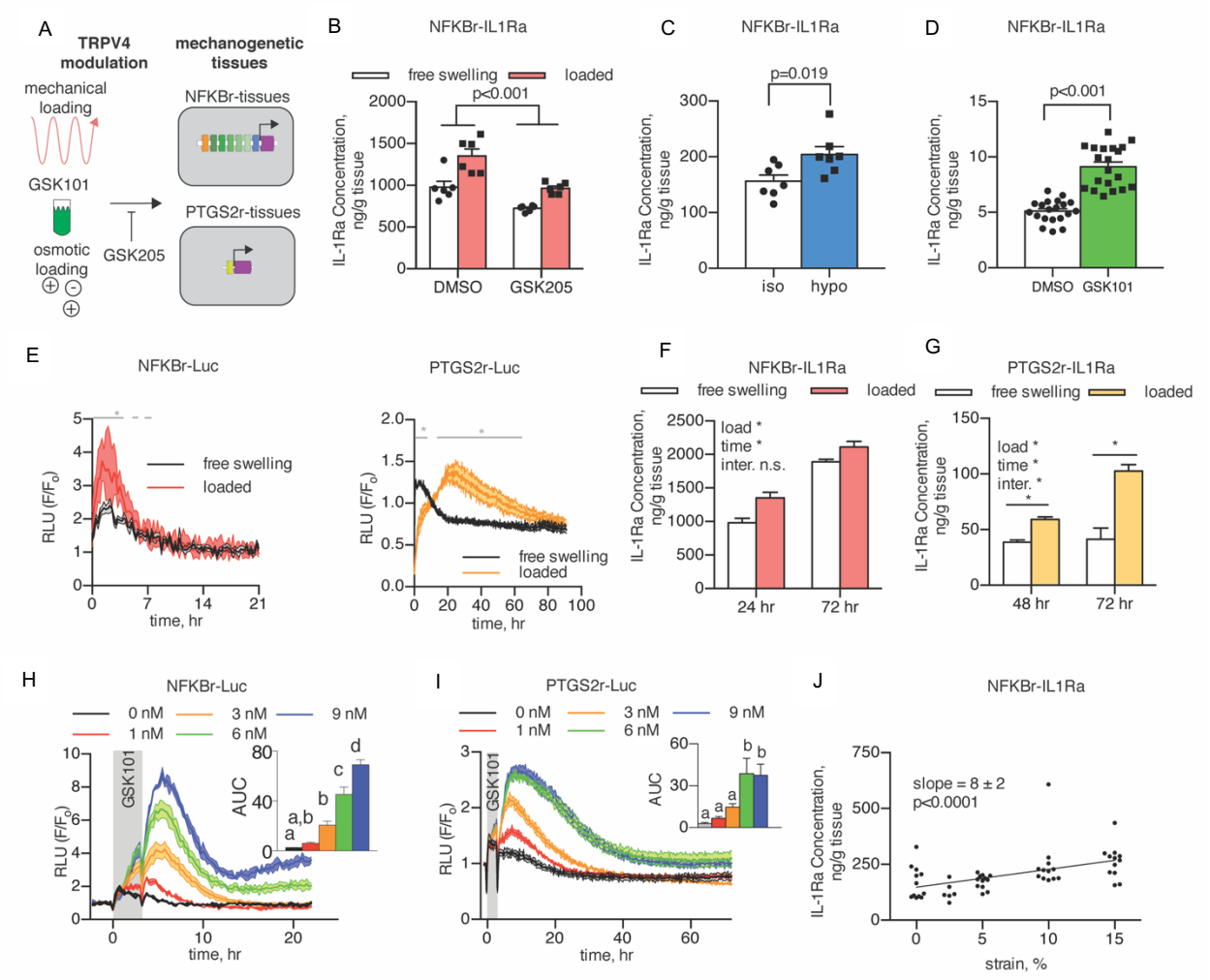

Figure 3.4 Mechanogenetic constructs respond to TRPV4 activation. (**A**) Mechanical loading, osmotic loading, or GSK101 stimulation was applied to mechanogenetic tissues; GSK205 inhibit TRPV4 activation. (**B**) NFKBr-IL1Ra tissues respond to mechanical loading through increased IL-1Ra ($p<0.001$). IL-1Ra is reduced with GSK205 supplementation ($p<0.001$, n=6 per treatment). (**C**) Exposure of NFKBr-IL1Ra to hypo-osmotic medium produces more IL-1Ra than iso-osmotic medium exposure ($p=0.019$, n=7 per group). (**D**) NFKBr-IL1Ra tissues exposed to GSK101 stimulation produce more IL-1Ra than vehicle controls ($p<0.001$, n=20 per group). (**E**) Mechanical loading of NFKBr-Luc tissues quickly activates and inactivates circuits, while PTGS2r-Luc tissues take longer to reach the peak and return to baseline (gray line denotes $p<0.05$ between free-swelling and load, n=3-6 per group). (**F**) NFKBr-IL1Ra tissue response to loading after 24 and 72 hours, indicating differential expression in first 24 hours. (**G**) PTGS2r-IL1Ra tissues respond to loading through 72 hours. (**H**) NFKBr-Luc tissues respond dose-dependently to TRPV4 activation via GSK101 through 9 nM GSK101 ($p<0.05$, n=2-4 per group). (**I**) PTGS2r-Luc tissues are sensitive to GSK101 up to 6 nM ($p<0.05$, n=2-4 per group). (**J**) NFKBr-IL1Ra tissue response is dose-dependent to compressive mechanical loading strain from 0 to 15 % ($p<0.001$, n=5-12). Data are presented as mean ± SEM.

To determine the sensitivity and temporal response kinetics of our engineered tissue system, factors critical for the effectiveness of any drug delivery system, we used bioluminescence imaging of NFKBr-Luc or PTGS2r-Luc constructs to determine the dynamic response of mechanogenetic cartilage constructs to TRPV4 activation by mechanical loading or GSK101 pharmacologic stimulation. In response to 10% compressive mechanical loading (Figure 3.4E), NFKBr-Luc tissue constructs rapidly peaked (1.8 ± 0.2 hours to peak) and decayed ($T_{50\%}$ decay time = 3.4 ± 0.4 hours) with loaded samples returning to baseline 4 hours after loading. PTGS2r-Luc tissue constructs were slower to activate (21.7 ± 2.7 hours to peak) and remained activated for a longer duration ($T_{50\%}$ decay time = 22.3 ± 1.7 hours). This differential in time delivery kinetics may provide strategies by which mechanical loading inputs can drive both short- and long-term drug production by judicious mechanogenetic circuit selection in a single therapeutic tissue construct. To test whether IL-1Ra production followed similar differential production rates, we mechanically loaded NFKBr-IL1Ra and PTGS2r-IL1Ra tissue constructs and measured protein levels of IL-1Ra released in the medium. One round of mechanical loading activated NFKBr-IL1Ra tissues by 24 hours, as measured by an increase in IL-1Ra produced by loaded tissue constructs compared to unloaded constructs (an increase in IL-1Ra production of 372 ± 265 ng/g, mean ± 1 SD). This differential in IL-1Ra concentration between loaded and free swelling constructs remained unchanged by 72 hours (loaded tissues produced 220 ± 223 ng/g more than unloaded constructs at this time point), indicating that loaded NFKBr-tissues were not continually activated and resumed baseline activity levels after 24 hours (Figure 3.4F). Conversely, in a preliminary experiment, a single round of mechanical loading did not differentially activate PTGS2r-IL1Ra in the 24 hours after loading (Figure S3.6). Informed by the bioluminescent imaging, we measured conditioned medium of PTGS2r-IL1Ra

tissues 48 and 72 hours after a single round of mechanical loading, however, and found that tissues produced more IL-1Ra after 48 hours compared to free swelling tissues (difference in means of 21 ng/g) and that the IL-1Ra difference between loaded and free swelling tissues continued to increase by 72 hours (difference in means of 61 ng/g). This increased effect size confirmed that mechanically loaded PTGS2r tissue constructs remained activated up to 72 hours after loading and demonstrated a longer acting mechanogenetic response in the PTGS2r system (Figure 3.4G). Based on the bioluminescent imaging results, we did not measure IL-1Ra levels past 72 hours. These results show that complex drug delivery strategies can be programmed into a single mechanogenetic tissue constructs to produce multiple modes and timescales of therapeutic or regenerative biologic drug delivery.

For insight into the dose-response relationship and sensitivity of the mechanogenetic gene circuits, we imaged NFKBr-Luc and PTGS2r-Luc bioluminescence in response to different doses of GSK101. Temporal imaging revealed that GSK101 stimulation produced similar rise and decay kinetics as TRPV4 activation from mechanical loading (Figure 3.4E) in NFKBr-Luc (Figure 3.4H) and PTGS2r-Luc (Figure 3.4I) cartilage tissue constructs compared to unstimulated controls. Both mechanogenetic tissue constructs displayed a clear dose-dependent activation from GSK101 stimulation as demonstrated by the area under the curve (AUC). NFKBr-Luc tissue constructs were responsive from 1 to 9 nM GSK101, whereas PTGSr-Luc tissue constructs plateaued in response at 6 nM GSK101. On the basis of this pharmacologic sensitivity, we hypothesized that mechanogenetic constructs would be increasingly activated by higher mechanical loading strains through increased osmotic stimulation (Figure 3.2B). As NFKBr-Luc tissues demonstrated the most pronounced GSK101 dose-dependent response, we applied dynamic compressive strain amplitudes from 0 to 15% to NFKBr-IL1Ra tissue

constructs to span the range of physiologic strains expected for articular cartilage *in vivo* (*159*). We measured elevated production of IL-1Ra with increasing compressive strains (Figure 3.4J) (slope = 8 ± 2 ng/g IL-1Ra per %strain, $p<0.001$), demonstrating that drug production is directly responsive to the magnitude of mechanical loading in our mechanogenetic engineered tissues.

3.4.4 Mechanogenetic engineered cartilage activation protects cartilage tissues from IL-1α-induced inflammation-driven degradation

The long-term success of engineered cartilage implants depends on the ability of implants to withstand the extreme loading and inflammatory stresses within an injured or osteoarthritic joint (*109*). We hypothesized that TRPV4 activation would activate mechanogenetic tissue constructs to produce therapeutic levels of IL-1Ra and protect engineered cartilage constructs and the surrounding joint from destructive inflammatory cytokines. As our mechanogenetic circuits rely on signaling pathways that overlap with the cellular inflammatory response, we examined the dose-response of IL-1Ra production in response to the inflammatory cytokine IL-1α (Figure 3.5A and 3.5C). NFKBr-IL1Ra mechanogenetic constructs responded to exogenous IL-1α supplementation following a dose-dependent characteristic, consistent with findings of IL-1-induced NF-κB signaling in chondrocytes (Figure 3.5B) (*101*). This dose-dependent response to IL-1α was present up to 10 ng/mL and offered prolonged and robust production of IL-1Ra, promoting the notion that cell-based tissues may offer a more sustained ability to produce therapeutic biomolecules relative to traditional acellular approaches (Figure S3.7). Mechanical loading further enhanced IL-1Ra production in the presence of IL-1α, demonstrating that even in the presence of high levels of inflammation, mechanical loading further potentiates NF-κB signaling (Figure S3.8). Mechanogenetic PTGS2r-IL1Ra and PTGS2r-Luc constructs demonstrated no sensitivity to IL-1α (Figure 3.5D and 3.5E). In contrast to NFKBr tissue

constructs, the selective sensitivity to TRPV4 activation and not to IL-1α in PTGS2r tissue constructs suggests that this system is distinctively sensitive to mechano- or osmo-activation of TRPV4. This distinction was further demonstrated in tissues exposed to both IL-1α inflammation and osmotic loading, wherein only loading played a significant influence (Figure S3.9) (p=0.0002 for loading and p=0.14 for inflammation).

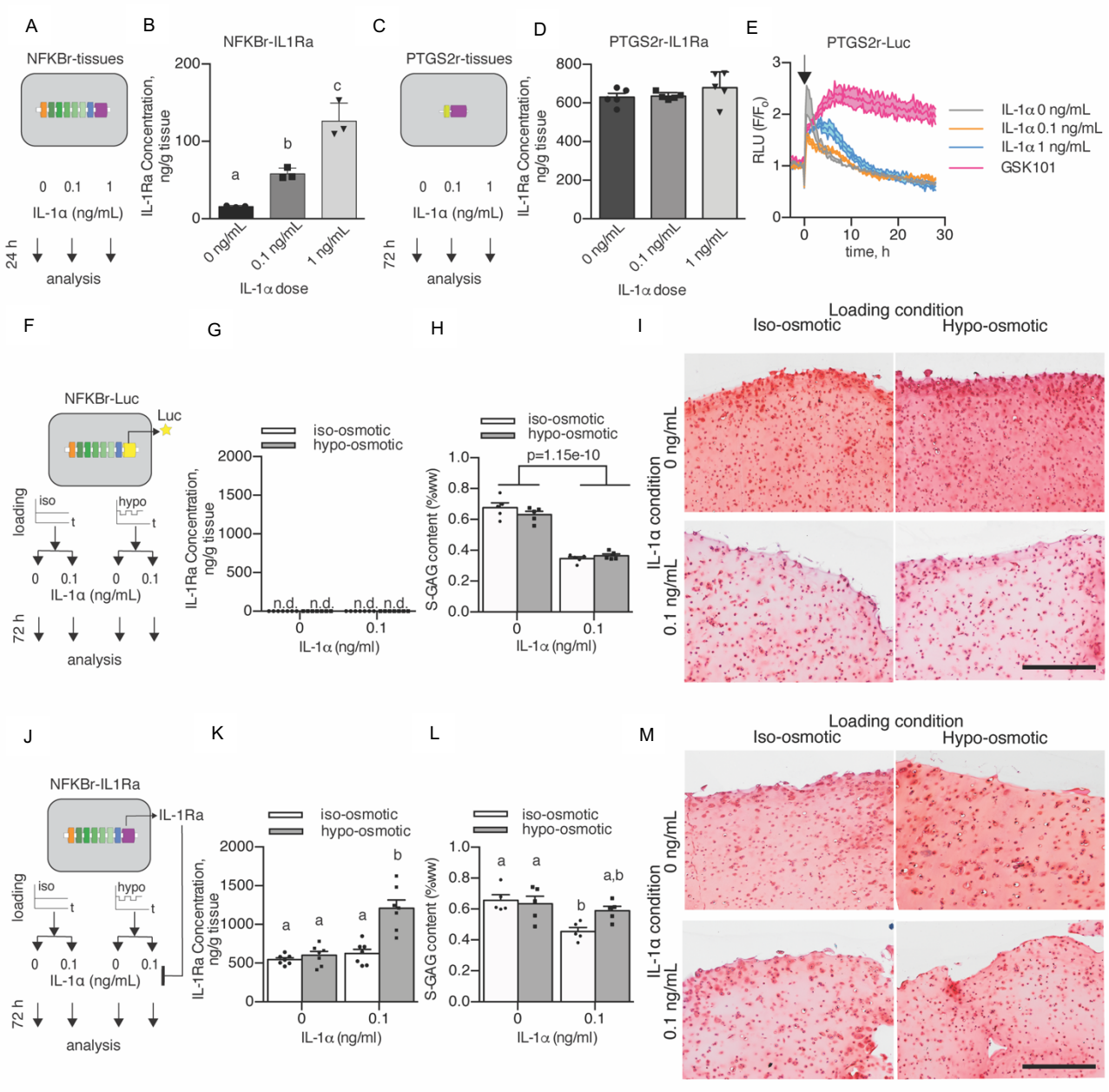

Figure 3.5 Activation of TRVP4 via osmotic loading of mechanogenetic constructs protects against IL-1α. (**A**) Inflammatory response of NFKBr-IL1Ra constructs under IL-1α supplementation. (**B**) NFKBr-IL1Ra tissues produce IL-1Ra in response to IL-1α (n=3, $p<0.001$). (**C**) Inflammatory response of PTGS2r-IL1Ra tissues under IL-1α supplementation. (**D**) PTGS2r-IL1Ra tissues do not respond to IL-1α (n=5). (**E**) PTGS2r-Luc tissues that are not altered by IL-1α are modulated by chronic GSK101 (n=2 per condition, arrow indicates stimulation). (**F**) Osmo-inflammatory response of NFKBr-Luc tissues using osmotic loading (3 hours/day) and IL-1α (0 or 0.1 ng/mL) applied to NFKBr-Luc tissues. (**G**) NFKBr-Luc tissues do not produce IL-1Ra (n=7). n.d., no difference. (**H**) NFKBr-Luc tissues lost S-GAG in the presence of IL-1α (n=5 per group). (**I**) Histological reduction of safranin-O staining with IL-1α supplementation. (**J**) Osmo-inflammatory response of NFKBr-IL1Ra tissues using osmotic loading (3 hours/day) and IL-1α (0 or 0.1 ng/mL). (**K**) IL-1Ra was increased with inflammation and osmotic loading (n=7, $p<0.001$). (**L**) S-GAG content in NFKBr-IL1Ra tissues with IL-1α supplementation (0 or 0.1 ng/mL) and/or osmotic loading (different letters denote significant differences, $p<0.05$, n=5). (**M**) NFKBr-IL1Ra tissues displayed similar safranin-O staining without IL-1α supplementation, while IL-1α supplementation reduced safranin-O staining in iso-osmotic tissues but not hypo-osmotic tissues. Data are presented as mean ± SEM.

To test whether TRPV4 activation induced IL-1Ra production would protect engineered mechanogenetic tissue constructs against IL-1α, we cocultured mature, 21-day-old NFKBr tissue constructs with articular cartilage explants in the presence of IL-1α inflammation and daily hypo-osmotic loading (incubation in 180 mOsm medium for 3 hours/day; standard iso-osmotic medium was maintained 380 mOsm) to model the inflammation and osmotic conditions present in the cartilage of arthritic joints exposed to daily loading (Figure 3.5F and 3.5J). Using NFKBr-Luc tissue constructs, which lack an anti-inflammatory response to TRPV4 or IL-1α activation (Figure 3.5G), to simulate how conventional engineered cartilage constructs would respond in an arthritic joint, constructs lost 45.6% of their sulfated glycosaminoglycan (S-GAG) content after 72 hours of IL-1α treatment (Figure 3.5H). S-GAGs are essential structural molecules that impart mechanical integrity and strength in both engineered and native cartilage (*160, 161*). Osmotic loading did not modulate this response and the substantial S-GAG loss was observable histologically through diminished safranin-O staining throughout the tissue (Figure 3.5I). In the

anti-inflammatory NFKBr-IL1Ra tissue constructs, osmotic loading in the presence of inflammatory IL-1α increased IL-1Ra production by 93% over iso-osmotic control tissues also cultured with IL-1α (Figure 3.5K). After 72 hours of treatment, IL-1α induced a 30.8% loss of S-GAG in NFKBr-IL1Ra engineered cartilage constructs under iso-osmotic conditions, while NFKBr-IL1Ra engineered cartilage that was incubated with IL-1α and osmotically loaded did not significantly lose their S-GAG content (Figure 3.5L). Histologically, hypo-osmotic loading NFKBr-IL1Ra engineered cartilage constructs maintained rich safranin-O staining of S-GAG throughout the constructs, even in the presence of IL-1α (Figure 3.5M). Explant proteoglycan levels were similar across all IL-1α treatment groups. Together, these data demonstrate engineered mechanogenetic cartilage constructs that can produce anti-inflammatory IL-1Ra in response to osmotic loading at levels sufficient for engineered tissue protection in a proinflammatory environment mimicking the conditions present in an osteoarthritic joint (*162*).

3.5 Discussion

By combining synthetic biology and tissue engineering, we developed a novel class of bioartificial material that is mechanogenetically sensitive. This system functions by redirecting endogenous mechanically sensitive ion channels to drive synthetic genetic circuits for converting mechanical inputs into programmed expression of a therapeutic transgene. By engineering these cells into a functional tissue construct, this system provides the potential to repair or resurface damaged cartilage, while providing site-specific, mechanically induced anti-cytokine therapy against inflammation. Our approach is based on redirection of the downstream response to activation of the TRPV4 ion channel – a critical mechanosensor in cartilage – to transduce tissue-scale deformational mechanical loading via mechano-osmotic coupling in the charged

extracellular matrix. By deconstructing the GRNs activated by mechanically induced TRPV4, we coopted chondrocyte-endogenous signaling machinery to drive synthetic circuits for the production of therapeutic biologic drugs, using the anti-inflammatory drug IL-1Ra as a model system for proof of concept. Our results also demonstrate the use of distinct signaling networks for defining the specificity, timing, and dose-response for the expression of therapeutic biologic drugs. We show that a single round of mechanical loading can induce short-term and long-term responses based on the particular response of the synthetic circuit. While we targeted a treatment for cartilage repair and osteoarthritis, pathologic mechanical loading and mechanosignaling play a role in a broad range of acute and chronic diseases (*5*), suggesting a wide range of potential therapeutic applications for mechanogenetically regulated cells or tissues requiring autonomous cellular control systems.

While we developed mechanogenetic cartilage tissues based on TRPV4 activation here, the use of other native, mechanically sensitive ion channels and receptors provide an attractive source of mechanosensors that can be elicited to provoke synthetic outputs. Expanding mechanogenetic approaches to additional mechanosensors with applications to other tissues would increase the range of physical stimuli that synthetic circuits can respond to but requires an in-depth understanding of both the mechanical contexts necessary for mechanosensor activation and the resulting downstream signaling pathways. The fact that primary chondrocytes have an array of different mechanically sensitive ion channels and receptors highlights the potential opportunities to layer mechanosensor specific circuits and produce systems responsive to different mechanical inputs that drive specific synthetic outputs. Our analysis here demonstrates that physiologic (~10%, 1 Hz) mechanical loading of engineered cartilage is converted to a mechano-osmotic signal that activates TRPV4, evidenced by the GSK205 inhibition of

chondrocyte calcium signaling in response to mechanical loading or osmotic loading of engineered cartilage but not to direct cellular deformation or membrane deformation. To this end, we examined the mechanoresponsiveness of TRPV4 signaling and developed two genetic circuits that respond to TRPV4 activation. Note that while endogenous *PTGS2* regulation subsided within 24 hours after mechanical loading, our PTGS2r-circuit remained activated up to 72 hours after loading, highlighting the role that endogenous mechanisms of gene regulation may play, which are likely absent in our synthetic circuits. In this regard, the use of alternate chondrocyte mechanosensors remains an attractive area of research. For instance, the lack of a TRPV4-dependent response to high-strain compression via AFM loading is consistent with our earlier finding that high, potentially injurious, cellular strains are transduced via the PIEZO family of ion channels (*149*). The multimodal nature of TRPV4, and the TRP family more generally (*163*), suggests that additional genetic circuits may be developed for alternate activation modes by characterizing the downstream signaling networks that respond to temperature or biochemical activation of the channel (*164*). Moreover, engineering novel mechanosensors may open the opportunity for developing custom mechanical activation modes and orthogonal downstream signaling in future mechanogenetic systems.

Our findings offer a detailed perspective of the complex cellular events initiated by TRPV4 activation in chondrocytes. TRPV4 has been thought to play a largely anabolic role in chondrocytes through enhanced synthesis of matrix molecules, S-GAG and collagen, and upregulation of transforming growth factor-β (TGF-β3) (*141*), which is evident in our Gene Ontology (GO)/Kyoto Encyclopedia of Genes and Genomes (KEGG) pathway hits of "TGF-β signaling" and "glucocorticoid receptor signaling." However, our findings also revealed the presence of an acute, transiently resolving inflammatory response (pathways including

"chondrocytes in RA," "IL-6 signaling," "April mediated signaling," and "B cell activating factor signaling"). These findings are particularly striking, as the physiologic levels of mechanical loading applied here (10% compressive strain) are typically associated with promoting chondrocyte anabolism (*141*), although our data are consistent with other reports suggesting a proinflammatory role of TRPV4 (*10, 165, 166*). Together, the rapidly resolving mechanical load induced inflammation in this context may be part of a natural cascade by which a quickly decaying inflammatory response is characteristic of the regenerative, anabolic response to mechanical loading (*167, 168*). In addition, increasing evidence suggests a potential role for TRPV4 in mediating cellular and tissue inflammation, and studies of chondrocyte-specific TRPV4 knockout mice report decreased severity of age-associated osteoarthritis (*165*). A load-induced mechanism of chondrocyte inflammation through TRPV4 may provide a target for osteoarthritis and other age-related diseases (*10, 166, 169*). The synthetic gene circuits developed in this study highlight the opportunities to target different responses through downstream pathway selection, namely, using an NFKBr circuit that is sensitive to IL-1α inflammation and a PTGS2r circuit that is IL-1α insensitive. To this end, the pathologic conditions present in osteoarthritis generate a milieu of inflammatory agents and factors that may, in addition to TRPV4 activation, induce NF-κB signaling and *PTGS2* regulation. Deep RNA-sequencing and promotor engineering may provide a unique strategy for developing distinct, mechano-responsive tools in an inflammatory, osteoarthritic joint. Additional therapeutic targets can also be readily inhibited or activated as well; our laboratory has investigated using intracellular inhibitors of NF-κB signaling and the soluble tumor necrosis factor receptor 1 as two alternative options for inhibiting inflammation (*59, 60*).

It is important to note some potential limitations, and future directions of this work. The microarray analysis offers us a first-ever look at the unique transcriptomic landscape induced by TRPV4 activation. To this end, while we used a positive strategy for the groups, i.e., comparing mechanical loading to GSK101 TRPV4 activation, using a negative strategy, i.e., comparing the mechanical loading response to mechanical loading in the presence of GSK205, may offer alternative transcriptomic targets that are TRPV4 regulated. Similarly, with the advent of next-generation sequencing technologies, performing a transcriptomic analysis of the targets of TRPV4 activation would likely increase target resolution, allowing more precise analysis of GRNs induced by TRPV4 activation. Subsequent GRN analysis would permit identification and discrimination between uniquely mechanically responsive and uniquely inflammation responsive networks to enable our long-term goals toward identifying precise genetic regulatory events driven by TRPV4 activation. Next-generation sequencing technologies may also reveal more robust negatively regulated transcript targets of mechanical loading. Our data here only uncovered several TRPV4 repressed targets, including collagen type VIII $\alpha 1$, suggesting that more refined transcript resolution may be necessary to detect additional targets.

Using an engineered, living tissue construct for coordinated drug delivery obviates many of the traditional limitations of "smart" materials, such as long-term integration, rapid dynamic responses, and extended drug delivery without the need for replacement or reimplantation of the drug delivery system. The modular approach of using cells as both the mechanosensors and the effectors within engineered tissues allows for regulation and sensitivity at the mechanically sensitive channel or receptor level, the signal network level, and the gene circuit level. While we used the primary chondrocyte's endogenous TRPV4 to drive our synthetic system, engineering novel mechanically sensitive proteins may beckon a new frontier for coordinating inputs or

driving receptor activation from novel and precise mechanical inputs. Together, this framework for developing mechanically responsive engineered tissues is a novel approach for establishing new autonomous therapeutics and drug delivery systems for mechanotherapeutics.

3.6 Supplemental Figures

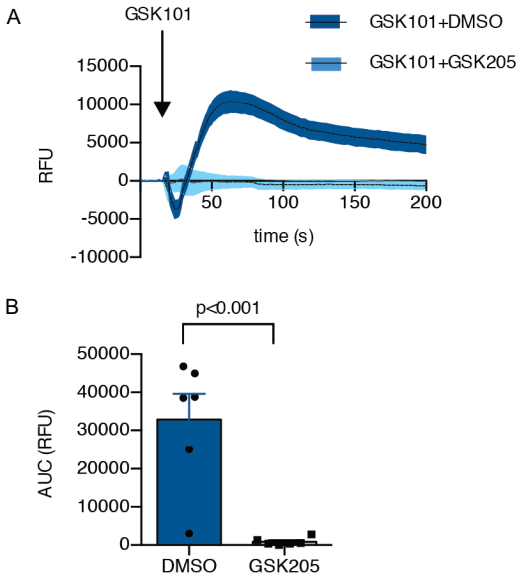

Figure S3.1 The TRPV4 agonist GSK101 stimulated intracellular calcium signaling immediately after addition (top) and this signaling was potently abolished by the antagonist GSK205. (**A**) Calcium signaling temporal dynamics of GSK101 activation. (**B**) Cumulative area-under-curve (AUC) of the temporal data ($p<0.001$, $n=6$). RFU, relative fluorescence units.

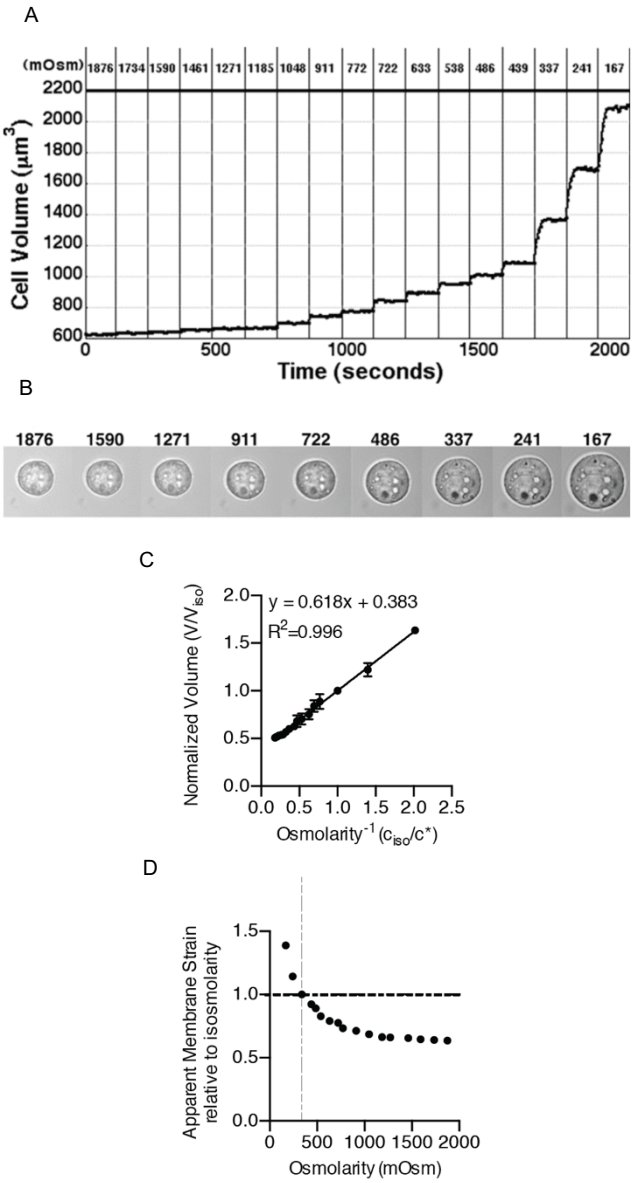

Figure S3.2 (**A**) Chondrocytes respond mechanically to changes in external osmolarity through a wide range of osmolarities as measured by cell volume. (**B**) DIC images from isolated chondrocytes undergoing osmotic loading. (**C**) Chondrocytes behave as ideal osmometers to changes osmolarity as displayed on a Ponders plot which plots the normalized inverse osmolarity to the normalized cell volume. The slope of the line (0.618) corresponds to the volume fraction that is osmotically active within the chondrocyte (n=18 cells). (**D**) Figure in (C) converted to demonstrate non-linear influence on apparent membrane strain resulting from osmotic fluctuations.

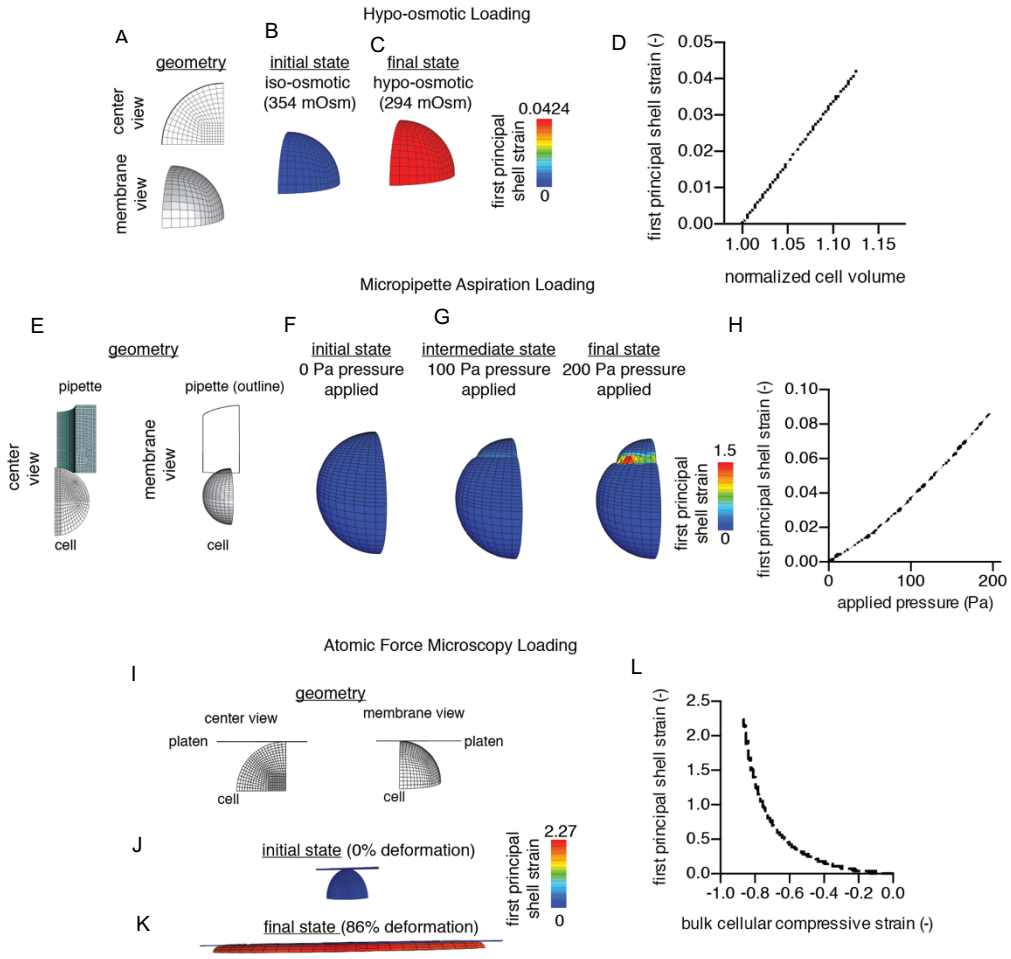

Figure S3.3 Finite element models of cellular loading conditions: hypo-osmotic (**A-D**), micropipette aspiration (**E-H**), and direct AFM loading (**I-L**). Models are run of an octant or quadrant cell by employing appropriate axisymmetry boundary conditions. Simulation figures represent the original geometry (A, E, I, center and membrane views), the pre-strained membrane state (B, F, J), and the deformed states (C, G, K). For osmotic loading, a hypo-osmotic step of -60 mOsm was applied; for micropipette aspiration 100 and 200 Pa pressures were applied; for AFM compression a 86% cell deformation was applied. Scale bar depicts the first principle strain of the cell membrane. Plots (D, H, L) represent the relationship between the applied deformation method and the first principal membrane strain; the micropipette plotted relationship is shown for a membrane element residing within the pipette and the AFM plotted relationship is shown for a membrane element residing along the equatorial (peak) region of membrane strain.

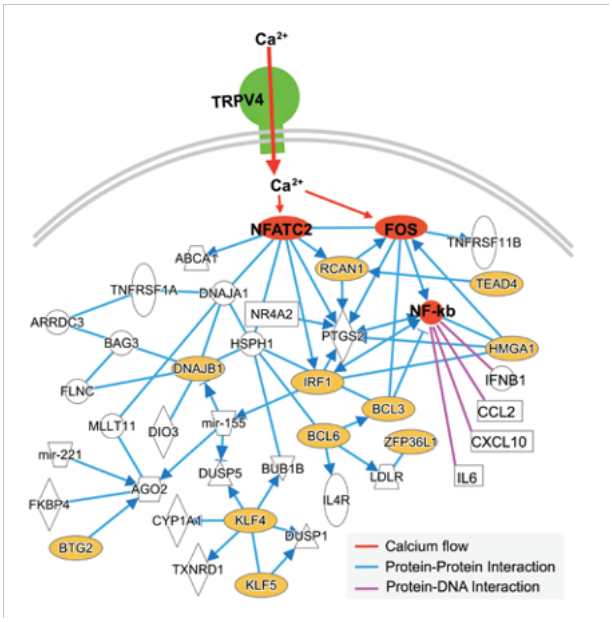

Figure S3.4 Network schematic for intracellular pathways stimulated by TRVP4 activation

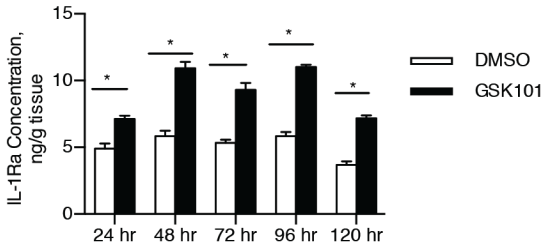

Figure S3.5 Daily IL-1Ra production from NKFBr-IL1Ra mechanogenetic cartilage exposed to either 1 nM GSK101 or vehicle (DMSO) constructs for 3 hour/day every 21 hours. Data are pooled and presented cumulatively in Fig. 4C. n=4 per group/timepoint, * denotes $p<0.05$ between GSK101 and vehicle compared on each day.

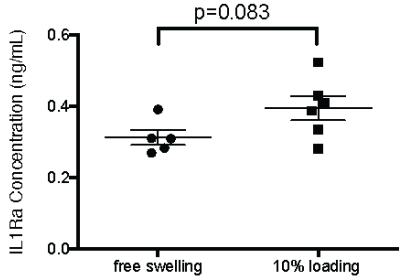

Figure S3.6 Preliminary study of PTGS2r-IL1Ra response to mechanical loading after 24 hours demonstrated no significant changes in IL-1Ra levels prior to 24 hours.

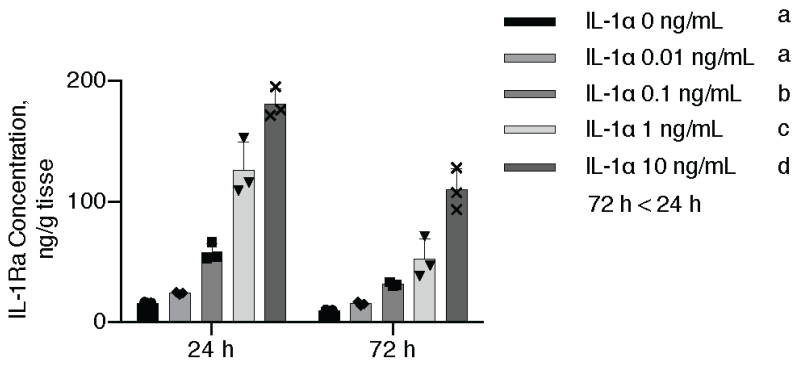

Figure S3.7 NFKBr-IL1Ra engineered cartilage responds in a dose-dependent manner to IL-1α robustly for extended durations (24 and 72 hours of exposure). Subset data from 24 hours exposure depicted in Fig. 5A. Different letters depict significant differences in groups.

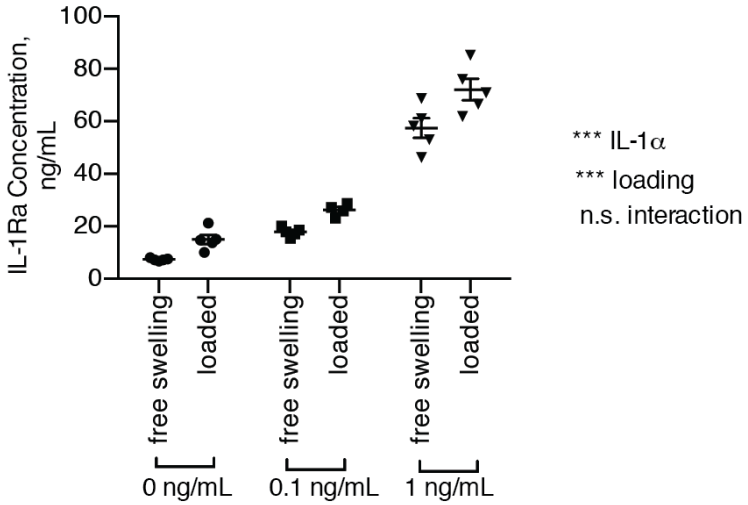

Figure S3.8 NFKBr-IL1Ra mechanogenetic tissues respond to both IL-1α and deformational mechanical loading at 24 hours in a coculture system with graded IL-1α conditions (interaction n.s., $p>0.05$; *** denotes $p<0.05$). n.s., not significant.

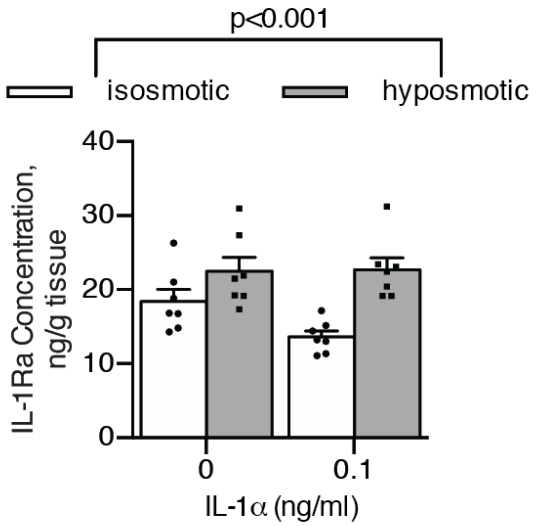

Figure S3.9 Iso-osmotic (control) and hypo-osmotic (loaded) treatments of PTGS2r-IL1Ra constructs in the presence of 0 or 0.1 ng/mL IL-1α in a coculture setting responded only to the loading factor produced a significant difference in IL-1Ra production response ($p<0.001$). Data are presented as mean ± SEM.

3.7 Conclusions

We engineered two mechanogenetic synthetic transcription systems that can sense mechanical loading via TRPV4 activation and produce a biologic drug, IL-1Ra, in response. The first mechanogenetic circuit relies on TRPV4 mediated NF-κB signaling (NFKBr circuit) while the second mechanogenetic circuit is responsive to TRPV4 mediated upregulation of PTGS2 (PTSG2r circuit). Both circuits respond to both compressive mechanical stimuli, osmotic loading, and pharmacologic activation of TRVP4 in a dose-dependent manner and can protect engineered cartilage from IL-1α mediated degradation. The NFKBr circuit showed fast-acting short term drug delivery and was also responsive to IL-1α, while the PTSG2r circuit showed longer term drug delivery kinetics and was solely responsive to mechanical stimuli. This mechanogenetic system is a novel approach for establishing new autonomous biologic drug delivery systems for mechanotherapeutics.

Chapter 4: Synthetic gene circuits for preventing disruption of the circadian clock due to inflammation

Partially adapted from: Pferdehirt, L.*, Damato, A.*, Dudek, M., Meng, Q.J., Herzog, E.D., & Guilak, F. (2021). Synthetic gene circuits for preventing disruption of the circadian clock due to inflammation. *PNAS*, *in submission.*

4.1 Abstract

The circadian clock regulates and maintains tissue homeostasis through temporal control of tissue-specific clock-controlled genes. In articular cartilage, disruptions in the circadian clock are linked to disruptions in anabolic pathways within chondrocytes, leading to a pro-catabolic state and cartilage degradation. In the presence of inflammation, the cartilage circadian clock is disrupted, which can further contribute to the pathogenesis of diseases such as osteoarthritis. Using synthetic biology and tissue engineering, we developed genetically engineered cartilage constructs from murine induced pluripotent stem cells (miPSCs) capable of preserving the circadian clock in the presence of inflammation. We tested the ability of three cellular engineering approaches to preserve circadian pace-making function. We found that circadian rhythms arise following miPSC differentiation into tissue-engineered cartilage. Exposure of tissue-engineered cartilage to inflammatory cytokine interleukin-1 (IL-1) disrupted circadian rhythms and degraded cartilage extracellular matrix (ECM). In contrast, tumor necrosis factor-α (TNFα) did not lead to circadian rhythm disruption or ECM loss. The three cell lines engineered to resist inflammation (CRISPR/Cas9 gene-edited cells lacking a functional IL-1 receptor 1, gene-edited cells programmed to produce IL-1 receptor antagonist (IL-1Ra) in response to

inflammation, and cells transduced using lentivirus expressing a synthetic promoter activated by inflammatory signaling to produce IL-1Ra) all showed similar protection against IL-1 induced ECM degradation and loss of circadian rhythms. These synthetic gene circuits reveal a unique approach to support daily rhythms in cartilage and provide a strategy for creating cell-based therapies to preserve the functional circadian clock.

4.2 Introduction

The circadian clock is an internal genetic timing mechanism that exists in the brain and nearly all cells in peripheral tissues, operating on a roughly 24-hour period (*13-15*). The circadian clock coordinates tissue-specific physiology with different cycles such as light and darkness, body temperature, and rest and activity (*13*). The core clock mechanism, comprised of transcriptional activators *Bmal1* and *Clock* and transcriptional repressors *Per1/2* and *Cry1/2* and output genes, such as *Rev-erbs, Dbp,* and *Nfil3*, forms an auto-regulatory negative feedback loop that drives rhythmic gene expression (*14, 15*). The circadian clock drives expression of many other genes, referred to as clock-controlled genes, that are tissue-specific and play important roles in maintaining tissue homeostasis through their temporal nature (*13, 16, 170, 171*). Disruptions in the circadian clock and subsequent disruptions in expression of these clock-controlled genes have been linked to several diseases such as obesity, diabetes, cardiovascular disease, and osteoarthritis (OA) (*14, 16, 172, 173*).

Clock genes play a critical role in maintaining tissue homeostasis in many different musculoskeletal tissues including muscle, tendon, bone, and articular cartilage (*16, 22*). Articular cartilage consists of an abundant ECM synthetized by the only resident cell type, chondrocytes (*2, 3, 174*). Articular cartilage is avascular and aneural and is maintained through a balance

between anabolic and catabolic activities. Disruption to this balance, for example through increased inflammation, drives the degradation of articular cartilage which is a key characteristic of OA, the leading cause of pain and disability worldwide (*27, 28, 175*). It has been shown that many anabolic and catabolic pathways in articular cartilage have different daily dynamics, driven by a functional circadian clock in chondrocytes, that help maintain cartilage homeostasis (*16, 17, 19-22, 176-179*). Pathways that have different activity at different times include metabolic, ECM remodeling, and catabolic pathways (*16, 21*), and disruptions in the clock cause loss in rhythmic expression and altered expression of these pathways (*21*). For example, the cartilage-specific knockout of one of the core clock genes, *Bmal1,* results in a catabolic response and cartilage degradation in mice (*19*). These findings suggest that the disruption of the circadian clock in cartilage could be an important contributor to the pathogenesis of OA (*34*).

Inflammation is a key driver in the pathogenesis of OA, characterized by increased levels of proinflammatory cytokines interleukin-1 (IL-1) and tumor necrosis factor-α (TNFα), which in turn induce ECM degradation through the enhanced production of degradative enzymes and other pro-inflammatory mediators that shift chondrocyte activity to a pro-catabolic state (*24, 26, 29-31*). Importantly, inflammation has been shown to disrupt circadian rhythms in cartilage (*33*). The addition of IL-1 to cartilage explants caused a loss in circadian rhythms that was only rescued with the administration of dexamethasone (dex), an anti-inflammatory agent (*33*). Anti-cytokine therapies such as IL-1 receptor antagonist (IL-1Ra, anakinra) have shown promise in alleviating symptoms of post-traumatic OA (*36-38*); however, systemically delivered anti-cytokine therapies are administered at high doses, which may have significant off-target effects,

including an increased susceptibility to infection and certain autoimmune diseases (*43*) as well as limited tissue regeneration and repair (*75-77*).

Because of the drawbacks with anti-cytokine therapies and lack of effective disease-modifying treatments to address both the symptoms and structural changes of OA (*45, 47, 74*), we previously used genetic engineering to develop various self-regulating cellular systems to address these limitations (*59*). Using CRISPR/Cas9 gene editing we created murine induced pluripotent stem cells (miPSCs) lacking a functional IL-1 receptor 1 (IL1R1) that can successfully be differentiated into tissue engineered cartilage that is protected from IL-1 induced matrix degradation (IL1R1 KO) (*53*). We also used CRISPR/Cas9 gene editing in miPSCs to incorporate IL-1Ra, a competitive antagonist of IL-1, downstream of the *Ccl2* locus (Ccl2-IL1Ra) to drive controlled production of IL-1Ra in response to inflammation and subsequent activation of *Ccl2* (*60*). These cells were also able protect cartilage from inflammation (*60*). Furthermore, we have also developed a synthetic promoter that is activated by nuclear factor kappa-light-chain-enhancer of activated B cells (NF-κB) to drive production of our desired transgene, IL-1Ra (NFκBr-IL1Ra) (*59*). This lentiviral gene therapy has been shown to inhibit IL-1 in response to inflammation or mechanical loading in miPSC-derived tissue engineered cartilage and also in primary porcine chondrocytes (*59, 63*).

Due to the role of the circadian clock in maintaining cartilage tissue homeostasis shown by disruptions in circadian rhythms leading to altered gene expression (*21*) and cartilage degradation (*19*), and the recent finding that inflammation can drive disruption in the chondrocyte circadian clock, the goal of this study was to develop tissue-engineered cartilage using stem cells that have been genetically engineered to preserve the circadian clock in response to inflammation (Figure 4.1). Therefore, we sought to establish a platform for testing the role of

circadian rhythms in cartilage maintenance and accomplished this by first testing when circadian rhythms arise while differentiating our miPSCs into chondrocytes and then the consequences of inflammatory signals on chondrocyte circadian rhythms and cartilage integrity, before testing the ability of our genetically engineered circuits to preserve circadian rhythms. However, it is important to note that undifferentiated stem or progenitor cells generally do not exhibit circadian rhythms (*180*). Therefore, we first examined the hypothesis that miPSCs do not exhibit a clock but establish circadian rhythms as they progress through chondrogenic differentiation and the development of an engineered cartilage matrix. We next determined the effect of inflammatory cytokines on the circadian clock in our tissue engineered pellets and determined that IL-1α and IL-1β, but not TNFα, drive disruptions in circadian rhythm. We then tested the ability of our genetically engineered cell-based therapies targeting IL-1 to protect the clock from IL-1 induced disruption. We show the ability of our self-regulating synthetic gene circuits to preserve the circadian clock and protect against inflammation-mediated disruption and cartilage degradation. These findings further our understanding of the circadian rhythm synchronization in cartilage and its disruption in response to inflammatory cytokines, and introduce the concept of a "clock-preserving" mechanism through the combination of synthetic biology and tissue engineering of stem cell gene circuits.

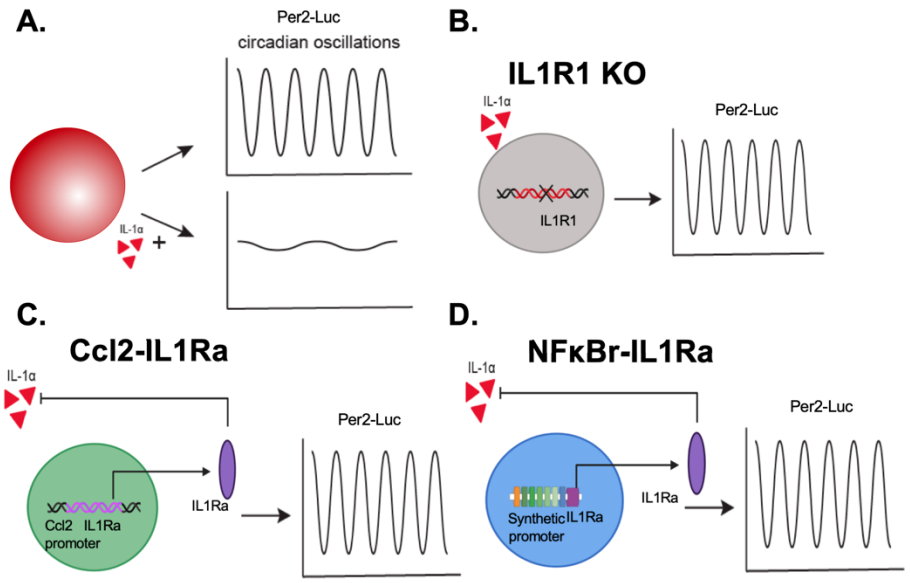

Figure 4.1 Inflammation resistant cell-based therapies and circadian measurements. Tissue engineered cartilage pellets with a circadian reporter (Per2-Luc) were tracked to measure their circadian clock. **(A)** In the presence of IL-1α the circadian clock was disrupted. Three different genetic engineering-based cell therapies were developed to be resistant to IL-1α: **(B)** IL1R1 KO – CRISPR/Cas9 edited cells lacking the IL-1 receptor 1; **(C)** Ccl2-IL1Ra – CRISPR/Cas9 edited cells that produce an IL-1 antagonist, IL-1Ra in response to inflammation and subsequent expression of *Ccl2*; and **(D)** NFκBr-IL1Ra – lentiviral gene therapy circuit with a synthetic promoter activated by NF-κB signaling driving production of IL-1Ra. The ability of these cell therapies to preserve the circadian clock in the presence of inflammation was tested.

4.3 Materials and Methods

4.3.1 Cell culture and differentiation

Murine induced pluripotent stem cells (miPSCs)

Murine induced pluripotent stem cells (miPSCs), derived from tail fibroblasts from adult C57BL/6 mice and validated for pluripotency as described by Diekman et al. (*49, 86*) were cultured in Dulbecco's Modified Eagle's Medium High Glucose (DMEM-HG, Gibco), 20% lot selected fetal bovine serum (FBS, Atlanta Biologicals), 100 nM minimum essential medium nonessential amino acids (NEAA, Gibco), 55 μM 2-mercaptoethanol (2-me, Gibco), 24 ng/mL

gentamicin (Gibco), and 1000 U/mL mouse leukemia inhibitory factor (LIF, Millipore), and maintained on mitomycin C-treated mouse embryonic fibroblasts (Millipore).

miPSCs were differentiated toward a mesenchymal state using a high-density micromass culture (*49*). Differentiation medium contained DMEM-HG, 1% culture medium supplement containing recombinant human insulin, human transferrin, and sodium selenite (ITS+, Corning), 100 nM NEAA, 55 μM 2-me, 24 ng/mL gentamicin, 50 μg/mL L-ascorbic acid, and 40 μg/mL L-proline. On days 3–5, this medium was supplemented with 100 nM dexamethasone and 50 ng/mL bone morphogenetic protein 4 (BMP-4; R&D Systems). After 15 days of culture, the micromasses were dissociated with pronase (Millipore Sigma) and collagenase type II (Worthington Biochemical) and the pre-differentiated iPSCs (PDiPSCs) were plated on gelatin-coated dishes in expansion medium containing DMEM-HG, 10% lot-selected FBS, 1% ITS+, 100 nM NEAA, 55 μM 2-me, 1% penicillin/streptomycin (P/S, Gibco), 50 μg/mL L-ascorbic acid, 40 μg/mL L-proline, and 4 ng/mL of basic fibroblast growth factor (bFGF, R&D Systems). To create a 3D PDiPSC system, passage 2 PDiPSCs were cast in agarose (4% molten type VII agarose, Sigma Aldrich) at a final density of 100 million cells/mL in 1% agarose (*49*).

To create tissue engineered cartilage passage 2 PDiPSCs were pelleted by centrifugation of 250K cells (*49*). Pellets were cultured for 14-21 days in chondrogenic medium consisting of DMEM-HG, 1% ITS+, 100 nM NEAA, 55 μM 2-me, 1% P/S, 50 μg/mL L-ascorbic acid, 40 μg/mL L-proline, 100 nM dexamethasone, and 10 ng/mL TGF-β3 (R&D Systems).

Porcine primary chondrocytes

Full-thickness porcine articular chondrocytes were enzymatically isolated using collagenase II (Worthington Biochemical) from the femurs of pigs obtained from a local abattoir (~30 kg; 12 to 16 weeks old) postmortem in accordance with an exemption protocol by the

Institutional Animal Care and Use Committee. Filtered cells were mixed 1:1 with 4% molten type VII agarose (Sigma-Aldrich) and the cell-agarose mixture was injected into a gel apparatus and allowed to set at room temperature. Chondrocyte-laden disks were punched out yielding engineered cartilage at a final concentration of 2% agarose and 15 to 20 million cells/mL. All constructs were cultured in chondrogenic medium for 2-21 days containing DMEM-HG, 10% FBS (Atlas), 100 nM NEAA, 15 mM HEPES (Gibco), 50 μg/mL L-ascorbic acid, 40 μg/mL L-proline, and 1% P/S (*12*).

4.3.2 Circadian reporter design

Two luciferase reporter lentiviral vectors, one driven by the murine Bmal1 promoter and one driven by the murine Period 2 (Per2) promoter, were used (*181*). These cassettes result in luciferase expression with the circadian promoters Bmal1 (Bmal1-Luc, B1L) or Per2 (Per2-Luc, P2L) are activated.

4.3.3 Development of inflammation resistant and self-regulating iPSCs

Three different cellular engineering approaches were used to test the ability to maintain the circadian clock in response to inflammatory cytokine interleukin-1α (IL-1α): a knockout miPSC line lacking the IL-1 receptor 1 (IL1R1 KO) (*53*), a CRISPR/Cas9 edited miPSC line that incorporates IL-1 receptor antagonist (IL-1Ra) downstream of the *Ccl2* promoter (Ccl2-IL1Ra) (*60*) , and cells transduced with a lentiviral gene therapy that includes a synthetic promoter activated by the nuclear factor kappa-light-chain enhancer of activated B cells (NF-κB) pathway that drives IL-1Ra production (NFκBr-IL1Ra) (*59*). IL1R1 KO, Ccl2-IL1Ra, and NFκBr-IL1Ra transduced PDiPSCs were all transduced with Per2-Luc (P2L) lentivirus and pelleted to grow into tissue engineered cartilage for experimentation.

IL1R1 KO miPSC line

The IL1R1 KO line was created using CRISPR/Cas9 technology to create a homozygous deletion of the IL1R1. These cells do not respond to the presence of IL-1α and have been previously shown to be effective in mitigating inflammation induce degradation of tissue engineered cartilage (*53*).

Ccl2-IL1Ra miPSC line

The Ccl2-IL1Ra line was created using CRISPR/Cas9 technology to insert IL-1Ra downstream of the *Ccl2* promoter creating a heterozygous cell line. *Ccl2* is a common gene upregulated with inflammation in cartilage and therefore the Ccl2-IL1Ra cells effectively sense inflammation and produce an anti-inflammatory therapeutic in an autoregulated manner (*60*).

NFκBr-IL1Ra lentiviral vector

To create the NFκBr-IL1Ra lentiviral vector, a synthetic NF-κB inducible promoter was designed to incorporate multiple NF-κB response elements as previously described (*59*). A synthetic promoter was developed containing five consensus sequences approximating the NF-κB canonical recognition motif based on genes upregulated through inflammatory challenge: *InfB1, Il6, Mcp1, Adamts5,* and *Cxcl10*. A TATA box derived from the minimal CMV promoter was cloned between the synthetic promoter and downstream target gene, murine *Il1rn*, and an NF-κB-negative regulatory element (NRE-5'-AATTCCTCTGA-3') was cloned upstream of the promoter to reduce background signal (*59, 79, 151*). This lentiviral vector has been shown to protect tissue engineered cartilage from inflammation mediated degradation and has been shown to be mechanoresponsive and utilized in porcine tissue engineered cartilage (*59, 63*).

4.3.4 Lentivirus production and cell transduction

Human embryonic kidney (HEK) 293T cell were co-transfected with second-generation packaging plasmid psPAX2 (No. 12260; Addgene), the envelope plasmid pMD2.G (No. 12259; Addgene), and the expression transfer vector (B1L, P2L, or NFκBr-IL1Ra plasmids) by calcium phosphate precipitation to make vesicular stomatitis virus glycoprotein pseudotyped lentivirus (*85*). The lentivirus was harvested at 24- and 48- hours post transfection and stored at -80°C until use. The functional titer of the virus was determined with quantitative real-time polymerase chain to determine the number of lentiviral DNA copies integrated into the genome of transduced HeLa cells (*85*). For all cell transductions, virus was thawed on ice and diluted in medium to obtain the desired number of viral particles to achieve a multiplicity of infection of 3 (*59*). Polybrene was added to a concentration of 4 μg/mL to aid in transduction. The medium of the cells was aspirated and replaced with virus-containing medium, and cells were incubated for 24 hours before aspirating the viral medium.

4.3.5 Circadian clock characterization through bioluminescence recordings and imaging

miPSCs and PDiPSCs were transduced with either Bmal1-Luc (B1L) or Per2-Luc (P2L) virus. PDiPSCs were either cultured in monolayer, cast in agarose, or pelleted. miPSCs, PDiPSCs, PDiPSCs freshly cast in agarose (PDiPSC agarose), and mature pellets (tissue engineered cartilage pellets) were plated in 35 mm petri dishes with 1 mL of recording medium containing D-luciferin (Goldbio), sealed with vacuum grease, and placed in a light-tight36º incubator containing photo-multiplier tubes (PMTs) (Hamamatsu Photonics). Each dish was placed under one PMT and the bioluminescence was recorded as photons per 180 seconds. Bioluminescence data were detrended with a 24h moving average and analyzed in ChronoStar

1.0 (*182*). Recoding medium contained DMEM powder (Sigma), B27 supplement (Invitrogen), P/S, L-glutamine (Invitrogen), HEPES (Sigma), and D-glucose (Invitrogen). Porcine chondrocytes were also transduced with P2L, cast in agarose, cultured, and then subjected to bioluminescence recordings in the dark incubator. As a control, the femoral head from 10 week old PER2::LUC reporter mice (founders generously provided by Dr. Joseph Takahashi, UTSW) (*170*) was obtained and the bioluminescent output from the cartilage explants was also recorded .

4.3.6 Inflammatory challenge and bioluminescence recordings and imaging

After 14 days of chondrogenic culture, pellets transduced with P2L underwent inflammatory challenge with 20 ng/mL TNFα, 1 ng/mL IL-1α, 1 ng/mL IL-1β, or a PBS control. Pellets were placed in recording medium and bioluminescence was recorded for 72 hours. After 72 hours of recording, cytokine or PBS was added to the dish and bioluminescence was recorded for an additional 72 hours. Pellets with a period of bioluminescence 18-32h, mean bioluminescence >30,000 photons, and pre-cytokine amplitude >20,000 photons were included in analysis. Damping ratio was calculated as amplitude two days following treatment divided by amplitude the day prior to treatment. Additional pellets were treated with cytokines or PBS and stored at -80℃ for quantitative reverse transcription polymerase chain reaction (qRT-PCR), -20℃ for biochemical analysis, or fixed in 10% neutral buffered formalin (NBF). As a comparison, Per2::Luc mouse femoral head articular cartilage was dissected from 4-6 week old mice. The cartilage explants were cultured in DMEM/F12 (without phenol red and FBS, with L-glutamine and non-essential amino acids). Explants were synchronized by 1h treatment with 100 nM dexamethasone and their bioluminescence was recorded in Lumicycle as described previously (*19*). 36 hours after synchronization explants underwent inflammatory challenge with 20 ng/mL TNFα, 1 ng/mL IL-1α, 1 ng/mL IL-1β, or a PBS control. After 48 hours of exposure to

cytokines 100 nM dexamethasone was added to the medium and bioluminescence recorded for another 48 hours. Damping of the circadian clock was assessed by measuring of the amplitude of peak before and after treatment. For each explant the peak before treatment was normalized as 100% and the peak after treatment was expressed as % of that value.

IL1R1 KO, Ccl2-IL1Ra, NFκBr-IL1Ra, and P2L control pellets were all subjected to inflammatory challenge with 1 ng/mL IL-1α or a PBS control. Bioluminescence was recorded 72 hours pre addition of cytokine and for 72 hours post addition of cytokine. Additional pellets were treated with cytokines or PBS, media was collected, and pellets were stored at -80℃ for qRT-PCR, -20℃ for biochemical analysis, or fixed in 10% NBF. Additionally, dishes with pellets in recording media were recorded for 72h using an Andor iKon-M electron multiplying charged coupled device (Oxford Instruments) at 20x magnification with 1h exposures and 2x2 binning. During multi-day recordings, samples were maintained at 36º in darkness. Image sequences were concatenated into videos using ImageJ.

4.3.7 Histological and biochemical analysis of pellet cultures

After 72 hours of inflammatory challenge, pellets were washed with PBS and fixed in 10% NBF for 24 hours, paraffin embedded, and sectioned at 8 μm thickness. Slides were stained for Safranin-O/hematoxylin/fast green (*91*).

For biochemical analysis, pellets were digested overnight in 125 μg/mL papain at 65℃. DNA content was measured with PicoGreen assay (Thermo Fisher) and total sulfated glycosaminoglycan (sGAG) content was measured using a 1,9-dimethylmethylene blue assay at 525 nm wavelength (*90*).

4.3.8 Gene expression with quantitative real time polymerase chain reaction

Pellets were homogenized using a miniature beat beater, lysed in Buffer RL, and RNA was isolated following the manufacturer's protocol (total RNA purification; Norgen Biotek). Reverse transcription was performed using Superscript VILO complementary DNA master mix (Invitrogen). qRT-PCR was performed using Fast SyBR Green master mix (Applied Biosystems). Primer pairs were synthesized by Integrated DNA Technologies, Inc: *Ccl2* [forward (F), 5'-GGCTCAGCCAGATGCAGTTAA-3'; reverse (R), 5'-CCTACTCATTGGGATCATCTTGCT-3'], *Il6* [F, 5'-GAGGATACCACTCCCAACAGACC-3'; R, 5'-AAGTGCATCATCGTTGTTCATACA-3'] *r18s* [F, 5'-CGGCTACCACATCCAAGGAA-3'; R, 5'-GGGCCTCGAAAGAGTCCTGT-3']. Data are reported as fold changes and were calculated using the $\Delta\Delta C_T$ method and are shown relative to the P2L PBS control group and ribosomal 18s is used as the reference gene.

4.3.9 Enzyme-linked immunosorbent assays

After 72 hours of inflammatory challenge, culture media was collected from pellets and stored at -20°C. IL-1Ra concentration was measured with DuoSet enzyme-linked immunosorbent assay (ELISA) specific to mouse IL-1Ra/IL-1F3 (R&D Systems).

4.3.10 Statistical Analysis

Statistical analysis was performed using Prism. A one-way ANOVA with Dunnett's post hoc test was used to analyze all biochemistry data for P2L pellets given TNF-α, IL-1α, IL-1β, or PBS with PBS as the control ($\alpha = 0.05$). A one-way ANOVA with Fisher's LSD post hoc test was used to analyze damping ratios for pellets given TNF-α, IL-1α, IL-1β, or PBS with PBS as the control ($\alpha = 0.05$). Additionally, a one-way ANOVA with Dunnet's post hoc test was used to

analyze biochemistry data for IL1R1 KO, Ccl2-IL1Ra, and NFκBr-IL1Ra pellet experiments within each group with 0 ng/mL dose as the control ($\alpha = 0.05$). A two-way ANOVA with Tukey's HSD post hoc test was used to analyze qRT-PCR data for P2L pellets given cytokines and all biochemistry, qRT-PCR, and ELISA data for IL1R1 KO, Ccl2-IL1Ra, and NFκBr-IL1Ra pellet experiments ($\alpha = 0.05$). Statistical analysis for cartilage explants and their response to inflammatory cytokines was performed using student t-test comparing the values of the peak after control or cytokine treatment.

4.4 Results

4.4.1 The circadian clock develops by chondrogenic stage of murine iPSC chondrogenesis

To assess the development of the circadian clock in our *in vitro* chondrogenesis protocol of murine iPSCs (miPSCs), we transduced miPSCs and pre-differentiated iPSCs (PDiPSCs) with Per2-Luc (P2L) or Bmal1-Luc (B1L) lentivirus and tracked the bioluminescence output of miPSCs, PDiPSCs in monolayer, PDiPSCs freshly cast in agarose, and chondrogenic cartilage pellets (Figure 4.2A). We found that miPSCs expressed P2L and B1L, but with no evidence of circadian oscillation (e.g., periods >32h), Figure 4.2B). Additionally, at the PDiPSC differentiation stage, P2L transduced PDiPSCs began to oscillate (average period=28.12±3.1h, mean±SEM), and B1L oscillation, which appears after *Per2* expression in development (*180*), had not yet occurred (period length >32h, Figure 4.2B). However, PDiPSCs cast in a 3D agarose system showed enhanced rhythmicity in *Per2* (average period=26.3±2.2h), while *Bmal1* remained arrhythmic (period length >32h, Figure 4.2B). Tissue engineered cartilage pellets showed high amplitude oscillations of *Per2* and *Bmal1* in anti-phase, meaning the circadian

clock had fully developed in our tissue engineered cartilage (P2L period=23.2±3.1h, B1L period=21.5±4.9h, Figure 4.2B).

Murine cartilage explants were taken from the femoral head of 10 week old homozygous PER2::LUC mice (*170*). Bioluminescence recording of these cartilage explants demonstrated sustained circadian rhythms, as shown previously (Figure 4.2C). Our tissue engineered cartilage pellets had similar period length compared to PER2:LUC oscillations in the cartilage explants, further confirming the development and maturation of the circadian clock in our tissue engineered cartilage (engineered cartilage period=23.2±3.1h, explant period=23.9±1.5h). Additionally, we transduced primary porcine chondrocytes with our P2L lentivirus, and these porcine chondrocytes also showed sustained daily oscillations similar to our tissue engineered pellets (period=23.5±3.3h, Figure 4.2D). Together, these findings suggest that our *in vitro* chondrogenesis protocol develops a circadian clock in our tissue engineered cartilage that has robust and sustained oscillations similar to mature cartilage explants and primary chondrocytes in another species.

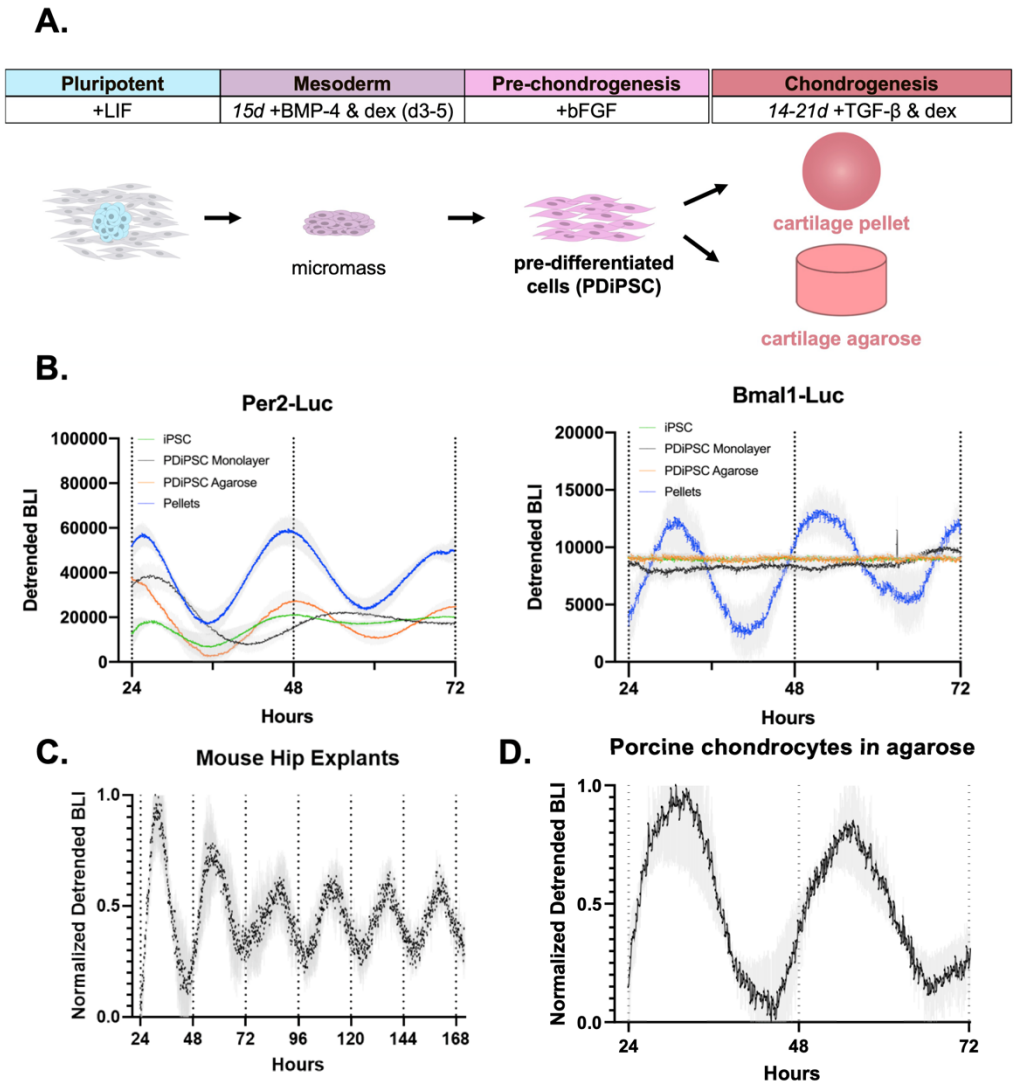

Figure 4.2 Development of the circadian clock in miPSC chondrogenesis. **(A)** Differentiation of miPSCs to chondrocytes. miPSCs were subjected to high-density micromass culture to create PDiPSCs. PDiPSCs were then either cast in agarose or pelleted and cultured in chondrogenic media for 14-21 days to create tissue engineered cartilage. **(B)** Per2-Luc bioluminescence intensity (BLI) of miPSCs (n=10), PDiPSCs (n=2), PDiPSCs in agarose (n=4), and pellets (n=10) (left) and Bmal1-Luc bioluminescence intensity (BLI) of miPSCs (n=5), PDiPSCs (n=4), PDiPSCs in agarose (n=5), and pellets (n=5). **(C)** BLI of femoral head cartilage explant from PER2::LUC mice (n=3, 1 hip per mouse). **(D)** Per2-Luc BLI in porcine chondrocytes cast in agarose (n=5).

4.4.2 Inflammation disrupts the circadian clock in native and tissue engineered cartilage

We next sought to understand the effect of inflammatory cytokines IL-1α, IL-1β, and TNFα on the circadian clock in tissue engineered cartilage pellets. It has previously been shown that IL-1β causes disruption in the circadian rhythms of murine cartilage explants through loss in bioluminescence oscillations and changes in clock gene expression, however TNFα had no effect (*33*). For these studies, we treated mature tissue engineered cartilage transduced with the P2L lentiviral reporter with 1 ng/mL IL-1α, 1 ng/mL IL-1β, 20 ng/mL TNFα, or PBS as a control. Bioluminescence tracking of P2L was recorded for 3 days prior to addition of cytokines. Cytokines were added in 2 µL volumes to not disrupt circadian rhythms and pellet bioluminescence was tracked for an additional 3 days post-cytokine addition. Pellets subjected to inflammatory challenge were also collected for histological and biochemical analysis of a main component of articular cartilage, sulfated glycosaminoglycans (sGAG) and analyzed for upregulation of inflammatory genes *Il6* and *Ccl2*. Pre-cytokine addition, all pellets showed circadian oscillations of P2L (n=45, Figure 4.3A). Pellets given PBS maintained circadian rhythms to the end of the recording (n=20, pre-PBS period=25.4±3.1h, post-PBS period=25.6±7.2h, Figure 4.3A). Pellets treated with TNFα also continued to maintain circadian oscillations (n=7, Figure 4.3A). Pellets treated with IL-1β showed a lengthening of period in all pellets and a 2.5-fold decrease in mean bioluminescence (n=8, Figure 4.3A) Additionally, 5 pellets treated with IL-1α showed rapid loss in circadian rhythms and all pellets show dramatically reduced amplitude of rhythms following a 2.8-fold decrease in bioluminescence (n=12, Figure 4.3A). The amplitude of bioluminescence was significantly decreased (p=0.0236) following IL-1α treatment (Figure 4.3B). Cartilage explants from PER2::LUC mice were also subjected to inflammatory challenge and bioluminescence output was recorded (Figure 4.4).

Similar to our tissue engineered cartilage pellets, TNFα had no effect on the circadian rhythm of the cartilage explants, however both IL-1α and IL-1β given at 1 ng/mL showed a rapid loss in circadian rhythms compared to controls and significant decrease in amplitude compared with controls ($p<0.05$) (Figure 4.4). The difference between the effect of TNFα and IL-1β on the circadian clock has previously been attributed to the activation of NF-κB signaling pathway by IL-1β and lack of activation by TNFα (*33*). The similar response of the effect of inflammatory cytokines on the circadian rhythm of our tissue engineered cartilage compared to *ex vivo* cartilage explants is encouraging for using our tissue engineered cartilage pellets as an *in vitro* model system.

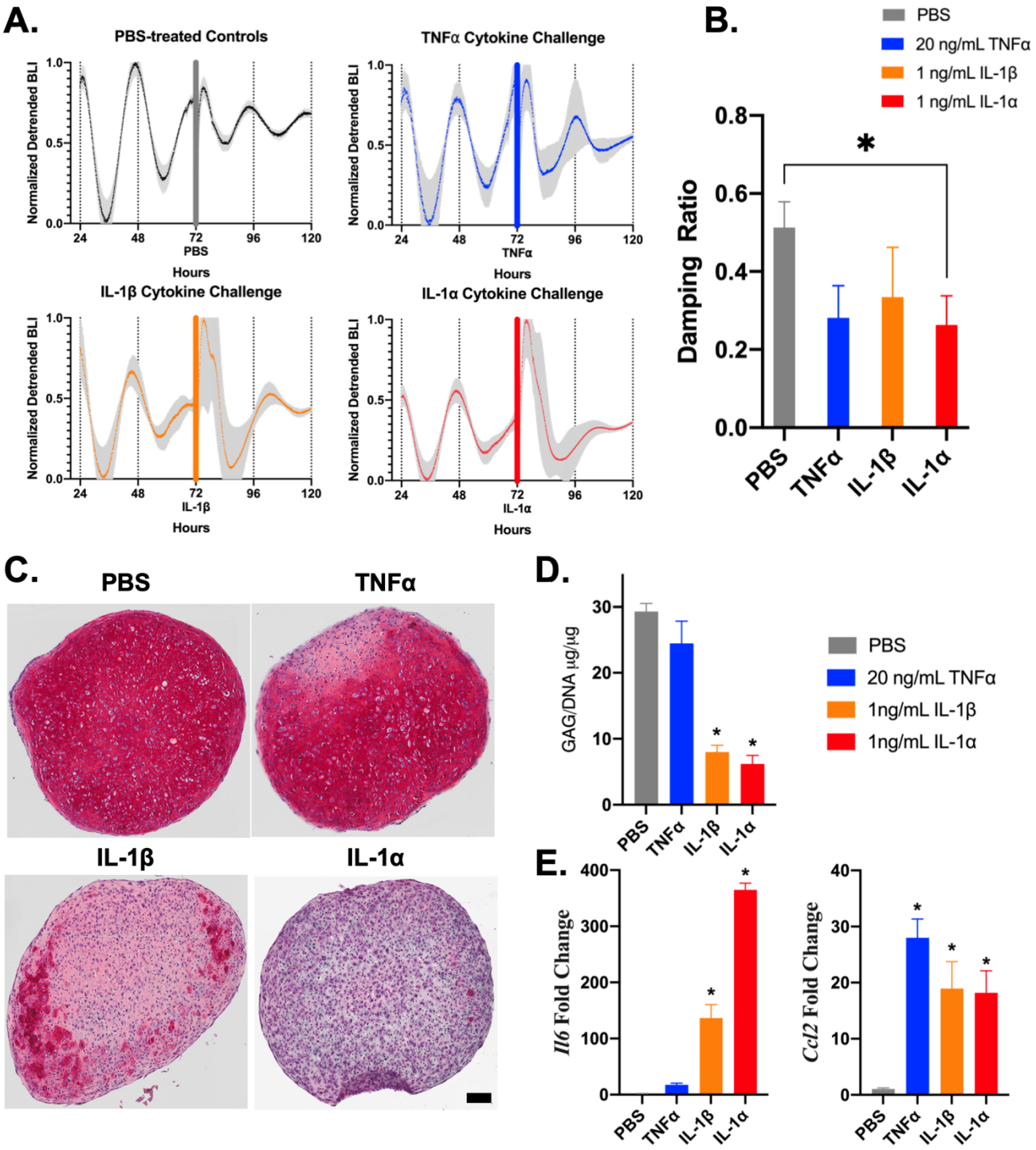
A.
PBS-treated Controls
TNFα Cytokine Challenge
IL-1β Cytokine Challenge
IL-1α Cytokine Challenge
Normalized Detrended BLI
Hours
PBS
TNFα
IL-1β
IL-1α
B.
PBS
20 ng/mL TNFα
1 ng/mL IL-1β
1 ng/mL IL-1α
Damping Ratio
C.
PBS
TNFα
IL-1β
IL-1α
D.
GAG/DNA μg/μg
1ng/mL IL-1β
1ng/mL IL-1α
E.
Il6 Fold Change
Ccl2 Fold Change

Figure 4.3 Tissue engineered cartilage response to inflammatory cytokines. **(A)** Tissue engineered cartilage pellets were treated with TNFα, IL-1β, IL-1α, or PBS control for 72 hours. Bars show addition of cytokine or PBS control. **(B)** Bioluminescence traces of pellets pre and post cytokine (TNFα (n=7), IL-1β (n=8), IL-1α (n=12), or PBS (n=20)). **(C)** Pellets treated with IL-1α show rapid decrease in bioluminescence, followed by lower amplitude circadian rhythm (p=0.0236). Asterisks represent significance compared to PBS control. **(D)** Safranin-O staining for sGAGs (n=4/treatment, scale bar = 100 μM). Pellets treated with IL-1β and IL-1α show loss in stain. **(E)** Quantification of sGAGs normalized to DNA content within each pellet (n=4/treatment). Pellets treated with IL-1β and IL-1α show significant loss in sGAG compared to PBS controls ($p < 0.0001$). Asterisks represents significant differences as compared to PBS controls. **(F)** Gene expression analysis of *Il6* and *Ccl2* (n=4/treatment, fold change relative to PBS control). Only IL-1β and IL-1α treatment caused upregulation of *Il6* ($p = 0.0002$). All cytokine treatments caused upregulation in *Ccl2* ($p < 0.05$). Different letters denote groups that are significantly different.

To better understand the effect of each cytokine on circadian rhythm and begin to elucidate the functional outputs of the cartilage clock we examined the effect of cytokines on the degradation of cartilage extracellular matrix, since the circadian clock is known to maintain cartilage homeostasis (*16, 17, 19-22, 176*). Pellets were stained with safranin-O to look at sGAG content (n=4/group, Figure 4.3C). Additionally, sGAG content within pellets was quantified by biochemical analysis and normalized to DNA content within each pellet (n=4/group, Figure 4.3D). The staining for sGAG showed rich red stain in the PBS control pellets as well as the pellets treated with TNFα, while pellets treated with IL-1β showed reduced sGAG staining and pellets treated with IL-1α showed a loss in sGAG (Figure 4.3D). The quantification of sGAG content matched the histological images, where the TNFα treated pellets had similar sGAG content compared to PBS controls, whereas the IL-1β and IL-1α treated pellets showed significant sGAG loss compared to PBS controls ($p<0.0001$, Figure 4.3D). This loss in ECM components in pellets treated with IL-1 but not TNFα suggests that pathways activated by IL-1

leading to matrix degradation could also be driving the loss of the circadian clock, which in turn exacerbates matrix loss.

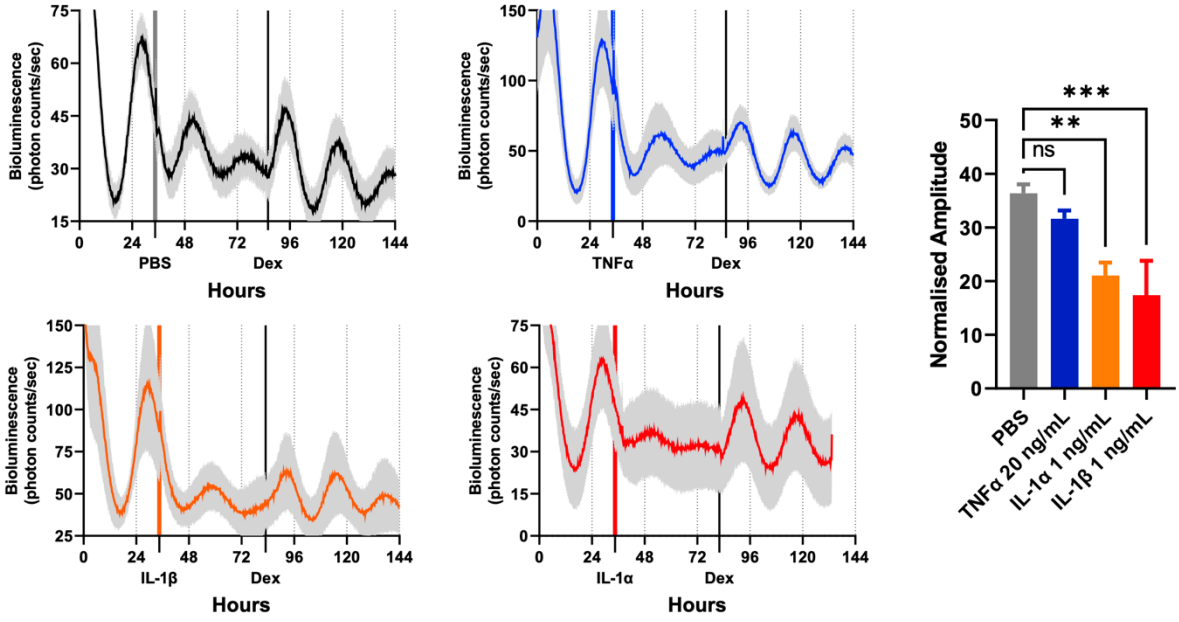

Figure 4.4 Cartilage circadian clock in response to inflammatory cytokines. Cartilage explants from the femoral head of PER2::LUC mice were recorded for bioluminescence intensity. Explants were treated with 1 ng/mL of IL-1β, IL-1α, 20 ng/mL of TNFα, or vehicle controls (n=3 per each condition). Loss of circadian rhythm was seen in explants given IL-1 and circadian rhythm was rescued with the administration of dexamethasone (dex). Grey, blue, orange, and red bars indicate administration of cytokine, black bars indicate administration of dex. Asterisks represent significance compared to controls ($p<0.05$).

Finally, inflammatory genes *Il6* and *Ccl2* were examined in pellets treated with cytokines. IL-6 is a cytokine that upregulates inflammatory pathways within the joint and CCL-2 is a chemokine that attracts immune cells to the joint. Here we see that treatment of pellets with TNFα caused significantly upregulated *Ccl2* gene expression compared to PBS controls (n=4, p=0.0002), but did not cause any significant upregulation in *Il6* (n=4, Figure 4.3E). However, addition of IL-1β and IL-1α caused a significant increase in *Ccl2* compared to PBS controls (n=4, p=0.0086 & p=0.0122 respectively) and a significant upregulation of *Il6* especially in the pellets given IL-1α (n=4, $p<0.0001$ for both IL-1β and IL-1α, Figure 4.3E). This data also

suggests that, although upregulation of chemokines such as *Ccl2* for immune cell recruitment is important, cytokines such as IL-1 and IL-6 are more likely to be involved in the disruption of the circadian clock. Taken together, this suggests that inflammatory cytokines IL-1β and IL-1α can disrupt the cartilage circadian clock in cartilage explants and our tissue engineered cartilage, and this effect might be through the upregulation of inflammatory cytokines, such as IL-6, that lead to matrix degradation.

4.4.3 IL-1 resistant engineered tissues are resistant to circadian disruption

Cartilage explants treated with IL-1α and IL-1β recovered the loss in circadian rhythms with the addition of dex, an anti-inflammatory agent (Figure 4.4). Because of the ability to recover the circadian clock with an anti-inflammatory treatment, we sought to test whether our anti-inflammatory cell therapies could preserve the circadian clock in the presence of IL-1α. Due to the enhanced impact of IL-1α on the disruption of the circadian clock, increased matrix degradation, and upregulation of *Il6* we used IL-1α in these studies. For these studies we used miPSCs CRISPR/Cas9 edited without IL1R1 that do not respond to IL-1 (IL1R1 KO) (*53*), miPSCs edited with CRISPR/Cas9 to incorporate IL-1Ra downstream of the *Ccl2* locus to drive IL-1Ra production in response to inflammation (Ccl2-IL1Ra) (*60*), and a lentiviral circuit incorporating a synthetic promoter activated by the NF-κB signaling pathway that drives production of IL-1Ra (NFκBr-IL1Ra) (*59*). All of the miPSC lines or miPSCs were transduced with the lentiviral vector containing the P2L reporter and differentiated into tissue engineered cartilage pellets. We then treated with IL-1α (Figure 4.5A) and assessed the ability of these pellets to maintain cartilage integrity and circadian expression.

First, the ability of the two self-regulating therapeutic groups, Ccl2-IL1Ra and NFκBr-IL1Ra pellets, to produce IL-1Ra was determined. As expected, all four groups (P2L controls,

IL1R1 KO, Ccl2-IL1Ra, and NFκBr-IL1Ra) showed no difference in IL-1Ra production when given no IL-1α and the P2L and IL1R1 KO pellets also showed no difference in IL-1Ra production when treated with 1 ng/mL of IL-1α (n=10/group, Figure 4.5B). Both Ccl2-IL1Ra and NFκBr-IL1Ra had significantly increased IL-1Ra production in response to 1 ng/mL of IL-1α, with the NFκBr-IL1Ra producing the highest amount of IL-1Ra (n=10/group, Ccl2-IL1Ra ~36 ng/mL IL-1Ra, NFκBr-IL1Ra ~74 ng/mL IL-1Ra, $p<0.0001$, Figure 4.5B).

After confirming that our self-regulating cells were producing sufficient IL-1Ra to inhibit IL-1 activity, we next tracked P2L through bioluminescence before the addition of cytokine and for 3 days after addition of 1 ng/mL of IL-1α. All four groups before the addition of cytokine were rhythmic, showing that the addition of any gene editing did not disrupt the clock (n=13, pre-IL-1α period=24.6±2.9h, Figure 4.5C). All three of our cell therapy groups showed maintained circadian rhythms in response IL-1α (n=13, post-IL-1α period=24.4±2.0h, Figure 4.5C), whereas the non-engineered controls showed loss in circadian rhythm as shown previously (n=12, Figure 4.3A). Cytokine-treated resistant pellets show a similar consistency in period to what we observed in PBS-treated control pellets. In addition to whole-pellet bioluminescence data, we recorded bioluminescence videos of untreated and our cell therapy groups at single-cell resolution.

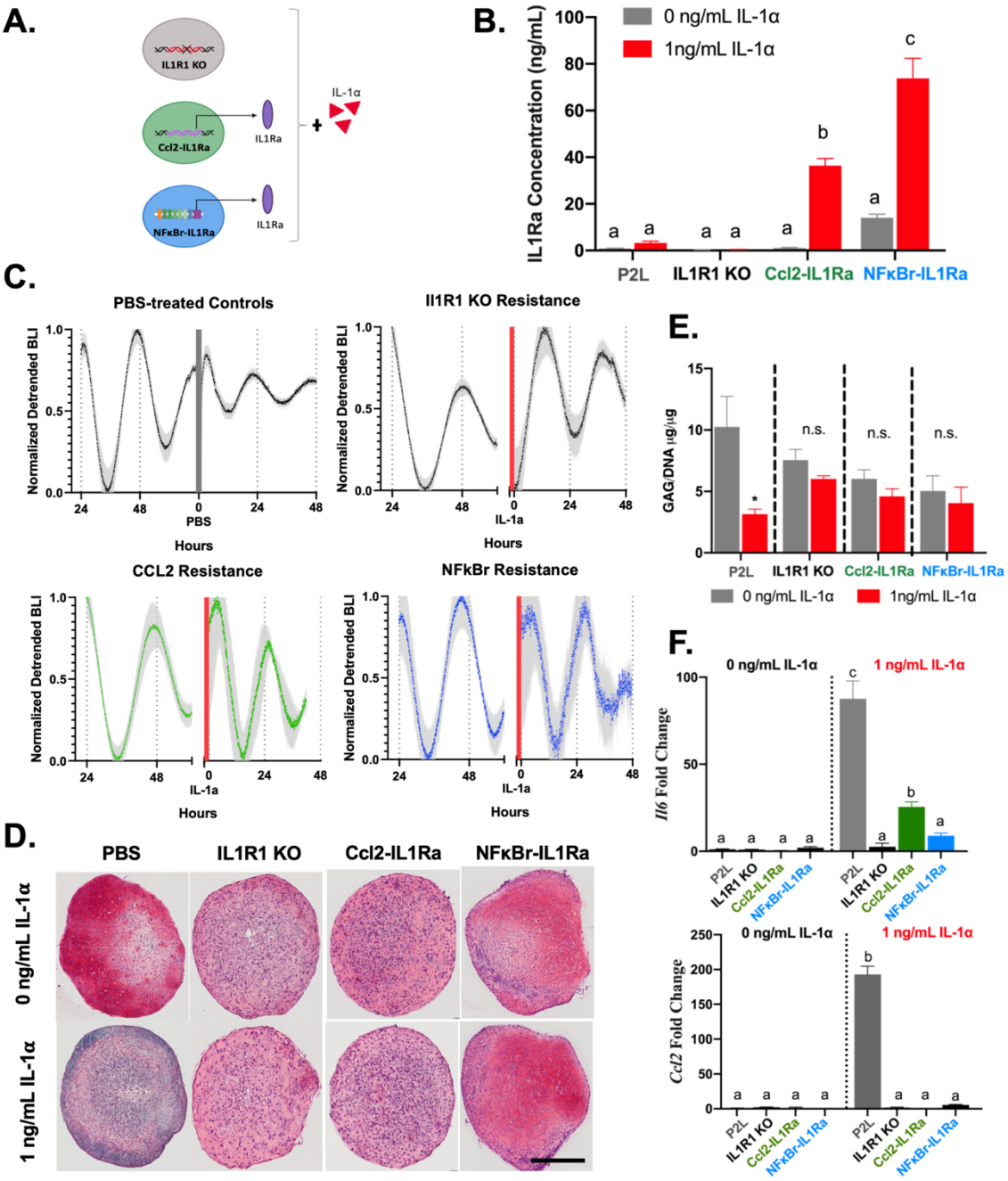
A.
IL1R1 KO
Ccl2-IL1Ra
NFκBr-IL1Ra
IL1Ra
IL1Ra
IL-1α
B.
0 ng/mL IL-1α
1ng/mL IL-1α
IL1Ra Concentration (ng/mL)
P2L
IL1R1 KO
Ccl2-IL1Ra
NFκBr-IL1Ra
C.
PBS-treated Controls
Il1R1 KO Resistance
CCL2 Resistance
NFkBr Resistance
Normalized Detrended BLI
PBS
IL-1a
Hours
D.
PBS
IL1R1 KO
Ccl2-IL1Ra
NFκBr-IL1Ra
0 ng/mL IL-1α
1 ng/mL IL-1α
E.
GAG/DNA μg/μg
n.s.
F.
Il6 Fold Change
Ccl2 Fold Change
0 ng/mL IL-1α
1 ng/mL IL-1α

Figure 4.5 Engineered cell therapies response to IL-1α. **(A)** Three different anti-inflammatory cell therapies were used to test the ability to protect the circadian rhythm of tissue engineered cartilage: CRISPR/Cas9 edited miPSCs lacking the IL1 receptor (IL1R1 KO), CRISPR Cas9 edited miPSCs that produce IL-1Ra downstream of the *Ccl2* promoter (Ccl2-IL1Ra), and a lentiviral gene therapy comprised of a NF-κB responsive synthetic promoter that drives production of IL-1Ra (NFκBr-IL1Ra). **(B)** IL-1Ra concentration in response to IL-1α stimulation (n=10/group). The Ccl2-IL1Ra and NFκBr-IL1Ra groups showed increased IL-1Ra production in response to IL-1α. **(C)** Bioluminescence traces of pellets pre and post cytokine (n=13). All three cell therapy groups showed preservation of the clock post cytokine treatment. Grey bar represents addition of PBS, red bar represents addition of IL-1α. **(D)** Safranin-O staining for sGAGs (n=4-6/group, scale bar = 100 μM). **(E)** Quantification of sGAGs normalized to DNA content within each pellet (n=8=10/treatment). Cell therapy groups showed no significant loss in sGAG in response to IL-1α. Asterisks denotes significance compared to PBS control within group. n.s. = not significant **(F)** Gene expression analysis of *Il6* and *Ccl2* (n=6-8/group fold change relative to P2L untreated control). All cell therapy groups showed significantly less inflammatory gene expression compared to IL-1α treated controls.

Additionally, when examining staining and quantification of sGAG content of the cartilage ECM, the IL1R1 KO, Ccl2-IL1ra, and NFκBr-IL1Ra groups exhibited rich safranin-O staining similar to P2L controls and no difference in sGAG content between control pellets (no cytokine treatment) and pellets treated with 1 ng/mL of IL-1α (n=4-6/group for histology, n=8-10/group for biochemical analysis, Figure 4.5D,E). Maintaining that there could be a potential link between protection of the cartilage ECM and preservation of the circadian clock. Finally, when examining gene expression of *Il6* and *Ccl2* 72 hours after treatment, all groups showed no upregulation of genes in response to no cytokine, however when stimulated with 1 ng/mL of IL-1α only the P2L controls showed significant upregulation of *Ccl2* (n=6-8, $p<0.0001$, Figure 4.5F) and the P2L group had the highest expression of *Il6* (n=6-8, $p<0.0001$, Figure 4.5F). The Ccl2-IL1Ra group showed no upregulation of *Ccl2* when treated with IL-1α at 72 hours due to the self-regulating response that rapidly inhibits IL-1 signaling (*60*), however there was a moderate increase in *Il6* expression compared to the IL1R1 KO and NFκBr-IL1Ra groups given

no cytokine and cytokine (n=6-8, $p<0.05$, Figure 4.5F) most likely due to the lower production of IL-1Ra to inhibit IL-1α compared to the NFκBr-IL1Ra (Figure 4.5F). Together, these data demonstrate that our cell therapies edited to either be non-responsive to IL-1α (IL1R1 KO) or to be self-regulating and produce an anti-inflammatory therapeutic, IL-1Ra, can effectively protect their cartilage ECM from degradation and importantly maintain the circadian clock in the presence of IL-1α.

4.5 Discussion

By combining tissue engineering, synthetic biology, and circadian biology, we have developed cell-based therapies that are capable of preserving the cartilage circadian clock in response to disruptive stimuli such as inflammation. While significant advances have been made in understanding the physiology of the circadian clock in recent years, the use of genetic approaches has not been employed previously to create cell-based clock preserving therapeutic systems. Here we used chondrocytes and tissue engineered cartilage as our model system, which provides a homogeneous cell population that avoids the complexities of interpreting data from multiple cell types. Using this system, we have been able to uncover characteristics of cartilage circadian rhythms and established a robust system for peripheral clock studies. These types of tools can be utilized to mitigate disease where circadian disruption plays a role (*16*), can be used to create better engineered tissues by ensuring tissue homeostasis through clock-controlled genes (*16, 22*),and may be used to uncover important characteristics of the circadian clock not yet known. In combination with tissue engineering, the use of genetically modified cells may allow the formation of functional bioartificial tissues with intrinsic clock-preserving characteristics.

In quantifying the circadian clock in miPSCs, we observed that undifferentiated cells were not rhythmic and developed their circadian clock over the course of chondrogenic differentiation. This is consistent with prior reports that mouse embryonic stem cells and other stem/progenitor cells cannot generate circadian rhythms until they differentiate (*180*), suggesting that formation of a mature circadian clock is an integral characteristic of cellular differentiation. However, the circadian clock is developed in adult stem cell populations, as well as most somatic cells, further confirming the importance of the clock in regulating tissue and cell homeostasis after cell development (*183*). Furthermore, we observed that iPSC-derived chondrocytes or primary porcine chondrocytes in tissue-engineered cartilage pellets showed a similar circadian response as primary murine cartilage and responded similarly to inflammatory cytokines, indicating that this model of iPSC chondrogenesis replicates many of the features of native cartilage. In this respect, such *in vitro* model systems can be utilized to uncover key characteristics of the circadian clock development throughout chondrogenesis and in response to inflammatory cytokines that drive disease progression. This can be expanded to other iPSC differentiation lineages and additional stimuli to further understand the circadian clock in development.

Although it is clear that the circadian clock plays a critical role in articular cartilage physiology and OA pathology, the mechanisms by which clock genes maintain chondrocyte homeostasis remain to be determined. Here we showed different responses of the circadian clock to cytokines in cartilage (*33*). By examining the effect of the cytokines IL-1 and TNF-α on the circadian clock as well as the cartilage ECM and inflammation associated genes, we determine that cytokines, IL-1β and IL-1α, that lead to matrix degradation and upregulation of other pro-inflammatory cytokines such as *Il6,* drive the disruption in the circadian clock instead of

cytokines such as TNF-α that had no effect on the circadian clock, matrix degradation, or upregulation of *Il6.* This information and this model system to test cytokines will help elucidate what each cytokine is directly acting on and help us uncover the direct link between inflammatory cytokines and the circadian clock.

An interesting observation made throughout this study was the maintenance of the circadian rhythms in cartilage explants, porcine chondrocytes, and tissue engineered cartilage pellets over many days, where cells or tissues lack exogenous entrainment cues (*184*). Cartilage explants especially maintained their oscillations for over 10 days without any perturbations such as media changes or plate movement. This type of maintained circadian clock is not common in tissue explants and highlights a potential interesting area of study (*185, 186*). Although there is research looking into the cartilage circadian clock, it is not known how the chondrocytes maintain their circadian clock within articular cartilage. It is hypothesized that changes in body temperature and factors within the synovial fluid help with clock synchronization (*13, 22*) but the prolonged maintenance of the circadian clock *ex vivo* without any synchronizing cues highlights that there might be a factor secreted by the chondrocytes themselves that maintains this synchrony, or the abundant ECM maintains the biochemical and biomechanical niche for synchrony (*187*). Future work looking into potential synchronizing factors will be key in uncovering this mechanism.

The ability of our genetic engineering approaches to maintain the circadian clock also opens a different area of therapeutic development. There are many diseases that are associated with disruptions in the circadian clock (*14*). Using gene therapy approaches to create cell therapies that focus on preserving or synchronizing the clock can be a useful arsenal to help ameliorate diseases beyond OA. For example, in the context of clock preservation in the

presence of inflammation, these circuits can be used to protect the intervertebral disc (*16, 172, 181*). Additionally, with the use of iPSCs there is the capability to expand this to create autologous cellular therapeutics and treatments against diseases where circadian disruption plays a role, such as in age-related clock dampening or cancer (*188, 189*). Using tissue engineering and creating cells that are capable of maintaining the circadian rhythm can also be used to develop better engineered tissues through maintenance of the circadian clock and associated genes involved in tissue homeostasis (*16, 22*).

Using an engineered tissue that is capable of protecting itself against inflammation and preserving the circadian clock in response to inflammation can overcome the current limitations in OA therapies and articular cartilage repair. This work can be expanded to create clock preserving cell therapies across many tissues by differentiating already developed iPSC lines into other tissues or using lentiviral approaches. For example, the NFκBr-IL1Ra lentiviral system has been used in both miPSCs and primary porcine chondrocytes for inflammation-activated and mechano-responsive drug delivery (*59, 63*). Future work in comparing rhythmic transcriptomes and understanding the beneficial effects of rhythm preservation will additionally help further insights into the physiology of the cartilage clock. This approach opens an innovative frontier for creating cell-based therapies to maintain the circadian clock. Together, this framework for developing clock preserving cell systems is an innovative approach to establish therapeutics and enhance tissue repair.

4.6 Conclusions

We engineered cell therapies that are capable of preserving the circadian clock in response to inflammation and protecting tissue engineered cartilage. Murine induced pluripotent stem cells (miPSCs) were differentiated into tissue engineered cartilage and the circadian rhythm of the cells undergoing chondrogenesis was tracked. We found that miPSCs do not have developed circadian rhythms, however the tissue engineered cartilage has fully developed circadian rhythms. Both our tissue engineered cartilage and cartilage explants from C57 mice showed loss in circadian rhythms with the addition of IL-1, however TNFα had no effect on the circadian rhythms. We developed three cell therapies capable of preserving circadian rhythms in the presence of IL-1. The first cell therapy was engineered using CRISPR/Cas9 to lack the functional IL-1 receptor 1 (IL1R1 KO) so it could not sense the presence of IL-1. The second cell therapy was engineered using CRISPR/Cas9 to produce IL-1 receptor antagonist downstream of the *Ccl2* promoter which is activated by inflammation (Ccl2-IL1Ra). The final circuit was a lentiviral system with a synthetic promoter activated by NF-κB signaling that produced IL-1Ra (NFκBr-IL1Ra). All three of these systems were capable of preserving the circadian clock and cartilage ECM from IL-1 induced inflammation. This is the first approach at using cellular engineering to preserve the circadian clock in peripheral tissues.

Chapter 5: A synthetic chronogenetic therapy gene circuit for temporal drug delivery

5.1 Abstract

Chronotherapy, the delivery of therapeutic interventions personalized to patient's circadian rhythms, has shown enhanced therapeutic efficacy and reduced side-effects. Currently, many drugs taken in the United States target the product of a circadian gene and therefore there is a need to focus on the timing of drug delivery. In rheumatoid arthritis, patients exhibit diurnal changes in cytokines that lead to inflammatory flares and enhanced disease severity in the early morning. There has been important work showing the administration of anti-inflammatory treatments in the early morning, immediately before the inflammatory flare, in reducing symptoms of RA. Using synthetic biology, we developed chronotherapy-based gene circuits, chronogenetic therapies, that produce our prescribed transgene downstream of the core circadian clock component, Per2. We transduced these lentiviral chronogenetic therapies into murine induced pluripotent stem cells and developed tissue-engineered cartilage as our model system for timed drug delivery. Our anti-inflammatory chronogenetic circuit was capable of producing interleukin-1 receptor antagonist (IL-1Ra) in an oscillatory manner tracking with circadian rhythms *in vitro.* Additionally, the tissue engineered pellets were able to entrain to host circadian rhythms when implanted into mice and produce differing levels of IL-1Ra in the serum at

different times of day. The chronogenetic synthetic gene circuits provide a novel cell therapy driving by the circadian clock for controlled biologic delivery at prescribed times of day.

5.2 Introduction

Chronotherapy, or the delivery of therapeutic interventions based on the patient's circadian rhythm, is emerging as an important method for minimizing side effects and increasing efficacy of drugs. Circadian rhythms are driven by the circadian clock, an internal genetic timing mechanism that operates on a roughly 24-hour period and exists within the brain and nearly all cells in peripheral tissues (*13-15*). The core clock genes, comprised of transcriptional activators *Bmal1* and *Clock* and transcriptional repressors *Per1/2* and *Cry1/2* and output genes, such as *Rev-erbs, Dbp,* and *Nfil3*, create an auto-regulatory negative feedback loop that drives the oscillatory and timed behavior of the clock (*14, 15*). These core clock genes drive expression of many other tissue-specific clock-controlled genes that help maintain tissue homeostasis (*16*). Recently, it was discovered that around 50% of mammalian genes are expressed with 24-hour rhythms and their expression is regulated in some way by the circadian clock (*65*). Therefore, there has been an increase in research trying to understand the importance of therapeutic delivery and matching it to circadian rhythms.

Recently it was found that over half (56) of the top 100 selling drugs in the United States target the product of a circadian gene (*64*). To this end, there are research and clinical trials looking into timed delivery of drugs for increasing their efficacy and minimizing side effects (*16,*

17, 20, 64-68). Studies have shown that time of day is critical to outcomes in heart surgery (*190*), cardiovascular disease treatment (*64*), cancer treatment (*69, 191, 192*), as well as others.

In musculoskeletal diseases, such as rheumatoid arthritis (RA) and osteoarthritis (OA), there are diurnal expression patterns in cytokines that demonstrate circadian patterns in the intensity of symptoms, with inflammatory flares occurring in the early morning (*16, 17, 66, 67, 193*). There is great evidence for the importance of chronotherapy in patients with RA. In trials of non-steroidal anti-inflammatory drugs (NSAIDs) or methotrexate, patients that took these drugs at night showed improved outcomes and reduced adverse effects to the drugs. Additionally, patients who received drugs at night instead of in the morning, to combat the increase in IL-6 in the early morning, reported reduced joint pain and inflammation (*68*). Therefore, there is a need for intermittent or timed delivery of biologics at specific times of day for enhanced efficacy in musculoskeletal diseases such as RA.

Unfortunately, this process of taking drugs at specific times of day can be difficult to maintain since it requires constant daily injections or delivery of drugs at inconvenient times, such as the case of arthritis where delivery of the drug in the early morning immediately before an inflammatory flare would be best. However, with recent advances in synthetic biology and genetic engineering, cell-based therapies that harness cells for localized, controlled, and long-lasting delivery of prescribed biologic drugs, can be a promising approach to ensure drug delivery at specific times of day and over specific frequencies. To this end, the goal of this study was to create cell-based chronotherapy gene circuits, chronogenetic therapies, that use the cell's own biologic circadian rhythm to provide gene-based delivery of biologic drugs at prescribed times and frequencies. Therefore, we developed two lentiviral synthetic gene circuits driven by the core clock gene, *Per2*, to produce a destabilized green fluorescence protein (d2eGFP) as an

initial proof-of-concept reporter circuit (Per2-d2eGFP-t2a-Luc) and interleukin-1 receptor antagonist (IL-1Ra) as an anti-inflammatory approach to target RA (Per2-IL1Ra-t2a-Luc). All circuits contained a 2A linker to produce luciferase in addition to the therapeutic drug for circadian monitoring. We first examined the ability of the GFP reporter circuit to produce protein in an oscillating manner in transduced murine induced pluripotent stem cells (miPSCs) differentiated into tissue-engineered cartilage. Tissue-engineered cartilage was used as the model delivery system due to the fact that its avascular and aneural and can easily be implanted and survive in any location (*23, 61*). We then worked to characterize the Per2-IL1Ra-t2a-Luc circuit *in vitro* to ensure oscillating production of IL-1Ra and to determine if this circuit could maintain its circadian clock in the presence of inflammatory cytokines, which has previously been shown to disrupt the clock (*33*). We then worked to test our Per2-IL1Ra-t2a-Luc circuit *in vivo* to understand tissue-engineered cartilage circadian clock entrainment to the host and the ability for timed drug delivery and IL-1Ra concentrations in the serum (Figure 5.1). We show the ability of these chronogenetic circuits to deliver our therapeutic biologics at specific times of day, driven by *Per2* expression both *in vitro* and *in vivo*. This approach is the very first creation of a cell-based therapy for chronotherapy applications through the use of synthetic biology and tissue engineering of stem cell gene circuits.

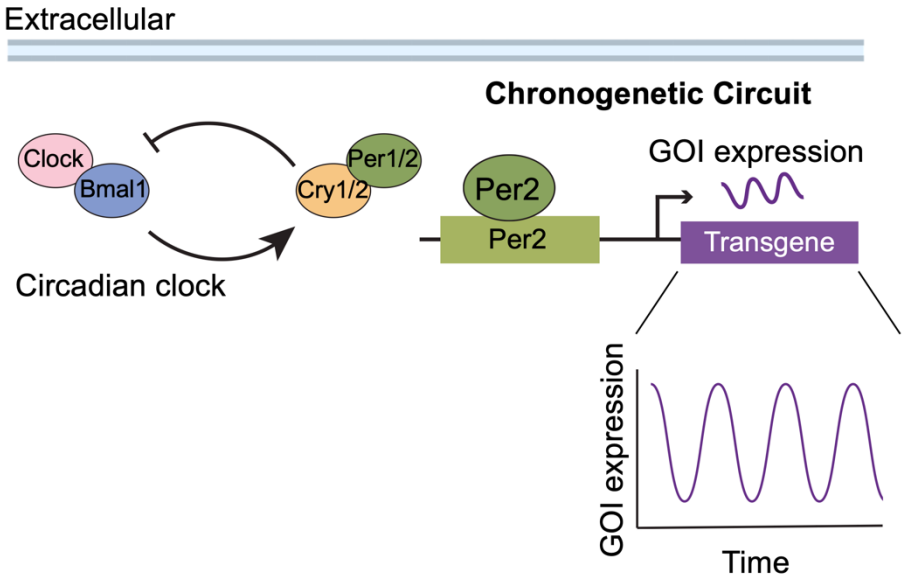

Figure 5.1 Cell-based chronotherapy approach. The therapeutic chronogenetic circuit was created and transduced into murine induced pluripotent stem cells (miPSCs) using lentivirus. These miPSCs were then differentiated into tissue engineered cartilage. The circuit was driven by the Per2 promoter, activated by core clock component Per2 and produced both a luciferase reporter and the therapeutic drug, IL-1Ra. The Per2-IL1Ra-t2a-Luc circuit is capable of delivering an anti-inflammatory drug to target inflammatory flares.

5.3 Materials and Methods

5.3.1 Murine induced pluripotent stem cell culture and differentiation

Murine induced pluripotent stem cells (miPSCs) were derived from tail fibroblasts from adult C57BL/6 mice and validated for pluripotency as described by Diekman et al. (*49, 86*). miPSCs were cultured in Dulbecco's Modified Eagle's Medium High Glucose (DMEM-HG, Gibco), 20% lot selected fetal bovine serum (FBS, Atlanta Biologicals), 100 nM minimum essential medium nonessential amino acids (NEAA, Gibco), 55 µM 2-mercaptoethanol (2-me, Gibco), 24 ng/mL gentamicin (Gibco), and 1000 U/mL mouse leukemia inhibitory factor (LIF, Millipore), and maintained on mitomycin C-treated mouse embryonic fibroblasts (Millipore).

miPSCs were differentiated toward a mesenchymal state using a high-density micromass culture (*49*) in differentiation medium containing DMEM-HG, 1% culture medium supplement containing recombinant human insulin, human transferrin, and sodium selenite (ITS+, Corning), 100 nM NEAA, 55 μM 2-me, 24 ng/mL gentamicin, 50 μg/mL L-ascorbic acid, and 40 μg/mL L-proline. On days 3–5, this medium was supplemented with 100 nM dexamethasone and 50 ng/mL bone morphogenetic protein 4 (BMP-4; R&D Systems). After 15 days, the micromasses were dissociated with pronase (Millipore Sigma) and collagenase type II (Worthington Biochemical) and the pre-differentiated iPSCs (PDiPSCs) were plated on gelatin-coated dishes in expansion medium containing DMEM-HG, 10% lot-selected FBS, 1% ITS+, 100 nM NEAA, 55 μM 2-me, 1% penicillin/streptomycin (P/S, Gibco), 50 μg/mL L-ascorbic acid, 40 μg/mL L-proline, and 4 ng/mL of basic fibroblast growth factor (bFGF, R&D Systems).

To create tissue engineered cartilage, passage 2 PDiPSCs were pelleted by centrifugation of 250K cells (*49*). Pellets were cultured for 14-21 days in chondrogenic medium consisting of DMEM-HG, 1% ITS+, 100 nM NEAA, 55 μM 2-me, 1% P/S, 50 μg/mL L-ascorbic acid, 40 μg/mL L-proline, 100 nM dexamethasone, and 10 ng/mL TGF-β3 (R&D Systems).

5.3.2 Cell-based chronotherapy circuit design

We developed two lentiviral systems activated by *Per2* expression, a core circadian clock gene. All circuits contained a t2a component that linked luciferase (Luc) downstream of the transgene, with the goal of creating a chronotherapy circuit that had its own luciferase reporter system. Therefore, upon activation of the repressive arm of the circadian clock and subsequent activation of Per2, the chronotherapy circuits would be activated and produce either a short-lived green fluorescence protein (Per2-d2eGFP-t2a-Luc) or interleukin-1 receptor antagonist (Per2-IL1Ra-t2a-Luc) over a 24-hour period.

Per2-d2eGFP-t2a-Luc circuit

The murine Per2 promoter was obtained from a lentiviral Per2-Luc plasmid (*181*). This promoter was cloned in place of the CMV promoter in a CMV-GFP-t2a-Luc lentiviral cassette purchased from Systems Biosciences. The CMV promoter was removed with restriction enzymes and the Per2 promoter was incorporated using Gibson Assembly (*82*). A destabilized green fluorescence protein (d2eGFP) was obtained [No. 26821, Addgene] and cloned in place of the stable GFP in the backbone cassette using restriction enzymes and Gibson Assembly (*82*) to create the Per2-d2eGFP-t2a-Luc circuit. The d2eGFP transgene came from the pcDNA3.3_d2eGFP plasmid which was a gift from Derrick Rossi (*194*). Therefore, a dual reporter chronotherapy gene circuit was created that would express both short-lived GFP and luciferase downstream of Per2 activation for initial concept characterization.

Per2-IL1Ra-t2a-Luc circuit

Murine interleukin-1 receptor antagonist (IL-1Ra) was incorporated into the Per2-d2eGFP-t2a-Luc cassette in place of the d2eGFP through restriction enzyme removal of d2eGFP and Gibson Assembly (*82*) to incorporate IL-1Ra. The IL-1Ra was obtained from a plasmid created to sense and respond to inflammation (*62, 63*). This lentiviral circuit was then able to produce IL-1Ra and luciferase in response to Per2 activation (Per2-IL1Ra-t2a-Luc) and can be used as an anti-inflammatory therapeutic.

5.3.3 Lentivirus production and cell transduction

Human embryonic kidney (HEK) 293T cells were co-transfected with second-generation packaging plasmid psPAX2 (No. 12260; Addgene), the envelope plasmid pMD2.G (No. 12259; Addgene), and the expression transfer vector (Per2-d2eGFP-t2a-Luc or Per2-IL1Ra-t2a-Luc) by calcium phosphate precipitation to make vesicular stomatitis virus glycoprotein pseudotyped

lentivirus (*85*). The lentivirus was harvested at 24- and 48- hours post transfection and stored at -80°C until use. The functional titer of the virus was determined with quantitative real-time polymerase chain to determine the number of lentiviral DNA copies integrated into the genome of transduced HeLa cells (*85*). PDiPSCs were transduced before being pelleted. For PDiPSC transductions, virus was thawed on ice and diluted in medium to obtain the desired number of viral particles to achieve a multiplicity of infection of 3 (*62*). Polybrene was added to a concentration of 4 μg/mL to aid in transduction. The medium of the cells was aspirated and replaced with virus-containing medium, and cells were incubated for 24 hours before aspirating the viral medium.

5.3.4 *In vitro* characterization of chronogenetic therapy circuits

All chronogenetic therapy circuits were characterized *in vitro* once the cells had become tissue engineered cartilage pellets after 14 days in chondrogenic culture. Both circuits were subject to bioluminescence recordings to track circadian oscillations. Per2-d2eGFP-t2a-Luc constructs were also subject to fluorescence imaging to quantify GFP expression over time. Media from the Per2-IL1Ra-t2a-Luc pellets was collected every 3 hours for 72 hours to determine IL-1Ra production, and pellets were harvested every 3 hours for 72 hours for *Il1rn* gene expression.

Bioluminescence recordings

Tissue engineered cartilage pellets (Per2-d2eGFP-t2a-Luc or Per2-IL1Ra-t2a-Luc) were plated in 35 mm petri dishes with 1 mL of recording medium containing D-luciferin (Goldbio), sealed with vacuum grease, and placed in a light-tight36º incubator containing photo-multiplier tubes (PMTs) (Hamamatsu Photonics). Each dish was placed under one PMT and the bioluminescence was recorded as photons per 180 seconds. Bioluminescence data were

detrended with a 24h moving average and analyzed in ChronoStar 1.0 (*182*). Recoding medium contained DMEM powder (Sigma), B27 supplement (Invitrogen), P/S, L-glutamine (Invitrogen), HEPES (Sigma), and D-glucose (Invitrogen).

Fluorescence imaging

After 14 days of chondrogenic culture Per2-d2eGFP-t2a-Luc pellets were digested with collagenase type II (Worthington Biochemicals), cast in a thin layer of agarose at a density of 10 million cells/mL on glass bottom black 96-well plates (Grier Bio), and cultured in chondrogenic medium. Plates were placed in a Cytation5 plate reader (BioTek) and agarose was subjected to fluorescence imaging at 4x magnification for 48 hours with images taken every hour. Image sequences were concatenated into videos using Gen5 software and individual cells were visualized and traced for GFP output.

Gene expression with quantitative real time polymerase chain reaction

Per2-IL1Ra-t2a-Luc pellets were collected every 3 hours for 72 hours. Pellets were homogenized using a miniature beat beater, lysed in Buffer RL, and RNA was isolated following the manufacturer's protocol (total RNA purification; Norgen Biotek). Reverse transcription was performed using Superscript VILO complementary DNA master mix (Invitrogen). qRT-PCR was performed using Fast SyBR Green master mix (Applied Biosystems). Primer pairs were synthesized by Integrated DNA Technologies, Inc: *Il1rn* [forward (F), 5'-GTCCAGGATGGTTCCTCTGC-3'; reverse (R), 5'-TCTTCCGGTGTGTTGGTGAG-3'] and *r18s* [F, 5'-CGGCTACCACATCCAAGGAA-3'; R, 5'-GGGCCTCGAAAGAGTCCTGT-3']. Data are reported as fold changes with a 6h moving average and were calculated using the $\Delta\Delta C_T$ method and are shown relative to the non-transduced (NT) control group at 0 hours and ribosomal 18s is used as the reference gene.

Enzyme-linked immunosorbent assays

Media from Per2-IL1Ra-t2a-Luc pellets was collected every 3 hours for 72 hours and stored at -20℃. IL-1Ra concentration was measured with DuoSet enzyme-linked immunosorbent assay (ELISA) specific to mouse IL-1Ra/IL-1F3 (R&D Systems). Data are reported as rates of formation with a 6h moving average.

Histological and biochemical analysis of tissue engineered cartilage

After 14 days of chondrogenic culture pellets were washed with PBS and fixed in 10% NBF for 24 hours, paraffin embedded, and sectioned at 8 μm thickness. Slides were stained for Safranin-O/hematoxylin/fast green (*91*).

For biochemical analysis, pellets were digested overnight in 125 μg/mL papain at 65℃. DNA content was measured with PicoGreen assay (Thermo Fisher) and total sulfated glycosaminoglycan (sGAG) content was measured using a 1,9-dimethylmethylene blue assay at 525 nm wavelength (*90*).

5.3.5 Inflammatory challenge

Per2-IL1Ra-t2a-Luc pellets underwent inflammatory challenge with 1 ng/mL IL-1α. Pellets were placed in recording medium and bioluminescence was recorded for 72 hours. After 72 hours of recording, cytokine was added to the dish and bioluminescence was recorded for an additional 72 hours.

5.3.6 *In vivo* characterization of chronogenetic therapy circuits

Per2-IL1Ra-t2a-Luc pellets were implanted into mice subcutaneously for circuit characterization and evaluation of therapeutic effect. 4 pellets per group were implanted into adult C57B/6 mice and were subject to evaluation. All procedures were approved by IACUC at Washington University in St. Louis.

Per2-IL1Ra-t2a-Luc entrainment characterization

Per2-IL1Ra-t2a-Luc pellets were characterized based on ability to entrain to mouse circadian rhythms through mouse actigraphy collection and bioluminescence imaging. Additionally, the ability for the Per2-IL1Ra-t2a-Luc circuit was evaluated through IL-1Ra serum concentration.

Mice were subjected to normal light/dark cycle and wheel running activity was collected. Bioluminescence was imaged every 4 hours for 36 hours. After bioluminescence imaging, pellet peak and trough were determined to be ZT 13 and ZT 5 respectively. To account for IL-1Ra translation, blood draws were taken from mice 4 hours after luminescence peak through cheek stab and serum collection. IL-1Ra serum levels were assessed by ELISA (Quantikine-IL1Ra, R&D Systems).

To evaluate if pellets have the ability to continue to entrain to mice circadian rhythm, mice were phase delayed 12h using a reversed light/dark schedule. Actigraphy data was collected continuously to monitor entrainment of activity and after 14 days, pellets were imaged for bioluminescence every 12 hours for 48 hours at ZT1 and ZT13. Additionally, serum was collected at the new peak and trough of bioluminescence expression and IL-1Ra serum was quantified by ELISA.

5.3.7 Statistical Analysis

Statistical analysis was performed using Prism. For all *in vitro* characterization of Per2-d2eGFP-t2a-Luc and Per2-IL1Ra-t2a-Luc circuits a one-way ANOVA with Tukey's HSD post hoc test was used to analyze GFP expression, IL-1Ra concentration, and *Il1rn* expression ($\alpha = 0.05$). For biochemistry data a one-way ANOVA with Dunnett's post hoc test was used with NT as the control ($\alpha = 0.05$). *In vivo* IL-1Ra serum was analyzed with a paired t-test ($\alpha = 0.05$).

5.4 Results

5.4.1 Characterization of chronogenetic reporter circuits and tissue engineered cartilage

To first evaluate the ability to create chronogenetic circuits, the ability of our synthetic circuits to drive production of both bioluminescence and a destabilized green fluorescence protein reporter (d2eGFP) in an oscillating manner was assessed. We found that our Per2-d2eGFP-t2a-Luc circuit had oscillating expression of luminescence (n=3, period=22.73±1.31h, Figure 5.2A) and d2eGFP protein expression (n=5, period=25±1.4h, Figure 5.2B), showing that our chronogenetic circuit concept is capable of driving timed expression of a desired output. Additionally, tissue engineered cartilage was evaluated for sulfated glycosaminoglycans (sGAG), a main component of the cartilage extracellular matrix. Non-transduced (NT) pellets and Per2-d2eGFP-t2a-Luc pellets were stained with safranin-O and both showed rich red stain for sGAGs (n=4/group, Figure 5.2C). Additionally, sGAG content was quantified and normalized to DNA content within each pellet (n=7/group, Figure 5.2D). There were no significant differences in sGAG content between groups, showing that our lentiviral chronogenetic therapy did not impact tissue-engineered cartilage formation. Therefore, our reporter chronogenetic circuit, Per2-d2eGFP-t2a-Luc, showed protein production driven by the circadian clock at prescribed times of day.

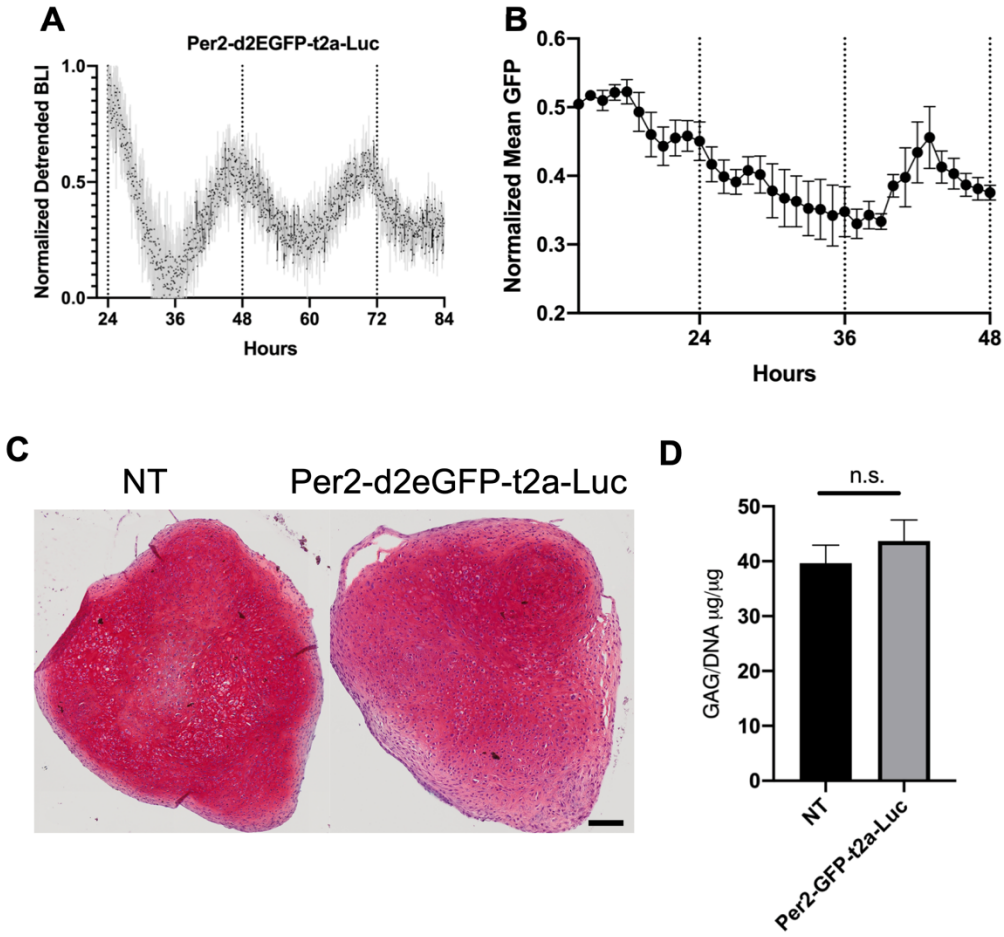

Figure 5.2 Characterization of chronogenetic therapy reporter circuit and tissue engineered cartilage. (A) Per2-d2eGFP-t2a-Luc bioluminescence intensity (BLI) in tissue engineered cartilage (n=3). (B) Mean GFP fluorescence intensity in digested pellets cast in agarose (n=5). (C) Safranin-O staining for sGAGs (n=4/group, scale bar=100 µM). (D) Quantification of sGAGs normalized to DNA content within each pellet (n=7/group). No significance between non-transduced (NT) and Per2-d2eGFP-t2a-Luc pellets (n.s.=no significance).

5.4.2 Synthetic chronogenetic IL-1Ra circuit produces IL-1Ra in a circadian manner

After seeing that our reporter circuit functioned well, we sought to test the ability of our Per2-IL1Ra-t2a-Luc chronogenetic circuit to produce IL-1Ra at different concentrations over time, with the overall goal of creating a circuit capable of inhibiting inflammatory flares at specific times of day. Per2-IL1Ra-t2a-Luc pellets showed circadian oscillations driven by Per2

(n=3, period=22.19±1.27h, Figure 5.3A). Additionally, it has been reported that inflammatory cytokines such as IL-1 can disrupt the circadian clock in cartilage (*33*) [See Chapter 4]. Therefore, we tested the ability of our Per2-IL1Ra-t2a-Luc circuit to maintain its oscillations in the presence of IL-1 and saw the maintenance of circadian oscillations after the addition of IL-1 (n=2, period=20.89±1.04h, Figure 5.3B). The maintenance of oscillations even in the presence inflammation provides additional support for the ability to use this circuit as a cell-based therapeutic to target inflammatory flares.

To determine the production of IL-1Ra, our therapeutic drug, we collected the media from Per2-IL1Ra-t2a-Luc pellets and collected the pellets for gene expression every 3 hours for 72 hours. Per2-IL1Ra-t2a-Luc pellets had increased *Il1rn* gene expression compared to NT controls (n = 6/group, $p<0.001$, Figure 5.3C). Additionally, *Il1rn* expression in our chronogenetic circuit showed circadian oscillations and a significant difference between one peak and trough of the *Il1rn* expression (period=22.8±3.6h, $p<0.05$, Figure 5.3C). Importantly, IL-1Ra production followed a similar oscillating trend to *Il1rn* gene expression and maintained a roughly 24-hour period of peak IL-1Ra expression driven by the circadian clock (n=6, period=22.5±2.9h, Figure 5.3D). Additionally, there were significant peaks of IL-1Ra production (33, 63, and 66 h, $p<0.04$) compared to troughs in IL-1Ra expression (42, 54, 57, 72 h, $p<0.01$, Figure 5.3D). Excitingly, this showed that our chronogenetic anti-inflammatory therapy had the ability to produce IL-1Ra at different times of day *in vitro.*

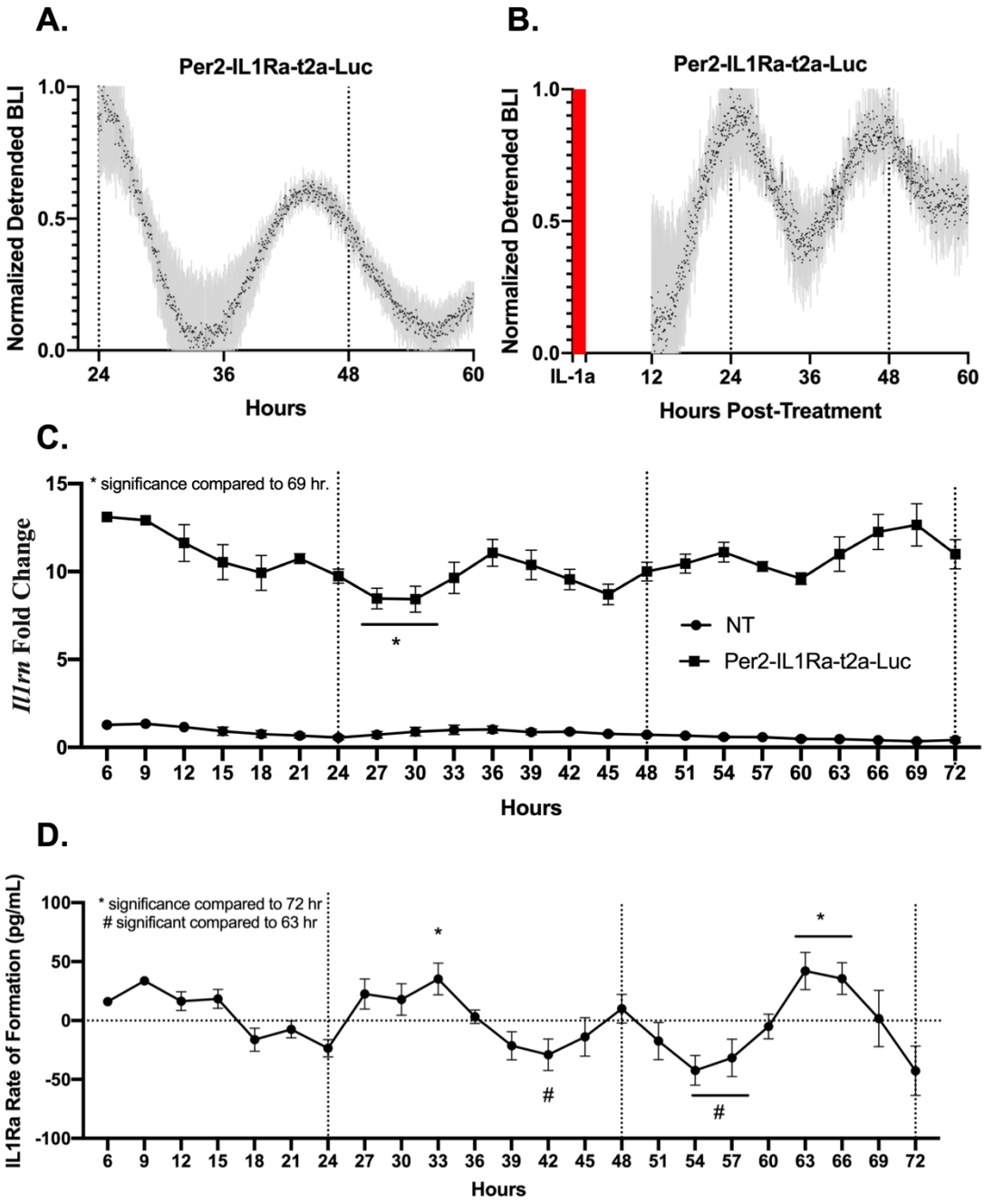
A.
Per2-IL1Ra-t2a-Luc
Normalized Detrended BLI
1.0
0.5
0.0
24
36
48
60
Hours
B.
Per2-IL1Ra-t2a-Luc
Normalized Detrended BLI
1.0
0.5
0.0
IL-1a
12
24
36
48
60
Hours Post-Treatment
C.
* significance compared to 69 hr.
Il1rn Fold Change
15
10
5
0
*
NT
Per2-IL1Ra-t2a-Luc
6 9 12 15 18 21 24 27 30 33 36 39 42 45 48 51 54 57 60 63 66 69 72
Hours
D.
* significance compared to 72 hr
# significant compared to 63 hr
IL1Ra Rate of Formation (pg/mL)
100
50
0
-50
-100
*
#
#
*
6 9 12 15 18 21 24 27 30 33 36 39 42 45 48 51 54 57 60 63 66 69 72
Hours

Figure 5.3 *In vitro* characterization of Per2-IL1Ra-t2a-Luc chronotherapy circuit. **(A)** BLI of Per2-IL1Ra-t2a-Luc pellets (n=3). **(B)** BLI of Per2-IL1Ra-t2a-Luc pellets after addition of 1 ng/mL of IL-1α (n=2). **(C)** Gene expression analysis of *Il1rn* (n=6/group, fold change relative to NT control at 0h). Samples collected every 3 hours for 72 hours. In the Per2-IL1Ra-t2a-Luc group there were oscillations of *Il1rn* expression and a significant decrease in expression at 27 and 39h compared to peak expression at 69h ($p<0.05$). Asterisks denotes significance compared to 69h. **(D)** IL-1Ra production over the course of 3 days in the Per2-IL1Ra-t2a-Luc circuits (n=6). The chronogenetic circuit produced oscillating IL-1Ra levels with a significant decrease in expression at 42, 57, and 60h compared to peak expression time of 63h ($p<0.01$) and a significant increase in expression at peak times 33, 63, and 66h compared to 72h ($p<0.04$). Asterisks denotes significance compared to 72h and hash denotes significance compared to 63h.

5.4.3 Chronogenetic IL-1Ra therapy circuits are capable of delivering IL-1ra at different times of day and can entrain to the circadian clock of the host *in vivo*

However, we wanted to test the effectiveness of this chronogenetic therapy approach *in vivo* both in our delivery mechanism and its ability to synchronize to the circadian clock of the host and in its ability to deliver therapeutic proteins at prescribed times. Therefore, we implanted the Per2-IL1Ra-t2a-Luc pellets into C57 mice in the flank. The bioluminescence of the pellets was monitored via around the clock (36h) bioluminescence intensity (BLI) imaging three days following implant and was found to be oscillatory, peaking at ZT13 (n=4, Figure 5.4B). Following the confirmation of circadian Per2-Luc gene expression *in vivo*, we assayed for IL-1Ra levels in serum through serial blood draws at 4h post BLI peak and trough, to account for the time to translation of IL-1Ra following peak Per2 promoter activation (Figure 5.4A). IL-1Ra concentration was significantly increased in the serum at 4h following the peak time of BLI compared to the trough of Per2 expression (n=4, p=0.0342, Figure 5.4C).

To assess entrainment of the implanted pellets to the mouse, the lighting schedule was reversed from standard 7a lights on/7p lights off to 8a lights off/8p lights on. For a week prior to

this transition and for a month following, mouse wheel-running actigraphy was tracked to monitor circadian entrainment to the light cycle. Within one-week post-delay, all mice were once again active during the dark phase and inactive in the light (Figure 5.4A). Following confirmation of re-entrainment via wheel running, the BLI of the implanted pellets was re-assessed. Bioluminescence imaging of pellets showed pellet entrainment to mouse circadian activity, with BLI peaking at ZT13, as observed previously (Figure 5.4D). Serum was again collected for IL-1Ra concentration 12 hours apart and IL-1Ra concentration was significantly increased during peak expression of *Per2* than during trough expression ($n=2$, $p = 0.046$, Figure 5.4E). Taken together, these results show the ability of our synthetic circuit to deliver IL-1Ra at different times of day, tracking with the clock component Per2, and the ability of our drug delivery system, a tissue engineered pellet, to entrain to the host for prescribed time of day treatment.

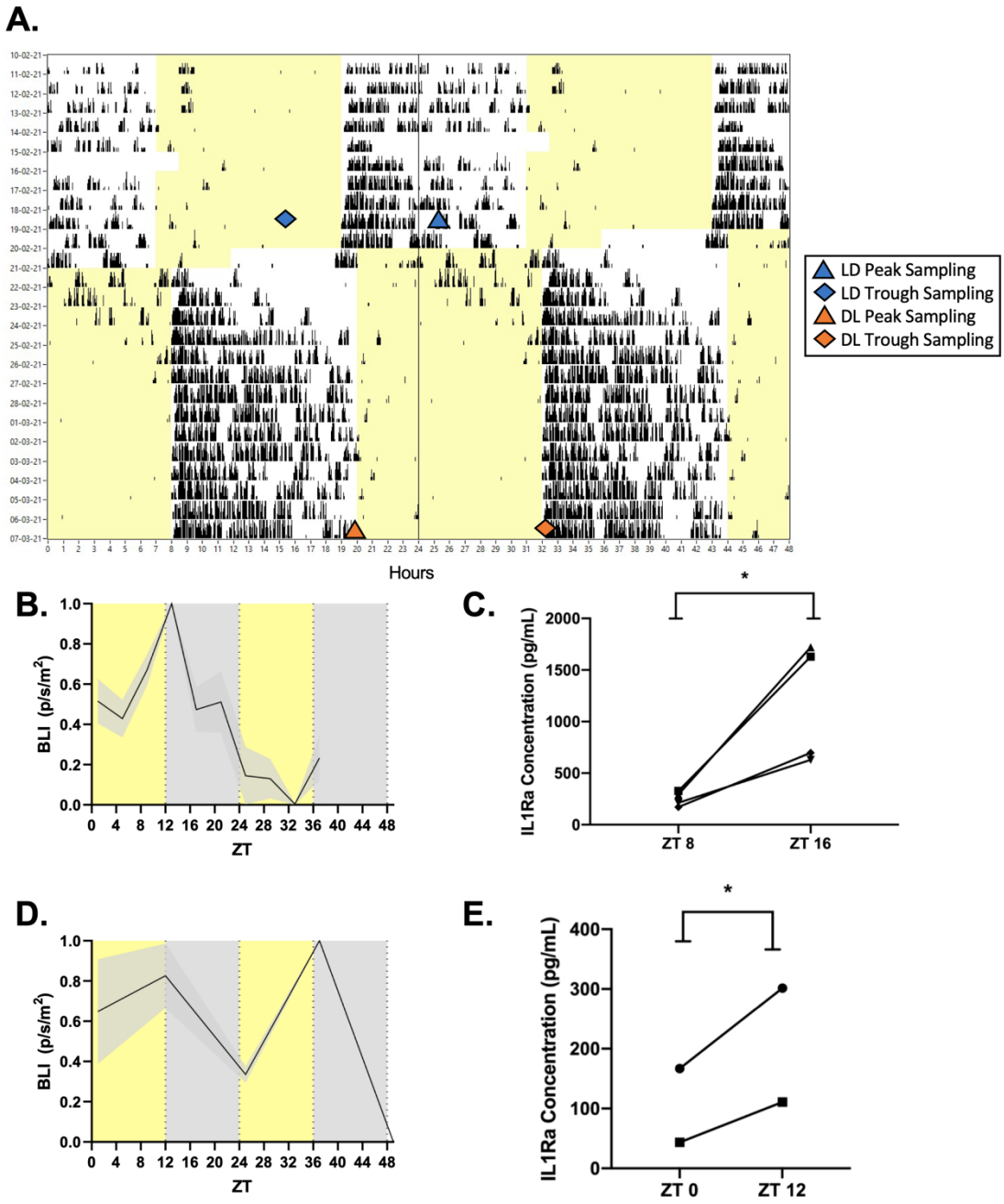

Figure 5.4 *In vivo* characterization of Per2-IL1Ra-t2a-Luc chronotherapy circuit. **(A)** Mouse wheel-running actigraphy recorded to monitor circadian entrainment to the light cycle. Yellow background is lights on; white background is lights off. **(B)** BLI of Per2-IL1Ra-t2a-Luc pellets implanted in mice three days after implant (n=4 mice 16 pellets). **(C)** Serum IL-1Ra concentration evaluated 4 hours post BLI peak and trough expression (n=4). Asterisks denotes significance within each sample, between timepoints. **(D)** BLI of pellets post entrainment to light/dark cycle (n=2 mice, 8 pellets). **(E)** Serum IL-1Ra concentration (n=2). Asterisks denotes significance within each sample, between timepoints.

5.5 Discussion

Going off the principles of chronotherapy, we used synthetic biology to develop cell-based chronogenetic therapies that are capable of delivering biologic drugs at prescribed times, tracking with circadian rhythms. To our knowledge, this is the first approach to create a cell therapy for timed drug delivery. While the notion of taking drugs in line with circadian rhythms is gaining popularity, the inconvenient times and need to take the drugs at the same time each day makes it difficult for patients to adhere to the chronotherapy approach. By harnessing the power of stem cells and creating a cell-therapy, we created a mechanism to deliver drugs at specific times without any burden on the patient that can also provide a more localized and controlled delivery of the drug. This approach can be used for disease targeting where symptoms or disease severity changes over the day and can be used for more effective delivery of growth factors or drugs targeting tissue homeostasis.

By developing an *in vitro* system to characterize our chronogenetic circuits we can create model systems to better understand the effect of chronotherapy on drug delivery and disease targets. Although circadian rhythms, clock-controlled genes, and their therapeutic counterparts are starting to be better understood, there are still many unknowns on the effect the core circadian clock has on specific genes, and the importance of timed drug delivery. Therefore, these synthetic circuits and *in vitro* characterization techniques can be used to better understand important connections between circadian rhythms and disease progression. Additionally, these systems can be used to deliver anabolic factors to cells to create better tissue engineered systems, as well as can be used to create *in vitro* model systems that can accurately depict cyclic disease states to better understand the effect of time.

Here we show that our anti-inflammatory chronogenetic circuit was capable of delivering the anti-inflammatory cytokine IL-1Ra in a timed and oscillating manner through different concentrations of protein in the serum. This system can be expanded beyond applications in RA and can be used for any inflammatory disease where there are inflammatory flares driven by the circadian clock. Additionally, this type of system can be used to deliver different concentrations of drugs at different times. Importantly, we also evaluated the ability of our tissue engineered cell therapy to entrain to its host, as this is important when producing chronogenetic therapies driven by the host circadian clock. Here we see that our tissue engineered constructs synchronize to the host and can continue to entrain even with shifts in circadian rhythms. The ability of the tissue engineered system to shift along with the mouse circadian clock is important in the ability of our tissue engineered systems to maintain prescribed drug delivery synchronized to personalized circadian rhythm even during perturbations or shifts in circadian rhythms that can happen with shift work, circadian disorders, and other disease pathologies that can affect the circadian clock.

Interestingly, we saw that our anti-inflammatory chronogenetic circuit was capable of maintaining its circadian rhythm in the presence of inflammatory cytokine, IL-1. Previously, it has been reported that inflammatory cytokines disrupt the circadian clock (*33, 181*) but that the administration of anti-inflammatory agents could restore the circadian clock. Therefore, our chronogenetic circuit is capable of being clock-preserving, which is important for its ability to deliver anti-inflammatory biologics at prescribed times of day. Additionally, this type of clock-preservation can help elucidate the relationship between circadian rhythms and inflammation.

The creation of these chronogenetic therapies opens up a whole new field of cell-based therapies and ways to enhance drug efficacy and mitigate side effects through the timed delivery

of drugs personalized to the patient's circadian rhythm. The chronogenetic circuits developed here were all driven by core clock gene *Per2*, however other core clock genes and the thousands of tissue-specific clock-controlled genes can be used for alternative timed delivery or for specific inputs. Additionally, multiple circuits can be used with antiphase drivers to create a two-pronged approach with one drug delivered at multiple peaks throughout the day or for two different drugs to be delivered at different times, depending on the need in disease progression. Additionally, mutations can be made in core clock genes to delay or advance the phase of the circadian clock, to tailor this approach to any timing of delivery (*195-197*).

Using this type of circadian clock driven chronogenetic therapy approach we can deliver drugs at specific times of day to enhance drug efficacy. This work can be directly used to targeting the inflammatory flares associated with RA. However, these approaches can also be expanded to create chronogenetic therapies for many different tissues and targeting different diseases where there are therapeutic targets for clock-controlled genes. Together, this framework for developing personalized chronogenetic therapies is a novel approach to establish a new generation of cell therapies that provide precision and effective therapeutic drug delivery.

5.6 Conclusions

We engineered cell therapies that are driven by the circadian clock component, Per2, to produced therapeutics at prescribed times of day driven by circadian rhythms. Tissue engineered cartilage pellets were used to deliver our chronogenetic therapies. *In vitro,* our Per2-IL1Ra-t2a-Luc circuit was capable of protecting itself from inflammation mediated circadian disruption and able to produce IL-1Ra at different concentrations throughout the day, tracking with *Per2* expression. *In vivo,* our tissue engineered pellets were capable of entraining their circadian rhythms to the host and were capable of producing IL-1Ra in the serum at different concentrations related to peak *Per2* expression and the trough of *Per2* expression. This is the first approach at creating temporally controlled synthetic cell circuits for cell-based chronotherapy of therapeutic interventions.

Chapter 6: Conclusions and Future Directions

With recent strides in the fields of synthetic biology and genome engineering, the ability to create cell-based therapies for disease treatment is more feasible than ever. We have applied these tools to target repair of articular cartilage in the presence of arthritic diseases such as osteoarthritis (OA) and rheumatoid arthritis (RA). In this way, we have created cell-based therapies that can deliver biologics in a prescribed, localized, and long-term manner mitigating many of the unwanted side-effects of systemic biologic delivery.

The work detailed in this dissertation establishes novel approaches for cell-based therapies targeting arthritis. By considering important stimuli that drive arthritis or are unique to articular cartilage, we first created synthetic circuits that can sense and respond to inflammation, can sense mechanical stimuli and respond, and can preserve the cartilage circadian clock even in the presence of desynchronizing stimuli such as inflammation. Finally, we build upon our circuits to create a novel cell therapy based on the principles of chronotherapy.

In Chapter 2 we discuss the development of a synthetic gene circuit that can sense activation of inflammatory signaling cascade NF-κB and produce an anti-inflammatory biologic in response, creating a self-regulating circuit. In Chapter 3 we show the creation of two synthetic circuits that are activated by mechanical loading, osmotic loading, or pharmacologic activation of TRPV4, a mechanobiologic ion channel in chondrocytes. These circuits have controlled production at different time scales in response to mechanical stimuli. In Chapter 4 we debut our clock-preserving cell therapies that can maintain the cartilage circadian clock even in the presence of inflammation. These cell-based therapies can be used to maintain the circadian clock to mitigate disease associated with clock desynchrony and can be used to elucidate

characteristics of the circadian clock that are not yet known. Finally, in Chapter 5 we introduce our revolutionary approach to cell-based chronotherapy, with the timed delivery of an anti-inflammatory agent driven by the circadian clock.

Although the main focus of these circuits was for use in tissue-engineered cartilage and targeting arthritis, these principles can be used to create smart cell therapies in any tissue or any field. Within cartilage, the therapeutic transgene can be replaced with a biologic to modulate arthritis pain or promote anabolic pathways to promote tissue regeneration. Additionally, these types of systems can be expanded to other musculoskeletal tissues. For example, we show in the Appendix a system in muscle cells to be able to sense and inhibit muscle fibrosis. These systems can be further expanded beyond musculoskeletal tissues and can be used in any diseases involving inflammation, mechanical stimuli, maintenance of the circadian clock, and/or requiring timed drug delivery. These systems will also further our understanding of important disease processes and can elucidate unknowns in disease pathologies. Finally, this work adds to the synthetic biology molecular toolkit of approaches to create better and more effective therapies to treat disease.

Appendix: Genome Engineered Muscle Derived Stem Cells for Autoregulated Anti-Inflammatory and Anti-Fibrotic Activity

Partially adapted from Pferdehirt L., Guo P., Lu A., Huard M., Guilak F.*, & Huard, J.* (2021). Genome engineered muscle derived stem cells for autoregulated anti-inflammatory and anti-fibrotic activity. *Orthopaedic Research Society 67th Annual Meeting.*

A.1 Abstract

Traumatic muscle injury leads to chronic and uncontrolled fibrosis in skeletal muscles, primarily driven through upregulation of transforming growth factor-β1 (TGF-β1). Cell-based therapies such as injection of muscle derived stem cells (MDSCs) has shown promise in muscle repair. However, these therapies remain challenging due to the harsh fibrotic environment within the injured muscle. Here, we created a "smart" cell-based drug delivery system using CRISPR-Cas9 to gene edit MDSCs capable of sensing TGF-β1 and producing an anti-fibrotic biologic, decorin. These gene edited smart cells, capable of inhibiting fibrosis in a dose-dependent and autoregulating manner, show anti-inflammatory and anti-fibrotic properties. Additionally, differentiation down a fibrotic lineage is eliminated in response to TGF-β1. Our results show that gene editing can be used to successfully create smart stem cells capable of producing biologic drugs in a controlled and localized manner. This autoregulating system provides a tool for cell-based drug delivery as the basis for a novel therapeutic approach for a variety of diseases.

A.2 Introduction

Muscle injuries commonly occur in teenagers and adults that participate in sports. While muscle injuries generally have good repair capacity, traumatic injury to the skeletal muscle usually causes fibrosis to develop, which leads to incomplete muscle repair and alters the functionality of the muscle. Fibrotic scar tissue not only blocks the regeneration process, but also predisposes the injured muscle to subsequent injuries (*198-200*). Muscle injury causes upregulation of inflammatory cytokines and infiltrating neutrophils, which increases the expression of transforming growth factor-β1 (TGF-β1), one of the main drivers of muscle fibrosis (*198, 199, 201-203*). TGF-β1 causes activation of my0fibroblasts and drives fibrotic scar tissue formation in the extracellular matrix (ECM) through upregulation of collagen 1 (*201*).

It has been shown that anti-fibrotic agents that inhibit TGF-β1, such as decorin, relaxin, suramin, gamma-interferon, and losartan, can reduce muscle fibrosis, leading to an improvement in muscle regeneration and repair (*202-213*). Decorin, a small leucine-rich proteoglycan, is a component of the ECM (*214*) and is important in regulating the assembly of collagenous matrices (*215*). Additionally, decorin interferes with muscle cell differentiation and migration, regulating connective tissue formation in skeletal muscle (*216-218*). Decorin has been shown to reduce muscle fibrosis by inhibiting TGF-β1 activity (*204, 212, 219, 220*). The delivery of decorin through an adeno-associated virus (AAV) gene therapy not only showed reduced muscle fibrosis, but also enhanced muscle regeneration (*202*).

In addition to anti-fibrotic agents, cell therapies have been shown to be effective in aiding in muscle repair. Muscle derived stem cells (MDSCs) are cells taken from neonatal mouse skeletal muscle and isolated through adhesion characteristics on collagen coated flasks (*221, 222*). Transplantation of MDSCs can improve muscle regeneration after injury (*201, 202*).

However, under the influence of TGF-β1 from the muscle injury microenvironment, the MDSCs themselves underwent differentiation down a fibrotic lineage and expressed TGF-β1, which further exacerbated the fibrosis cascade and limited the regenerative effect of the MDSCs (*201, 202, 223*). Therefore, to effectively use MDSCs as cell therapies for muscle repair, the fibrotic environment of the injured muscle must be inhibited. Combining losartan, an anti-fibrotic agent, with MDSC transplantation significantly improved the potential of the MDSCs to aid in muscle repair by inhibiting the differentiation of the MDSCs (*212*). However, systemic blockage of TGF-β1 through losartan or other anti-fibrotic therapeutics can be undesirable since TGF-β1 is important for the maintenance and repair of certain tissues (*224-226*). Additionally, pharmacologic therapies are given in high and unregulated doses and can have undesirable side effects, but new advances in cell therapies can overcome the disadvantages of pharmacologic therapies.

Previously, we have used CRISPR-Cas9 gene editing to create stem cells that can respond to inflammation in a feedback-controlled manner (*60*). Taking a similar approach, the goal of this study is to develop an autoregulated cell system with MDSCs that can respond to TGF-β1 by producing a biologic inhibitor of TGF-β1. In this way, we can create cell therapies that reduce fibrosis in the muscle, helping in overall muscle repair and promoting the reparative capabilities of MDSCs. To accomplish this goal, we first deconstructed the gene regulatory networks (GRNs) and signaling pathways activated in MDSCs by TGF-β1 to determine an optimal promoter to drive our gene circuit. We then used this promoter with CRISPR-Cas9 gene editing to create MDSCs responsive to TGF-β1 that produce decorin, promoting muscle repair by biologically inhibiting TGF-β1. Additionally, we incorporated luciferase within our circuit to as a reporter system (Figure A.1). Here, we show that TGF-β1 stimulation of our edited cells

elicits a dose-dependent and autoregulating response, reduces inflammatory and fibrotic markers, and eliminates the differentiation of MDSCs down a fibrotic lineage. This type of gene edited cell-based therapy could provide an effective method to inhibit muscle fibrosis after injury while overcoming limitations of current therapeutics.

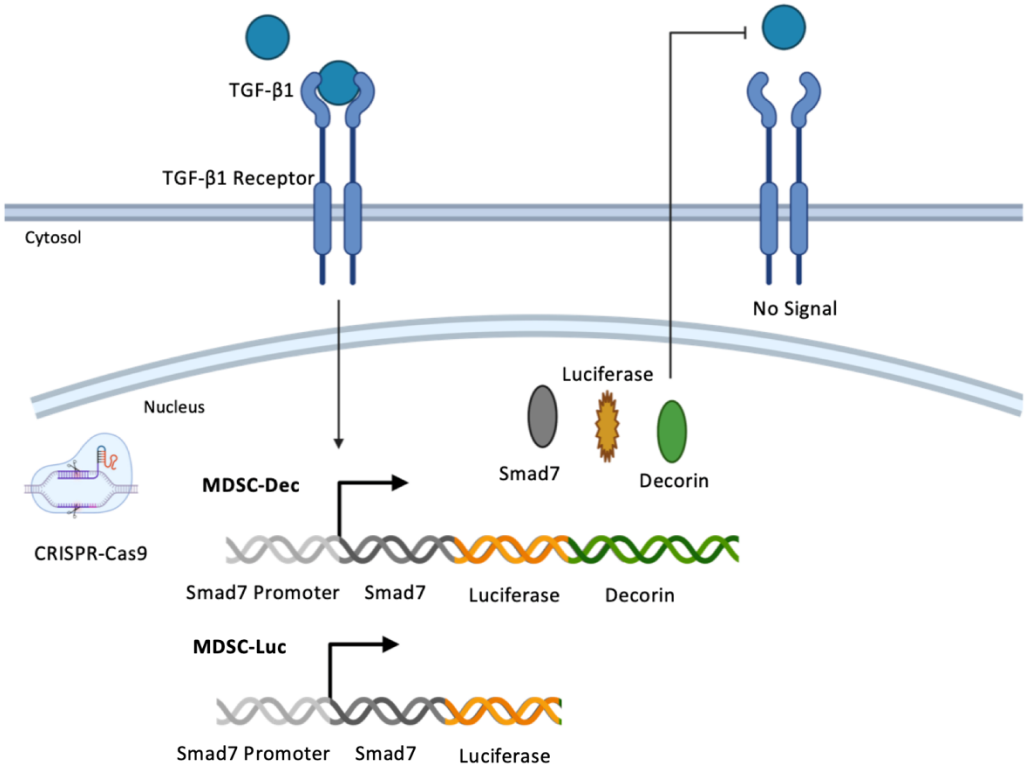

Figure A.1 Overview of design of CRISPR-Cas9 edited MDSCs. CRISPR-Cas9 was used to incorporate luciferase and murine decorin downstream of the functional Smad7 gene using a 2A component (MDSC-Dec). In the presence of TGF-β1, Smad7 is activated and the gene circuit produces Smad7, luciferase, and decorin. The production of decorin prevents TGF-β1from binding to the TGF-β1 receptor and inhibits activation of fibrotic cascades within the cell. A luciferase control line was also created without decorin (MDSC-Luc).

A.3 Materials and Methods

A.3.1 Isolation and Culture of MDSCs

MDSCs were isolated from C57BL/10J mice at 3 weeks of age by the pre-plate technique as previously described (*222*). MDSCs were cultured on collagen type I (Sigma-Aldrich) coated flasks in Dulbecco's Modified Eagle's Media-High Glucose (DMEM-HG, Gibco) containing 10% heat-inactivated fetal bovine serum (HI-FBS, Invitrogen), 10% horse serum (Invitrogen), 1% penicillin-streptomycin (P/S), and 0.5% chicken embryo extract (Gemini Bioproducts).

A.3.2 Gene Array Analysis

MDSCs were stimulated with 5ng/mL of TGF-β1 for 30 minutes. An untreated control was cultured under identical conditions without the TGF-β1. After 30 minutes, cells were collected and snap frozen in liquid nitrogen. Total RNA was extracted with Trizol reagent (Invitrogen) and subjected to a gene array. Significantly differentially expressed genes ($p<0.05$) were determined and fold changes in gene expression compared to untreated controls were calculated.

A.3.3 Gene Editing of MDSCs

Based on the gene array data, *Smad7* was determined as the target promoter to drive the gene circuit. Two cell lines were created, a luciferase control line (MDSC-Luc) and a decorin therapeutic line (MDSC-Dec). For the luciferase control line, targeting guides were produced in which coding sequences for the luciferase transgene were integrated directly downstream of the functional Smad7 transgene c-terminus with a t2a component incorporated. The therapeutic decorin line was produced by integrating decorin downstream of luciferase in the luciferase control line with a t2a component incorporated. Both lines are heterozygous edits. Cas9 and the

determined gRNAs were transfected into the MDSCs using Lipofectamine CRISPRMAX (Invitrogen) and clones were validated with junctional polymerase chain reaction (PCR) and sanger sequencing.

A.3.4 Luminescence Assay

Luciferase activity from MDSC-Luc and MDSC-Dec cells was measured using D-luciferin (Sigma-Aldrich) and a Cytation5 plate reader (Biotek). Luciferase activity is reported as a fold change of TGF-β1-stimulated cells over control cells cultured without TGF-β1 (n = 3).

A.3.5 Myogenic Differentiation Capacity

The myogenic differentiation capabilities of the MDSCs were assessed by switching the culture media into fusion media composed of DMEM-HG containing 2% HI-FBS and 1% P/S. After 3 days, the cells were strained for fast myosin heavy chain (MyHCf), which is a marker of terminal myogenic differentiation and 4',6-diamidino-2-phenylindole (DAPI). The level of myogenic differentiation was quantified as the percentage of MyHCf-expressing nuclei/total nuclei.

A.3.6 Decorin Gene Expression

Wild-type (WT), MDSC-Luc, and MDSC-Dec cells were stimulated with 0 ng/mL, 1 ng/mL, or 5 ng/mL TGF-β1 and collected for RNA isolation at 0, 0.5, 5, 12, and 24 hours (n = 3). RNA isolation was carried out following the manufacturer's protocol (Norgen). Reverse transcription was performed using Superscript VILO complementary DNA (cDNA) master mix (Invitrogen). Quantitative, reverse transcription polymerase chain reaction (qRT-PCR) was performed using Fast SyBR Green master mix (Applied Biosystems) following the manufacturer's protocol. Primer pairs were synthesized by Integrated DNA Technologies, Inc.

Genes were normalized to r18s. Fold changes were calculated using the $\Delta\Delta C_T$ method and are shown relative to the 0 hour no cytokine, WT control samples. For samples with no amplification, C_T threshold was set to the cycle limit.

A.3.7 Anti-Inflammatory and Anti-Fibrotic Activity of Engineered MDSCs

PCR for inflammatory (interleukin 1, *Il1* and interleukin 6, *Il6*) and fibrotic (fibronectin 1, *Fn1* and actin alpha 2, *Acta2*) was performed using ThermoScientific DreamTaq Green PCR Master Mix and the bands were imaged after agarose gel electrophoresis. The MDSC-Luc and MDSC-Dec lines were stimulated with 5 ng/mL of TGF-β1 and cells were harvested, and total RNA was extracted 12 hours post stimulation. Unstimulated control cells were harvested under identical conditions. *r18S* was used as the housekeeping control gene and normalized the bands.

Additionally, immunochemical labeling was performed for alpha-smooth muscle actin (α-SMA). Cultured cells were fixed in 5% formalin for 10 minutes and pre-incubated in 10% donkey serum in phosphate buffered saline for 1 hour at room temperature (RT). The cells were incubated for 3 hours at RT with primary antibodies for αSMA, Alexa 488-conjugated donkey anti-mouse IgG was used as secondary antibodies and DAPI was used for the nucleus.

A.3.8 Statistical Analysis

Statistical analysis was performed with Prism. Luminescence and decorin gene expression data were analyzed using analysis of variance (ANOVA) with Dunnet's post hoc testing using WT or unstimulated as the control ($\alpha = 0.05$). Data are displayed as mean ± SEM.

A.4 Results

A.4.1 Signaling pathways activated by TGF-β1 stimulation in MDSCs

MDSCs stimulated with 5 ng/mL of TGF-β1 showed 111 differentially expressed genes compared to unstimulated controls. Of the genes significantly upregulated compared to controls, four genes, *Smad7, Vegfa, Tgif1, and Spsb1,* showed the highest fold change in response to TGF-β1 by 30 minutes (Figure A.2) ($p<0.05$). Of the four genes, *Smad7* had the largest increase with a 17-fold change compared to unstimulated controls. Therefore, due to the rapid response and increased upregulation of *Smad7*, the *Smad7* promoter was utilized to drive our gene circuit. Additionally, due to the anti-fibrotic effects of *Smad7* (*227*), CRISPR-Cas9 was used to incorporate luciferase and murine decorin downstream of the functional *Smad7* gene using a 2A linker.

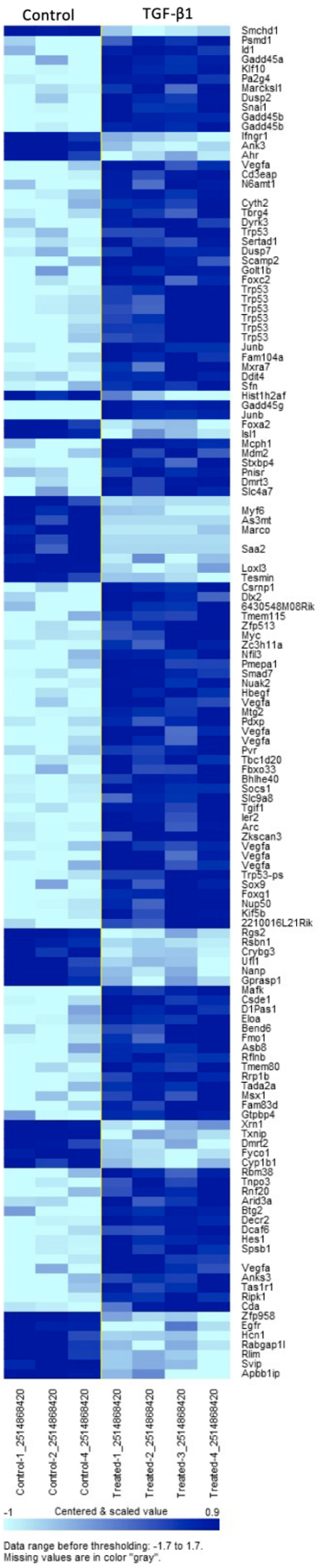

Figure A.2 Signaling pathways activated by TGF-β1 stimulation in MDSCs. MDSCs were treated with either 0 or 5 ng/mL of TGF-β1. 30 minutes after simulation, cells were collected for microarray. Displayed genes are scientifically differentially expressed ($p<0.05$) compared to controls (n=3-4).

A.4.2 Myogenic differentiation and response of gene edited MDSCs to TGF-β1

Gene edited MDSC-Luc and MDSC-Dec cells were tested in their ability to respond to TGF-β1 stimulation through luminescence output. MDSC-Luc and MDSC-Dec cells were treated with 5 ng/mL of TGF-β1 and compared with cells without TGF-β1. By 12 hours, both groups given TGF-β1 showed significant luminescence output compared to cells without cytokine (Figure A.3A) ($p<0.05$). This increase in luminescence shows that the gene circuit can sense and respond to TGF-β1 stimulation.

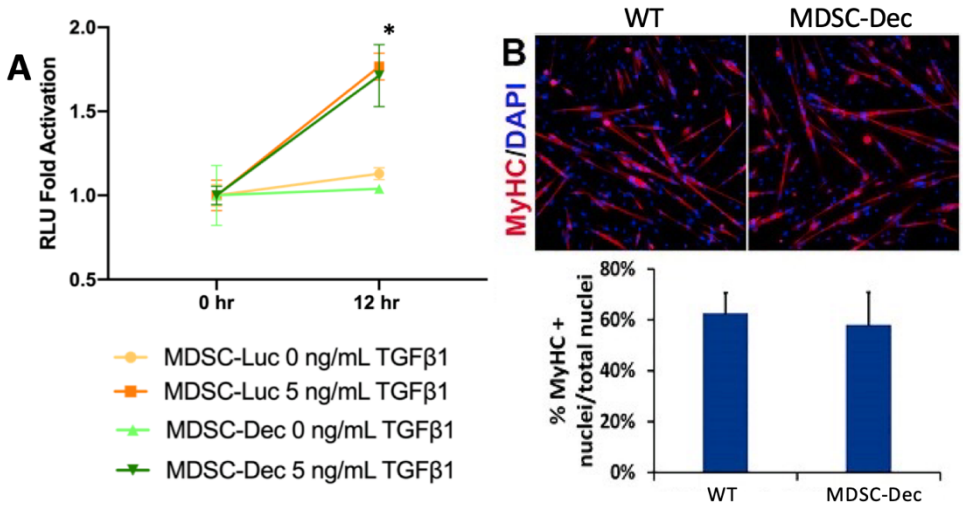

Figure A.3 Characterization of gene edited MDSCs to determine responsiveness to TGF-β1 and ability to myogenically differentiate. **(A)** MDSC-Luc and MDSC-Dec cells were stimulated with 0 or 5 ng/mL of TGF-β1, and luminescence was measured at 0 and 12 hours. Data represents mean relative luminescence (RLU) fold change ± SEM (n=3). Two-way ANOVA with Dunnett's post-hoc was used to determine significance. Asterisks represent significance ($p<0.05$) compared to 0-hour control. **(B)** Wild type (WT) MDSCs and MDSC-Dec cells stained with fast myosin heavy chain (MyHCf), a marker of terminal myogenic differentiation, and DAPI, a nuclear stain. Level of myogenic differentiation is quantified as the percentage of MyHCf-expression nuclei/total nuclei ± SEM.

To evaluate if the ability to myogenically differentiate was maintained after gene editing, MDSC-Dec cells were stained for fast myosin heavy chain (MyHCf), a marker of terminal myogenic differentiation. MDSC-Dec cells showed similar cell morphology and levels of MyHCf stain compared to WT MDSCs (Figure A.3B), indicating that gene editing and decorin expression in the cells does not affect the differentiation potential of the MDSCs.

A.4.3 Gene edited MDSC-Dec produce decorin in a dose-responsive and autoregulated manner

Non-edited wild type (WT) MDSCs and MDSC-Dec cells were stimulated with 1 ng/mL or 5 ng/mL of TGF-β1, and decorin expression was measured over time. Cells receiving no TGF-β1 were used as controls. At all timepoints, the MDSC-Dec groups at all doses of TGF-β1 showed significantly increased decorin expression compared to WT (Figure A.4) ($p<0.001$). MDSC-Dec cells responded to TGF-β1 in a dose dependent manner, where both the 1 ng/mL and 5 ng/mL dose of TGF-β1 showed significant decorin expression compared to unstimulated MDSC-Dec cells ($p<0.05$). The MDSC-Dec cells receiving 5 ng/mL showed increased decorin expression compared to 1 ng/mL TGF-β1 except at 24 hours (Figure A.4). Additionally, decorin expression in the MDSC-Dec cells was significantly decreased between 12 and 24 hours (Figure A.4) ($p<0.01$). This decrease in decorin expression shows the ability of the MDSC-Dec cells to produce enough decorin by 12 hours to inhibit TGF-β1 and turn the circuit off. Therefore, the MDSC-dec cells respond to TGF-β1 in a dose-dependent manner and the gene edited circuit is auto-regulating.

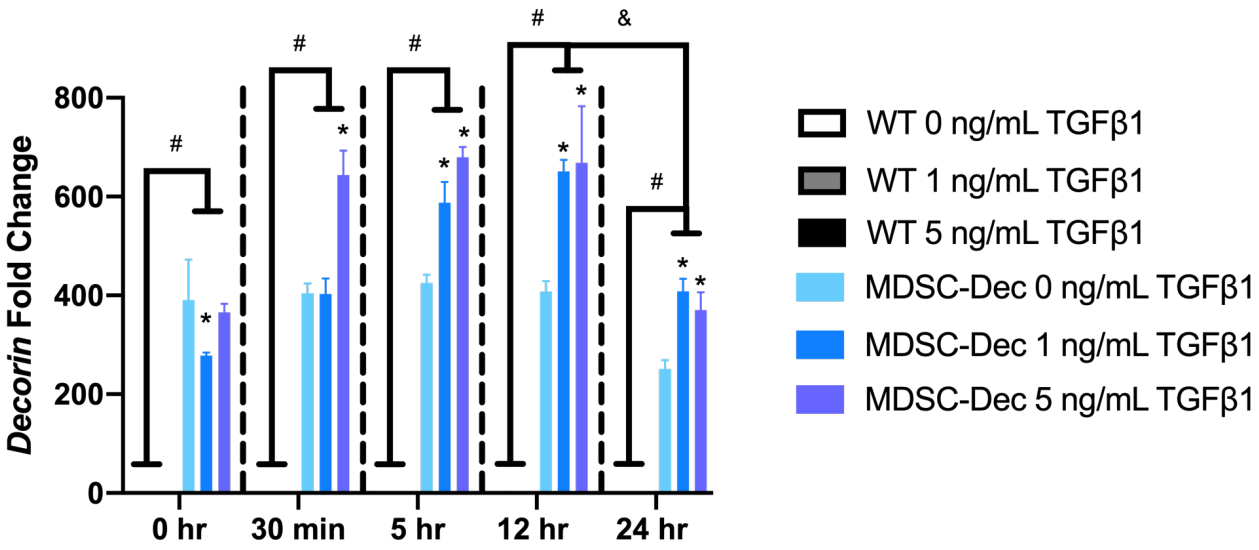

Figure A.4 Gene expression of WT and MDSC-Dec given 0, 1, or 5 ng/mL TGF-β1. Fold changes were determined relative to 0-hour WT cells without TGF-β1. Error bars represent means of fold change ± SEM (n=3). Asterisks represent significance within MDSC-Dec groups compared to MDSC-Dec group given 0 ng/mL of TGF-β1 ($p<0.05$). Hashes represent significance relative to WT control group ($p<0.05$). Ampersand represents significance within MDSC-Dec groups between 12 and 24 hours ($p<0.05$). Statistics analyzed with two-way ANOVA.

A.4.4 MDSC-Dec cells reduce inflammatory and fibrotic markers and eliminate fibrotic differentiation of MDSCs

MDSC-Luc and MDSC-Dec cells were stimulated with 5 ng/mL of TGF-β1 and compared to untreated MDSC-Luc and MDSC-Dec controls. Inflammatory cytokines *Il6* and *Il1* were downregulated in the MDSC-Dec cells in response to TGF-β1 compared to MDSC-Luc cells (Figure A.5A). Additionally, pro-fibrotic gene *Fn1* was also decreased in the MDSC-Dec cells in response to TGF-β1 after 12 hours compared to MDSC-Luc cells (Figure A.5A). This shows the anti-inflammatory and anti-fibrotic activity of the MDSC-Dec cells.

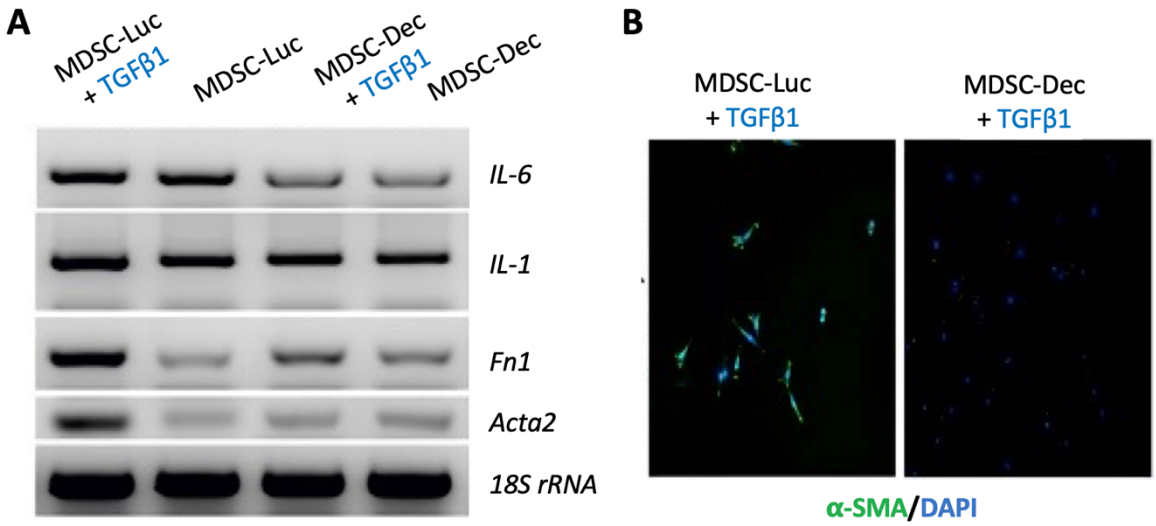

Figure A.5 Assessment of MDSC-Dec ability to reduce inflammation, fibrosis, and fibrotic differentiation. **(A)** Expression of inflammatory markers *Il6* and *Il1,* fibrotic marker *Fn1,* and *Acta2,* a gene encoding alpha smooth muscle actin (α-SMA) in MDSC-Dec and MDSC-Luc lines with and without TGF-β1 stimulation after 12 hours. *18S* rRNA used as housekeeping gene. **(B)** Staining for α-SMA (green) and DAPI (blue) in MDSC-Luc and MDSC-Dec cells treated with TGF-β1.

TGF-β1 stimulated MDSC-Dec cells also showed a decrease in *Acta2*, a gene encoding α smooth muscle actin (α-SMA) which is highly expressed in myofibroblasts, compared to MDSC-Luc cells (Figure A.5A). This result was further supported by the inability to detect α-SMA in MDSC-Dec cells treated with TGF-β1 compared to MDSC-Luc (Figure A.5B). Together, these results indicate that the TGF-β1 induced differentiation of MDSCs towards myofibroblasts, which can further exacerbate fibrosis, was reduced or eliminated.

A.5 Discussion

A major challenge in muscle repair and regeneration after injury is the injury-associated fibrotic microenvironment causing cell differentiation down a fibrotic lineage, further exacerbating fibrosis. We developed a MDSC-based smart cell using CRISPR-Cas9 in which cells sense and respond to fibrotic stimuli by producing anti-fibrotic biologic drugs. By utilizing

MDSCs that have the ability to engraft onto muscle and aid in muscle regeneration (*201, 202, 223*), this system provides the potential to repair muscle, while providing site-specific and autoregulated anti-fibrotic therapy. Our approach is based on the presence of TGF-β1, a main driver of muscle fibrosis, and coopting endogenous signaling pathways within MDSCs to produce anti-fibrotic biologic therapeutics. By deconstructing the differentially expressed genes activated by TGF-β1, we rewired endogenous gene expression to drive production of decorin, an anti-fibrotic, as a model system. Our results also demonstrate the use of this signaling pathway for defining the timing and dose-response for the expression of therapeutic biologic drugs. Additionally, we show the ability of the system to autoregulate itself. While we target a treatment for skeletal muscle repair in traumatic injury, fibrosis occurs in many tissues and in both acute and chronic diseases, suggesting a wide range of potential therapeutic applications for anti-fibrotic cell therapies.

An important advance of this work is the use of MDSCs, which provide an attractive cell source for muscle repair and regeneration because of their innate ability to differentiate into functional muscle cells *in vivo,* as well as their ability to reduce fibrosis and aid in muscle repair (*201, 202, 223*). Additionally, MDSCs have the ability to not only aid in skeletal muscle repair, but other musculoskeletal cell types as well, expanding the potential use for these MDSC smart cells (*221, 222*). Here, we show that our MDSC-Dec cells reduced pro-inflammatory and pro-fibrotic markers in the presence of TGF-β1, mitigating fibrosis. This indicates the potential use of this system for the repair of injured skeletal muscle and mitigation of fibrosis through a soluble release of decorin. Importantly, MDSC-Dec cells had no presence of α-SMA when given TGF-β1. Previous limitations in MDSC cell therapies were due to the differentiation of MDSCs into myofibroblasts in muscle injury microenvironment with high levels of TGF-β1, leading to

enhanced fibrosis (*201, 202, 223*). With our MDSC-Dec smart cells and the lack of α-SMA we show the TGF-β1-induced differentiation into myofibroblasts is eliminated in our cells, enhancing the ability of these MDSCs to maintain their regenerative capabilities.

Using CRSIPR-Cas9 gene editing, we engineered MDSC smart cells that produce luciferase and decorin downstream of the functional *Smad7* gene, creating a system that can dynamically respond to and attenuate TGF-β1. MDSC-Dec cells rapidly responded to TGF-β1 in a dose dependent manner, as cells given different doses of TGF-β1 had significant increases of decorin expression by 5 hours and higher doses of TGF-β1 resulted in increased decorin expression up to 12 hours. This dose response allows for controlled production of the therapeutic drug in response to different levels of fibrosis. Importantly, MDSC-Dec cells produced therapeutic levels of decorin so that TGF-β1 was inhibited and the gene circuit was shutting off by 24 hours. While we designed the MDSC smart cells to respond to TGF-β1 by producing decorin, there are many other drivers of fibrosis (*228*) as well as other anti-fibrotic agents that can be utilized as biologic therapeutics (*202-213*). Additionally, this approach can be readily expanded to other fibrotic diseases.

Current approaches for treatment of muscle fibrosis involve the use of anti-fibrotic agents (*202-213*). However, systemic inhibition of TGF-β1 leads to unwanted side effects (*224-226*). Additionally, for effective mitigation of fibrosis at the injured muscle, high doses of anti-fibrotic agents must be given because only a small amount makes it to the injury site. These approaches result in ineffective strategies to inhibit muscle fibrosis, calling for more effective and localized therapies. Previous approaches to target delivery of anti-fibrotic agents have used non-integrating viral vectors such as AAV (*202*). CRISPR-Cas9 editing techniques are advantageous for this system due to its precision in editing the cell, as well as use of endogenous pathways within the

cell, leading to prolonged life of the gene circuit and controlled activation of the circuit compared to non-integrating systems or synthetic circuits that do not utilize the endogenous pathways of the cell that can be subjected to silencing and random integration of the circuit.

Our gene edited cells have an autoregulating circuit that is capable of sensing and responding to fibrosis with a therapeutic level of biologic drug. The ability to use CRISPR-Cas9 allows the tunability of biologic drug produced, as well as endogenous signaling cascade as the input to the circuit. Similar approaches have been used to create CRISPR-based therapies for inflammation (*60*), broadening the applicability of this type of gene circuit beyond muscle injury-induced fibrosis. The continued development of designer circuits through gene switches (*114-116*), microRNA classifiers (*117, 229*), synthetic transcription systems (*119-121*), and lentiviral based cell-therapies (*62, 63*) provides a toolkit to engineer more complex circuits with specialized control. This work adds to our long-term goal of developing a molecular toolbox (*122, 123*) of biological building blocks for applications in mammalian cells for mitigating chronic diseases.

It is important to note potential limitations and future directions of this work. The microarray analysis offers us a look at the unique transcriptomic landscape in MDSCs in response to TGF-β1 stimulation. However, with the advent of next-generation sequencing technologies, performing a similar experiment and transcriptomic analysis would increase target resolution and give us a more precise analysis of genes activated by TGF-β1 and help us identify novel targets for future gene circuits. Additionally, although these cells have been tested *in vitro*, subsequent *in vivo* experiments will be necessary to fully determine the anti-fibrotic and reparative capabilities of the MDSC smart cells. Injecting the MDSCs into mice after muscle injury will help determine the efficacy of the circuit to inhibit fibrosis in the context of multiple

fibrotic inputs, in addition to TGF-β1 and determine the ability of MDSCs to maintain their regenerative phenotype instead of differentiating down a pro-fibrotic lineage.

The autoregulatory capabilities of this system, along with the use of a localized cell-based system, allows for applications in regenerative medicine or any chronic fibrotic disease. Applying these cells not only allows for localized anti-fibrotic therapies, but also provides regenerative potential to MDSCs. Together, this system allows for precise and localized delivery of therapeutics and can be broadly applicable in developing autoregulating systems for drug delivery in fibrotic diseases.

A.6 Conclusion

We created gene edited smart cells in MDSCs that can sense TGF-β1 and, instead of eliciting a fibrotic response and differentiation down a fibrotic lineage, produce decorin, a small molecule that inhibits TGF-β1 and reduces fibrosis. These cells respond in an autoregulating and dose-dependent manner to rapidly produce therapeutic levels of decorin. The anti-inflammatory and anti-fibrotic properties, as well as reduced differentiation down a fibrotic lineage of the gene edited MDSCs will allow for these cells to aid in muscle repair and regeneration, even in a fibrotic microenvironment. Broadly, this approach may be applicable in developing autoregulated biologic systems for drug delivery in fibrotic diseases.

References

1. Y. Luo *et al.*, The minor collagens in articular cartilage. *Protein Cell* **8**, 560-572 (2017).
2. Z. Lin, C. Willers, J. Xu, M. H. Zheng, The chondrocyte: biology and clinical application. *Tissue Eng* **12**, 1971-1984 (2006).
3. A. J. Sophia Fox, A. Bedi, S. A. Rodeo, The basic science of articular cartilage: structure, composition, and function. *Sports Health* **1**, 461-468 (2009).
4. V. C. Mow, A. Ratcliffe, A. R. Poole, Cartilage and diarthrodial joints as paradigms for hierarchical materials and structures. *Biomaterials* **13**, 67-97 (1992).
5. D. Ingber, Mechanobiology and diseases of mechanotransduction. *Annals of medicine* **35**, 564-577 (2003).
6. C. T. Lim, A. Bershadsky, M. P. Sheetz. (The Royal Society, 2010).
7. W. Liedtke *et al.*, Vanilloid receptor-related osmotically activated channel (VR-OAC), a candidate vertebrate osmoreceptor. *Cell* **103**, 525-535 (2000).
8. W. Liedtke, D. M. Tobin, C. I. Bargmann, J. M. Friedman, Mammalian TRPV4 (VR-OAC) directs behavioral responses to osmotic and mechanical stimuli in Caenorhabditis elegans. *Proceedings of the National Academy of Sciences* **100**, 14531-14536 (2003).
9. M. N. Phan *et al.*, Functional characterization of TRPV4 as an osmotically sensitive ion channel in porcine articular chondrocytes. *Arthritis & Rheumatism: Official Journal of the American College of Rheumatology* **60**, 3028-3037 (2009).
10. L. Ying *et al.*, The transient receptor potential vanilloid 4 channel modulates uterine tone during pregnancy. *Science translational medicine* **7**, 319ra204-319ra204 (2015).
11. M. Suzuki *et al.*, Localization of mechanosensitive channel TRPV4 in mouse skin. *Neuroscience letters* **353**, 189-192 (2003).
12. C. J. O'Conor, H. A. Leddy, H. C. Benefield, W. B. Liedtke, F. Guilak, TRPV4-mediated mechanotransduction regulates the metabolic response of chondrocytes to dynamic loading. *Proc Natl Acad Sci U S A* **111**, 1316-1321 (2014).
13. M. H. Hastings, A. B. Reddy, E. S. Maywood, A clockwork web: circadian timing in brain and periphery, in health and disease. *Nat Rev Neurosci* **4**, 649-661 (2003).
14. J. S. Takahashi, H. K. Hong, C. H. Ko, E. L. McDearmon, The genetics of mammalian circadian order and disorder: implications for physiology and disease. *Nat Rev Genet* **9**, 764-775 (2008).
15. T. Roenneberg, M. Merrow, Circadian clocks - the fall and rise of physiology. *Nat Rev Mol Cell Biol* **6**, 965-971 (2005).
16. M. M. Dudek, Q. J., Running on time: the role of circadian clocks in the musculoskeletal system. *Biochem* **463**, 1-8 (2014).
17. M. L. Andersson *et al.*, Diurnal variation in serum levels of cartilage oligomeric matrix protein in patients with knee osteoarthritis or rheumatoid arthritis. *Ann Rheum Dis* **65**, 1490-1494 (2006).
18. M. Dudek *et al.*, Circadian time series proteomics reveals daily dynamics in cartilge physiology. *Biorxiv*, (2019).
19. M. Dudek *et al.*, The chondrocyte clock gene Bmal1 controls cartilage homeostasis and integrity. *J Clin Invest* **126**, 365-376 (2016).

20. S. Y. S. Kong, T. V.; Criscione, L. G.; Elliott, A. L.; Jordan, J. M.; Kraus, V. B., Diurnal Variation of Serum and Urine Biomarkers in Patients with Radiographic Knee Osteoarthritis. *Arthritis Rheum* **54**, 2496-2504 (2006).
21. N. Gossan *et al.*, The circadian clock in murine chondrocytes regulates genes controlling key aspects of cartilage homeostasis. *Arthritis Rheum* **65**, 2334-2345 (2013).
22. N. Yang, Q. J. Meng, Circadian Clocks in Articular Cartilage and Bone: A Compass in the Sea of Matrices. *J Biol Rhythms* **31**, 415-427 (2016).
23. S. B. Abramson, M. Attur, Developments in the scientific understanding of osteoarthritis. *Arthritis Res Ther* **11**, 227 (2009).
24. M. Kapoor, J. Martel-Pelletier, D. Lajeunesse, J. P. Pelletier, H. Fahmi, Role of proinflammatory cytokines in the pathophysiology of osteoarthritis. *Nat Rev Rheumatol* **7**, 33-42 (2011).
25. P. Wehling *et al.*, Clinical responses to gene therapy in joints of two subjects with rheuamtoid arthritis *Human Gene Therapy* **20**, 97-101 (2009).
26. N. Wehling *et al.*, Interleukin-1beta and tumor necrosis factor alpha inhibit chondrogenesis by human mesenchymal stem cells through NF-kappaB-dependent pathways. *Arthritis Rheum* **60**, 801-812 (2009).
27. M. B. Goldring, S. R. Goldring, Articular cartilage and subchondral bone in the pathogenesis of osteoarthritis. *Ann N Y Acad Sci* **1192**, 230-237 (2010).
28. M. B. G. Goldring, S. R. , Osteoarthritis. *J. Cell. Physiol* **213**, 626-634 (2007).
29. M. B. Goldring, M. Otero, Inflammation in osteoarthritis. *Curr Opin Rheumatol* **23**, 471-478 (2011).
30. S. Rigoglou, A. G. Papavassiliou, The NF-kappaB signalling pathway in osteoarthritis. *Int J Biochem Cell Biol* **45**, 2580-2584 (2013).
31. Y. Bastiaansen-Jenniskens, D. Saris, L. B. Creemers, Pro- and Anti-inflammatory Cytokine Profiles in Osteoarthritis. 81-97 (2017).
32. J. Bondeson, S. Wainwright, C. Hughes, B. Caterson, The regulation of the ADAMTS4 and ADAMTS5 aggrecanases in osteoarthritis: a review. *Clin Exp Rheumatol* **26**, 139-145 (2008).
33. B. Guo *et al.*, Catabolic cytokines disrupt the circadian clock and the expression of clock-controlled genes in cartilage via an NFsmall ka, CyrillicB-dependent pathway. *Osteoarthritis Cartilage* **23**, 1981-1988 (2015).
34. N. Gossan, R. Boot-Handford, Q. J. Meng, Ageing and osteoarthritis: a circadian rhythm connection. *Biogerontology* **16**, 209-219 (2015).
35. W. M. Oo, S. P. Yu, M. S. Daniel, D. J. Hunter, Disease-modifying drugs in osteoarthritis: current understanding and future therapeutics. *Expert Opin Emerg Drugs* **23**, 331-347 (2018).
36. E. H. Choy, A. F. Kavanaugh, S. A. Jones, The problem of choice: current biologic agents and future prospects in RA. *Nat Rev Rheumatol* **9**, 154-163 (2013).
37. B. D. Furman *et al.*, Targeting pro-inflammatory cytokines following joint injury: acute intra-articular inhibition of interleukin-1 following knee injury prevents post-traumatic arthritis. *Arthritis Res Ther* **16**, (2014).
38. X. Chevalier *et al.*, Intraarticular injection of anakinra in osteoarthritis of the knee: a multicenter, randomized, double-blind, placebo-controlled study. *Arthritis Rheum* **61**, 344-352 (2009).

39. M. Grunke, H. Schulze-Koops, Successful treatment of inflammatory knee osteoarthritis with tumour necrosis factor blockade. *Ann Rheum Dis* **65**, 555-556 (2006).
40. A. Fioravanti, M. Fabbroni, A. Cerase, M. Galeazzi, Treatment of erosive osteoarthritis of the hands by intra-articular infliximab injections: a pilot study. *Rheumatol Int* **29**, 961-965 (2009).
41. J. P. Pelletier *et al.*, In vivo suppression of early experimental osteoarthritis by interleukin-1 receptor antagonist using gene therapy. *Arthritis Rheum* **40**, 1012-1019 (1997).
42. M. Schieker *et al.*, Effects of Interleukin-1beta Inhibition on Incident Hip and Knee Replacement : Exploratory Analyses From a Randomized, Double-Blind, Placebo-Controlled Trial. *Ann Intern Med* **173**, 509-515 (2020).
43. M. Ramos-Casals, P. Brito-Zeron, M. J. Soto, M. J. Cuadrado, M. A. Khamashta, Autoimmune diseases induced by TNF-targeted therapies. *Best Pract Res Clin Rheumatol* **22**, 847-861 (2008).
44. F. D. Keyser, Choice of Biologic Therapy for Patients with Rheumatoid Arthritis: The Infection Perspective. *Curr Rheumatol Rev* **7**, 77-87 (2011).
45. C. H. Evans, S. C. Ghivizzani, P. D. Robbins, Gene Delivery to Joints by Intra-Articular Injection. *Hum Gene Ther* **29**, 2-14 (2018).
46. C. H. Evans *et al.*, Gene transfer to human joints: progress toward a gene therapy of arthritis. *Proc Natl Acad Sci U S A* **102**, 8698-8703 (2005).
47. M. B. Goldring, F. Berenbaum, Emerging targets in osteoarthritis therapy. *Curr Opin Pharmacol* **22**, 51-63 (2015).
48. M. Cucchiarini, H. Madry, Biomaterial-guided delivery of gene vectors for targeted articular cartilage repair. *Nat Rev Rheumatol* **15**, 18-29 (2019).
49. B. O. Diekman *et al.*, Cartilage tissue engineering using differentiated and purified induced pluripotent stem cells. *Proc Natl Acad Sci U S A* **109**, 19172-19177 (2012).
50. V. P. Willard *et al.*, Use of cartilage derived from murine induced pluripotent stem cells for osteoarthritis drug screening. *Arthritis Rheumatol* **66**, 3062-3072 (2014).
51. H. Madry, P. Orth, M. Cucchiarini, Gene Therapy for Cartilage Repair. *Cartilage* **2**, 201-225 (2011).
52. S. Auslander, M. Fussenegger, Engineering Gene Circuits for Mammalian Cell-Based Applications. *Cold Spring Harb Perspect Biol* **8**, (2016).
53. J. M. Brunger, A. Zutshi, V. P. Willard, C. A. Gersbach, F. Guilak, CRISPR/Cas9 Editing of Murine Induced Pluripotent Stem Cells for Engineering Inflammation-Resistant Tissues. *Arthritis Rheumatol* **69**, 1111-1121 (2017).
54. P. S. Rachakonda, M. F. Rai, M. F. Schmidt, Application of inflammation-responsive promoter for an in vitro arthritis model. *Arthritis Rheum* **58**, 2088-2097 (2008).
55. J. L. Bondeson, S.; Wainwright, S.; Amos, N.; Evans, A.; Hughes, C.; Feldmann, M.; Caterson, B., Adenoviral gene transfer of the endogenous inhibitor IkappaBalpha into human osteoarthritis synovial fibroblasts demonstrates that several matrix metalloproteinases and aggrecanases are nuclear factor-kappaB-dependent. *Rheumatology* **34**, 523-523 (2007).
56. F. T. Moutos *et al.*, Anatomically shaped tissue-engineered cartilage with tunable and inducible anticytokine delivery for biological joint resurfacing. *Proc Natl Acad Sci U S A* **113**, E4513-4522 (2016).

57. J. M. Brunger *et al.*, Scaffold-mediated lentiviral transduction for functional tissue engineering of cartilage. *Proc Natl Acad Sci U S A* **111**, E798-806 (2014).
58. K. A. Glass *et al.*, Tissue-engineered cartilage with inducible and tunable immunomodulatory properties. *Biomaterials* **35**, 5921-5931 (2014).
59. F. Guilak *et al.*, Designer Stem Cells: Genome Engineering and the Next Generation of Cell-Based Therapies. *J Orthop Res* **37**, 1287-1293 (2019).
60. J. M. Brunger, A. Zutshi, V. P. Willard, C. A. Gersbach, F. Guilak, Genome Engineering of Stem Cells for Autonomously Regulated, Closed-Loop Delivery of Biologic Drugs. *Stem Cell Reports* **8**, 1202-1213 (2017).
61. Y. R. C. Choi, K. H.; Springer, L. E.; Pferdehirt, L.; Ross, A. K.; Wu, C. L.; Moutos, F. T.; Harasymowicz, N. S.; Brunger, J. M.; Pham, C. T. N.; Guilak, F., A genome-engineered bioartificial implant for autoregulated anti-cytokine drug delivery. *Biorxiv*, (2019).
62. L. Pferdehirt, A. K. Ross, J. M. Brunger, F. Guilak, A Synthetic Gene Circuit for Self-Regulating Delivery of Biologic Drugs in Engineered Tissues. *Tissue Engineering Part A* **25**, 809-820 (2019).
63. R. J. Nims *et al.*, A synthetic mechanogenetic gene circuit for autonomous drug delivery in engineered tissues. *Sci Adv* **7**, (2021).
64. R. Zhang, N. F. Lahens, H. I. Ballance, M. E. Hughes, J. B. Hogenesch, A circadian gene expression atlas in mammals: implications for biology and medicine. *Proc Natl Acad Sci U S A* **111**, 16219-16224 (2014).
65. M. D. Ruben *et al.*, A database of tissue-specific rhythmically expressed human genes has potential applications in circadian medicine. *Sci Transl Med* **10**, (2018).
66. M. Cutolo, Circadian rhythms and rheumatoid arthritis. *Joint Bone Spine* **86**, 327-333 (2019).
67. M. S. Cutolo, B.; Craviotto, C.; Pizzorni, C.; Sulli, A., Circadian rhythms in RA. *Ann Rheum Dis* **62**, 593-596 (2003).
68. F. Buttgereit, J. S. Smolen, A. N. Coogan, C. Cajochen, Clocking in: chronobiology in rheumatoid arthritis. *Nat Rev Rheumatol* **11**, 349-356 (2015).
69. A. R. Damato *et al.*, Temozolomide chronotherapy in patients with glioblastoma: a retrospective single institute study. *Neuro-Oncology Advances*, (2021).
70. D. Tay, S. Cremers, J. P. Bilezikian, Optimal dosing and delivery of parathyroid hormone and its analogues for osteoporosis and hypoparathyroidism - translating the pharmacology. *British Journal of Clinical Pharmacology* **84**, 252-267 (2018).
71. M. G. Cisternas *et al.*, Alternative Methods for Defining Osteoarthritis and the Impact on Estimating Prevalence in a US Population-Based Survey. *Arthritis Care Res (Hoboken)* **68**, 574-580 (2016).
72. P. H. Ousema *et al.*, The inhibition by interleukin 1 of MSC chondrogenesis and the development of biomechanical properties in biomimetic 3D woven PCL scaffolds. *Biomaterials* **33**, 8967-8974 (2012).
73. A. L. McNulty, F. T. Moutos, J. B. Weinberg, F. Guilak, Enhanced integrative repair of the porcine meniscus in vitro by inhibition of interleukin-1 or tumor necrosis factor alpha. *Arthritis Rheum* **56**, 3033-3042 (2007).
74. G. L. Matthews, D. J. Hunter, Emerging drugs for osteoarthritis. *Expert Opin Emerg Drugs* **16**, 479-491 (2011).

75. S. D. Gopinath, T. A. Rando, Stem cell review series: aging of the skeletal muscle stem cell niche. *Aging Cell* **7**, 590-598 (2008).
76. K. A. Kimmerling *et al.*, Sustained intra-articular delivery of IL-1Ra from a thermally-responsive elastin-like polypeptide as a therapy for post-traumatic arthritis. *European Cells and Materials* **29**, 124-140 (2015).
77. C. Mozzetta, G. Minetti, P. L. Puri, Regenerative pharmacology in the treatment of genetic diseases: the paradigm of muscular dystrophy. *Int J Biochem Cell Biol* **41**, 701-710 (2009).
78. C. A. Gersbach, S. R. Coyer, J. M. Le Doux, A. J. Garcia, Biomaterial-mediated retroviral gene transfer using self-assembled monolayers. *Biomaterials* **28**, 5121-5127 (2007).
79. C. H. Hou, J. Huang, R. L. Qian, Identification of α NF-κB site in the negative regulatory element (ε-NRAII) of human ε-globin gene and its binding protein NF-κ B p50 in the nuclei of K562 cells. *Cell research* **12**, 79-82 (2002).
80. M. Nourbakhsh, K. Hoffmann, H. Hauser, Interferon-β promoters contain a DNA element that acts as a position-independent silencer on the NF-. *EMBO Journal* **12**, 451-459 (1993).
81. M. Wiznerowicz, J. Szulc, D. Trono, Tuning silence: conditional systems for RNA interference. *Nat Methods* **3**, 682-688 (2006).
82. D. G. Gibson *et al.*, Enzymatic assembly of DNA molecules up to several hundred kilobases. *Nature methods* **6**, 343-345 (2009).
83. T. Kanda, K. F. Sullivan, G. M. Wahl, Histone-GFP fusion protein enables sensitive analysis of chromosome dynamics in living mammalian cells. *Curr. Biol.* **8**, 377-385 (1998).
84. J. Szulc, M. Wiznerowicz, M. O. Sauvain, D. Trono, P. Aebischer, A versatile tool for conditional gene expression and knockdown. *Nat Methods* **3**, 109-116 (2006).
85. P. Salmon, D. Trono, Production and titration of lentiviral vectors. *Current protocols in human genetics* **54**, 12.10. 11-12.10. 24 (2007).
86. B. W. Carey *et al.*, Reprogramming of murine and human somatic cells using a single polycistronic vector. *Proc Natl Acad Sci U S A* **106**, 157-162 (2009).
87. S. Hao, D. Baltimore, The stability of mRNA influences the temporal order of the induction of genes encoding inflammatory molecules. *Nat Immunol* **10**, 281-288 (2009).
88. W. W. Hu *et al.*, The use of reactive polymer coatings to facilitate gene delivery from poly (epsilon-caprolactone) scaffolds. *Biomaterials* **30**, 5785-5792 (2009).
89. F. T. Moutos, F. Guilak, Functional properties of cell-seeded three-dimensionally woven poly(epsilon-caprolactone) scaffolds for cartilage tissue engineering. *Tissue Eng Part A* **16**, 1291-1301 (2010).
90. R. W. Farndale, D. J. Buttle, A. J. Barrett, Improved quantitation and discrimination of sulphated glycosaminoglycans by use of dimethylmethylene blue. *Biochim Biophys Acta* **883**, 173-177 (1986).
91. B. T. Estes, B. O. Diekman, J. M. Gimble, F. Guilak, Isolation of adipose-derived stem cells and their induction to a chondrogenic phenotype. *Nat Protoc* **5**, 1294-1311 (2010).
92. K. Norrman *et al.*, Quantitative comparison of constitutive promoters in human ES cells. *PLoS One* **5**, e12413 (2010).
93. N. L. Fetter, H. A. Leddy, F. Guilak, J. A. Nunley, Composition and transport properties of human ankle and knee cartilage. *J Orthop Res* **24**, 211-219 (2006).

94. S. L.D., S. E., B. J., M. D.J., DNA delivery from polymer matrices for tissue engineering. *Nat Biotechnol* **17**, 551-554 (1999).
95. J. E. Phillips, K. L. Burns, J. M. Le Doux, R. E. Guldberg, A. J. Garcia, Engineering graded tissue interfaces. *Proc Natl Acad Sci U S A* **105**, 12170-12175 (2008).
96. E. Gouze *et al.*, In vivo gene delivery to synovium by lentiviral vectors. *Mol Ther* **5**, 397-404 (2002).
97. K. Kato, K. Miyake, T. Igarashi, S. Yoshino, T. Shimada, Human immunodeficiency virus vector-mediated intra-articular expression of angiostatin inhibits progression of collagen-induced arthritis in mice. *Rheumatology International* **25**, 522-529 (2004).
98. G. Yin *et al.*, Endostatin gene transfer inhibits joint angiogenesis and pannus formation in inflammatory arthritis. *Mol Ther* **5**, 547-554 (2002).
99. P. Basile *et al.*, Freeze-dried tendon allografts as tissue-engineering scaffolds for Gdf5 gene delivery. *Mol Ther* **16**, 466-473 (2008).
100. W.-W. Hu, M. W. Lang, P. H. Krebsbach, Digoxigenin modification of adenovirus to spatially control gene delivery from chitosan surfaces. *Journal of Controlled Release* **135**, 250-258 (2009).
101. T. Chowdhury, D. Salter, D. Bader, D. Lee, Signal transduction pathways involving p38 MAPK, JNK, NFκB and AP-1 influences the response of chondrocytes cultured in agarose constructs to IL-1β and dynamic compression. *Inflammation Research* **57**, 306-313 (2008).
102. W. W. Hu, Z. Wang, S. J. Hollister, P. H. Krebsbach, Localized viral vector delivery to enhance in situ regenerative gene therapy. *Gene Ther* **14**, 891-901 (2007).
103. M. Kumar, B. Keller, N. Makalou, R. Sutton, Systematic determination of he packaging limit of lentiviral vectors. *Human Gene Therapy* **12**, 1893-1905 (2001).
104. M. Wiznerowicz, D. Trono, Harnessing HIV for therapy, basic research and biotechnology. *Trends Biotechnol* **23**, 42-47 (2005).
105. M. C. Milone, U. O'Doherty, Clinical use of lentiviral vectors. *Leukemia* **32**, 1529-1541 (2018).
106. A. Schambach, C. Baum, Clinical application of lentiviral vectors - concepts and practice. *Curr Gene Ther* **8**, 474-482 (2008).
107. R. Zufferey *et al.*, Self-inactivatig lentivirus vector for seafe and efficient in vivo gene deliery. *Journal of Virology* **72**, 9873-9880 (1998).
108. P. K. Valonen *et al.*, In vitro generation of mechanically functional cartilage grafts based on adult human stem cells and 3D-woven poly(epsilon-caprolactone) scaffolds. *Biomaterials* **31**, 2193-2200 (2010).
109. C. E. Badr *et al.*, Real-Time Monitoring of Nuclear Factor κB Activity in Cultured Cells and in Animal Models. *Molecular Imaging* **8**, 278-290 (2009).
110. F. A. van de Loo *et al.*, An inflammation-inducible adenoviral expression system for local treatment of the arthritic joint. *Gene Ther* **11**, 581-590 (2004).
111. J. Adriaansen *et al.*, Reduction of arthritis following intra-articular administration of an adeno-associated virus serotype 5 expressing a disease-inducible TNF-blocking agent. *Ann Rheum Dis* **66**, 1143-1150 (2007).
112. M. Khoury *et al.*, Inflammation-inducible anti-TNF gene expression mediated by intra-articular injection of serotype 5 adeno-associated virus reduces arthritis. *The Journal of Gene Medicine* **9**, 596-604 (2007).

113. N. Farhang *et al.*, CRISPR-Based Epigenome Editing of Cytokine Receptors for the Promotion of Cell Survival and Tissue Deposition in Inflammatory Environments. *Tissue Eng Part A* **23**, 738-749 (2017).
114. M. Gossen, H. Bujard, Tight control of gene expression in mammalian cells by tetracycline-responsive promoters. *Proc Natl Acad Sci U S A* **89**, 5547-5551 (1992).
115. D. Greber, M. D. El-Baba, M. Fussenegger, Intronically encoded siRNAs improve dynamic range of mammalian gene regulation systems and toggle switch. *Nucleic Acids Res* **36**, e101 (2008).
116. B. P. Kramer *et al.*, An engineered epigenetic transgene switch in mammalian cells. *Nat Biotechnol* **22**, 867-870 (2004).
117. L. Wroblewska *et al.*, Mammalian synthetic circuits with RNA binding proteins for RNA-only delivery. *Nat Biotechnol* **33**, 839-841 (2015).
118. Z. Xie, L. Wroblewska, L. Prochazka, R. Weiss, Y. Benenson, Multi-input RNAi-based logic circuit for identification of specific cancer cells. *Science* **333**, 1307-1311 (2011).
119. Y. Y. Chen, M. C. Jensen, C. D. Smolke, Genetic control of mammalian T-cell proliferation with synthetic RNA regulatory systems. *Proc Natl Acad Sci U S A* **107**, 8531-8536 (2010).
120. P. Perez-Pinera *et al.*, Synergistic and tunable human gene activation by combinations of synthetic transcription factors. *Nat Methods* **10**, 239-242 (2013).
121. L. S. Qi *et al.*, Repurposing CRISPR as an RNA-guided platform for sequence-specific control of gene expression. *Cell* **152**, 1173-1183 (2013).
122. S. Auslander, M. Fussenegger, From gene switches to mammalian designer cells: present and future prospects. *Trends Biotechnol* **31**, 155-168 (2013).
123. P. M. Boyle, P. A. Silver, Harnessing nature's toolbox: regulatory elements for synthetic biology. *J R Soc Interface* **6 Suppl 4**, S535-546 (2009).
124. Y. Lu, A. A. Aimetti, R. Langer, Z. Gu, Bioresponsive materials. *Nature Reviews Materials* **2**, 16075 (2017).
125. H. D. Intengan, E. L. Schiffrin, Structure and mechanical properties of resistance arteries in hypertension: role of adhesion molecules and extracellular matrix determinants. *Hypertension* **36**, 312-318 (2000).
126. M. Plodinec *et al.*, The nanomechanical signature of breast cancer. *Nature nanotechnology* **7**, 757 (2012).
127. D. D. Anderson *et al.*, Post-traumatic osteoarthritis: improved understanding and opportunities for early intervention. *Journal of Orthopaedic Research* **29**, 802-809 (2011).
128. M. B. Larsen, A. J. Boydston, Successive mechanochemical activation and small molecule release in an elastomeric material. *Journal of the American Chemical Society* **136**, 1276-1279 (2014).
129. J. Wang, J. A. Kaplan, Y. L. Colson, M. W. Grinstaff, Mechanoresponsive materials for drug delivery: Harnessing forces for controlled release. *Advanced drug delivery reviews* **108**, 68-82 (2017).
130. L. Liu *et al.*, Mechanoresponsive stem cells to target cancer metastases through biophysical cues. *Sci Transl Med* **9**, (2017).
131. Y. Pan *et al.*, Mechanogenetics for the remote and noninvasive control of cancer immunotherapy. *Proc Natl Acad Sci U S A* **115**, 992-997 (2018).

132. B. Mohanraj *et al.*, Mechanically-Activated Microcapsules for 'On-Demand' Drug Delivery in Dynamically Loaded Musculoskeletal Tissues. *Adv Funct Mater* **29**, (2019).
133. G. R. Gossweiler *et al.*, Mechanochemical activation of covalent bonds in polymers with full and repeatable macroscopic shape recovery. *ACS Macro Letters* **3**, 216-219 (2014).
134. J. Di *et al.*, Stretch-triggered drug delivery from wearable elastomer films containing therapeutic depots. *ACS nano* **9**, 9407-9415 (2015).
135. J. Wu, A. H. Lewis, J. Grandl, Touch, tension, and transduction–the function and regulation of Piezo ion channels. *Trends in biochemical sciences* **42**, 57-71 (2017).
136. W. Lee, F. Guilak, W. Liedtke, in *Current topics in membranes*. (Elsevier, 2017), vol. 79, pp. 263-273.
137. S. S. Ranade, R. Syeda, A. Patapoutian, Mechanically activated ion channels. *Neuron* **87**, 1162-1179 (2015).
138. A. P. Christensen, D. P. Corey, TRP channels in mechanosensation: direct or indirect activation? *Nature Reviews Neuroscience* **8**, 510 (2007).
139. C. Moore, R. Gupta, S. E. Jordt, Y. Chen, W. B. Liedtke, Regulation of Pain and Itch by TRP Channels. *Neurosci Bull* **34**, 120-142 (2018).
140. W. Liedtke, J. M. Friedman, Abnormal osmotic regulation in trpv4-/- mice. *Proc Natl Acad Sci U S A* **100**, 13698-13703 (2003).
141. C. J. O'Conor, H. A. Leddy, H. C. Benefield, W. B. Liedtke, F. Guilak, TRPV4-mediated mechanotransduction regulates the metabolic response of chondrocytes to dynamic loading. *Proceedings of the National Academy of Sciences* **111**, 1316-1321 (2014).
142. D. T. Felson *et al.*, Osteoarthritis: new insights. Part 2: treatment approaches. *Annals of internal medicine* **133**, 726-737 (2000).
143. A. D. Cigan *et al.*, Nutrient channels aid the growth of articular surface-sized engineered cartilage constructs. *Tissue Engineering Part A* **22**, 1063-1074 (2016).
144. R. J. Nims *et al.*, (*) Constrained Cage Culture Improves Engineered Cartilage Functional Properties by Enhancing Collagen Network Stability. *Tissue Eng Part A* **23**, 847-858 (2017).
145. N. K. Lad *et al.*, Effect of normal gait on in vivo tibiofemoral cartilage strains. *J Biomech* **49**, 2870-2876 (2016).
146. A. T. Collins *et al.*, Obesity alters the in vivo mechanical response and biochemical properties of cartilage as measured by MRI. *Arthritis Res Ther* **20**, 232 (2018).
147. E. G. Sutter *et al.*, Effects of Anterior Cruciate Ligament Deficiency on Tibiofemoral Cartilage Thickness and Strains in Response to Hopping. *Am J Sports Med* **47**, 96-103 (2019).
148. W. R. Trickey, F. P. Baaijens, T. A. Laursen, L. G. Alexopoulos, F. Guilak, Determination of the Poisson's ratio of the cell: recovery properties of chondrocytes after release from complete micropipette aspiration. *J Biomech* **39**, 78-87 (2006).
149. W. Lee *et al.*, Synergy between Piezo1 and Piezo2 channels confers high-strain mechanosensitivity to articular cartilage. *Proceedings of the National Academy of Sciences* **111**, E5114-E5122 (2014).
150. J. C. Hou, S. A. Maas, J. A. Weiss, G. A. Ateshian, Finite Element Formulation of Multiphasic Shell Elements for Cell Mechanics Analyses in FEBio. *J Biomech Eng*, (2018).

151. M. Nourbakhsh, K. Hoffmann, H. Hauser, Interferon-beta promoters contain a DNA element that acts as a position-independent silencer on the NF-kappa B site. *The EMBO journal* **12**, 451-459 (1993).
152. R. L. Mauck *et al.*, Functional tissue engineering of articular cartilage through dynamic loading of chondrocyte-seeded agarose gels. *Journal of biomechanical engineering* **122**, 252-260 (2000).
153. D. A. Lee, T. Noguchi, S. P. Frean, P. Lees, D. L. Bader, The influence of mechanical loading on isolated chondrocytes seeded in agarose constructs. *Biorheology* **37**, 149-161 (2000).
154. F. Guilak, R. J. Nims, A. Dicks, C.-L. Wu, I. Meulenbelt, Osteoarthritis as a disease of the cartilage pericellular matrix. *Matrix Biology* **71**, 40-50 (2018).
155. Z. Deng *et al.*, Cryo-EM and X-ray structures of TRPV4 reveal insight into ion permeation and gating mechanisms. *Nature structural & molecular biology* **25**, 252 (2018).
156. S. Loukin, X. Zhou, Z. Su, Y. Saimi, C. Kung, Wild-type and brachyolmia-causing mutant TRPV4 channels respond directly to stretch force. *Journal of Biological Chemistry* **285**, 27176-27181 (2010).
157. M. R. Servin-Vences, M. Moroni, G. R. Lewin, K. Poole, Direct measurement of TRPV4 and PIEZO1 activity reveals multiple mechanotransduction pathways in chondrocytes. *Elife* **6**, e21074 (2017).
158. S. A. Maas, B. J. Ellis, G. A. Ateshian, J. A. Weiss, FEBio: finite elements for biomechanics. *J Biomech Eng* **134**, 011005 (2012).
159. J. Sanchez-Adams, H. A. Leddy, A. L. McNulty, C. J. O'Conor, F. Guilak, The mechanobiology of articular cartilage: bearing the burden of osteoarthritis. *Current rheumatology reports* **16**, 451 (2014).
160. R. J. Nims *et al.*, Continuum theory of fibrous tissue damage mechanics using bond kinetics: application to cartilage tissue engineering. *Interface Focus* **6**, 20150063 (2016).
161. N. O. Chahine, F. H. Chen, C. T. Hung, G. A. Ateshian, Direct measurement of osmotic pressure of glycosaminoglycan solutions by membrane osmometry at room temperature. *Biophys J* **89**, 1543-1550 (2005).
162. A. L. McNulty, N. E. Rothfusz, H. A. Leddy, F. Guilak, Synovial fluid concentrations and relative potency of interleukin-1 alpha and beta in cartilage and meniscus degradation. *J Orthop Res* **31**, 1039-1045 (2013).
163. H. A. Leddy, A. L. McNulty, F. Guilak, W. Liedtke, Unraveling the mechanism by which TRPV4 mutations cause skeletal dysplasias. *Rare Dis* **2**, e962971 (2014).
164. S. Heller, R. O'Neil, *Molecular Mechanisms of TRPV4 Gating.* W. Liedtke, S. Heller, Eds., TRP Ion Channel Function in Sensory Transduction and Cellular Signaling Cascades. (CRC Press/Taylor & Francis, Boca Raton (FL), 2007).
165. C. J. O'Conor *et al.*, Cartilage-specific knockout of the mechanosensory ion channel TRPV4 decreases age-related osteoarthritis. *Scientific reports* **6**, 29053 (2016).
166. L. Ye *et al.*, TRPV4 is a regulator of adipose oxidative metabolism, inflammation, and energy homeostasis. *Cell* **151**, 96-110 (2012).
167. S. Wu, D. Fadoju, G. Rezvani, F. De Luca, Stimulatory effects of insulin-like growth factor-I on growth plate chondrogenesis are mediated by nuclear factor-κB p65. *Journal of Biological Chemistry* **283**, 34037-34044 (2008).

168. S. Wu, J. K. Flint, G. Rezvani, F. De Luca, Nuclear factor-κB p65 facilitates longitudinal bone growth by inducing growth plate chondrocyte proliferation and differentiation and by preventing apoptosis. *Journal of Biological Chemistry* **282**, 33698-33706 (2007).
169. I. Cambré *et al.*, Mechanical strain determines the site-specific localization of inflammation and tissue damage in arthritis. *Nature communications* **9**, 4613 (2018).
170. S. H. Yoo *et al.*, PERIOD2::LUCIFERASE real-time reporting of circadian dynamics reveals persistent circadian oscillations in mouse peripheral tissues. *Proc Natl Acad Sci U S A* **101**, 5339-5346 (2004).
171. A. Patke, M. W. Young, S. Axelrod, Molecular mechanisms and physiological importance of circadian rhythms. *Nat Rev Mol Cell Biol* **21**, 67-84 (2020).
172. S. Q. Shi, T. S. Ansari, O. P. McGuinness, D. H. Wasserman, C. H. Johnson, Circadian disruption leads to insulin resistance and obesity. *Curr Biol* **23**, 372-381 (2013).
173. S. L. Chellappa, N. Vujovic, J. S. Williams, F. Scheer, Impact of Circadian Disruption on Cardiovascular Function and Disease. *Trends Endocrinol Metab* **30**, 767-779 (2019).
174. J. M. Mansour, Biomechanics of Cartilage. *Kinesiol Mech Pathomechanics Hum Mov*, 66-79 (2009).
175. J. Martel-Pelletier, C. Boileau, J. P. Pelletier, P. J. Roughley, Cartilage in normal and osteoarthritis conditions. *Best Pract Res Clin Rheumatol* **22**, 351-384 (2008).
176. M. Dudek *et al.*, Circadian time series proteomics reveals daily dynamics in cartilage physiology. *Osteoarthritis Cartilage*, (2021).
177. F. Dernie, D. Adeyoju, A matter of time: Circadian clocks in osteoarthritis and the potential of chronotherapy. *Exp Gerontol* **143**, 111163 (2021).
178. G. Chen *et al.*, Circadian Rhythm Protein Bmal1 Modulates Cartilage Gene Expression in Temporomandibular Joint Osteoarthritis via the MAPK/ERK Pathway. *Front Pharmacol* **11**, 527744 (2020).
179. H. Bekki *et al.*, Suppression of circadian clock protein cryptochrome 2 promotes osteoarthritis. *Osteoarthritis Cartilage* **28**, 966-976 (2020).
180. K. Yagita *et al.*, Development of the circadian oscillator during differentiation of mouse embryonic stem cells in vitro. *Proc Natl Acad Sci U S A* **107**, 3846-3851 (2010).
181. M. Dudek *et al.*, The intervertebral disc contains intrinsic circadian clocks that are regulated by age and cytokines and linked to degeneration. *Ann Rheum Dis* **76**, 576-584 (2017).
182. B. Maier, Loernzen, S., Finger, A., Herzel, H., Kramer, A., Searching novel clock genes using RNAi-based screening. *In Circadian Clocks, Methods and Protocols, Brown, S.A.* **Chapter 8**, (2020).
183. S. A. Benitah, P. S. Welz, Circadian Regulation of Adult Stem Cell Homeostasis and Aging. *Cell Stem Cell* **26**, 817-831 (2020).
184. C. Beaulé, D. Granados-Fuentes, L. Marpegan, E. D. Herzog, In vitrocircadian rhythms: imaging and electrophysiology. *Essays In Biochemistry* **49**, 103-117 (2011).
185. M. Abe *et al.*, Circadian rhythms in isolated brain regions. *J Neurosci* **22**, 350-356 (2002).
186. S. Yamazaki *et al.*, Resetting central and peripheral circadian oscillators in transgenic rats. *Science* **288**, 682-685 (2000).
187. J. Williams *et al.*, Epithelial and stromal circadian clocks are inversely regulated by their mechano-matrix environment. *J Cell Sci* **131**, (2018).

188. B. J. Altman *et al.*, MYC Disrupts the Circadian Clock and Metabolism in Cancer Cells. *Cell Metab* **22**, 1009-1019 (2015).
189. S. Hood, S. Amir, The aging clock: circadian rhythms and later life. *J Clin Invest* **127**, 437-446 (2017).
190. B. Lemmer, The clinical relevance of chronopharmacology in therapeutics. *Pharmacol Res* **33**, 107-115 (1996).
191. J. Sobrino, L. Casanas, C. Izquierdo, J. Clavell, [Circadian rhythm variability in arterial blood pressure]. *Rev Enferm* **29**, 50-52 (2006).
192. M. H. Smolensky, B. Lemmer, A. E. Reinberg, Chronobiology and chronotherapy of allergic rhinitis and bronchial asthma. *Adv Drug Deliv Rev* **59**, 852-882 (2007).
193. G. Kaur, C. Phillips, K. Wong, B. Saini, Timing is important in medication administration: a timely review of chronotherapy research. *Int J Clin Pharm* **35**, 344-358 (2013).
194. L. Warren *et al.*, Highly efficient reprogramming to pluripotency and directed differentiation of human cells with synthetic modified mRNA. *Cell Stem Cell* **7**, 618-630 (2010).
195. A. Patke *et al.*, Mutation of the Human Circadian Clock Gene CRY1 in Familial Delayed Sleep Phase Disorder. *Cell* **169**, 203-215 e213 (2017).
196. C. R. Jones, A. L. Huang, L. J. Ptacek, Y. H. Fu, Genetic basis of human circadian rhythm disorders. *Exp Neurol* **243**, 28-33 (2013).
197. L. H. Ashbrook, A. D. Krystal, Y. H. Fu, L. J. Ptacek, Genetics of the human circadian clock and sleep homeostat. *Neuropsychopharmacology* **45**, 45-54 (2020).
198. J. Huard, Y. Li, F. H. Fu, Muscle injuries and repair: current trends in research. *J Bone Joint Surg Am* **84**, 822-832 (2002).
199. Y. Li, F. H. Fu, J. Huard, Cutting-edge muscle recovery: using antifibrosis agents to improve healing. *Phys Sportsmed* **33**, 44-50 (2005).
200. D. Delos, T. G. Maak, S. A. Rodeo, Muscle injuries in athletes: enhancing recovery through scientific understanding and novel therapies. *Sports Health* **5**, 346-352 (2013).
201. Y. Li, J. Huard, Differentiation of muscle-derived cells into myofibroblasts in injured skeletal muscle. *Am J Pathol* **161**, 895-907 (2002).
202. Y. Li *et al.*, Decorin gene transfer promotes muscle cell differentiation and muscle regeneration. *Mol Ther* **15**, 1616-1622 (2007).
203. J. Zhu *et al.*, Relationships between transforming growth factor-beta1, myostatin, and decorin: implications for skeletal muscle fibrosis. *J Biol Chem* **282**, 25852-25863 (2007).
204. K. Fukushima *et al.*, The use of an antifibrosis agent to improve muscle recovery after laceration. *Am J Sports Med* **29**, 394-402 (2001).
205. Y. S. Chan *et al.*, Antifibrotic effects of suramin in injured skeletal muscle after laceration. *J Appl Physiol (1985)* **95**, 771-780 (2003).
206. M. Nozaki *et al.*, Improved muscle healing after contusion injury by the inhibitory effect of suramin on myostatin, a negative regulator of muscle growth. *Am J Sports Med* **36**, 2354-2362 (2008).
207. Y. S. Chan, Y. Li, W. Foster, F. H. Fu, J. Huard, The use of suramin, an antifibrotic agent, to improve muscle recovery after strain injury. *Am J Sports Med* **33**, 43-51 (2005).
208. W. Foster, Y. Li, A. Usas, G. Somogyi, J. Huard, Gamma interferon as an antifibrosis agent in skeletal muscle. *J Orthop Res* **21**, 798-804 (2003).

209. K. Sato *et al.*, Improvement of muscle healing through enhancement of muscle regeneration and prevention of fibrosis. *Muscle Nerve* **28**, 365-372 (2003).
210. S. Negishi, Y. Li, A. Usas, F. H. Fu, J. Huard, The effect of relaxin treatment on skeletal muscle injuries. *Am J Sports Med* **33**, 1816-1824 (2005).
211. Y. Li, S. Negishi, M. Sakamoto, A. Usas, J. Huard, The use of relaxin improves healing in injured muscle. *Ann N Y Acad Sci* **1041**, 395-397 (2005).
212. M. Kobayashi *et al.*, The Combined Use of Losartan and Muscle-Derived Stem Cells Significantly Improves the Functional Recovery of Muscle in a Young Mouse Model of Contusion Injuries. *Am J Sports Med* **44**, 3252-3261 (2016).
213. H. S. Bedair, T. Karthikeyan, A. Quintero, Y. Li, J. Huard, Angiotensin II receptor blockade administered after injury improves muscle regeneration and decreases fibrosis in normal skeletal muscle. *Am J Sports Med* **36**, 1548-1554 (2008).
214. A. M. Hocking, T. Shinomura, D. J. McQuillan, Leucine-rich repeat glycoproteins of the extracellular matrix. *Matrix Biol* **17**, 1-19 (1998).
215. J. Sottile, D. C. Hocking, P. J. Swiatek, Fibronectin matrix assembly enhances adhesion-dependent cell growth. *J Cell Sci* **111 (Pt 19)**, 2933-2943 (1998).
216. E. Brandan, M. E. Fuentes, W. Andrade, The proteoglycan decorin is synthesized and secreted by differentiated myotubes. *Eur J Cell Biol* **55**, 209-216 (1991).
217. J. C. Casar, B. A. McKechnie, J. R. Fallon, M. F. Young, E. Brandan, Transient up-regulation of biglycan during skeletal muscle regeneration: delayed fiber growth along with decorin increase in biglycan-deficient mice. *Dev Biol* **268**, 358-371 (2004).
218. N. Yoshida, S. Yoshida, K. Koishi, K. Masuda, Y. Nabeshima, Cell heterogeneity upon myogenic differentiation: down-regulation of MyoD and Myf-5 generates 'reserve cells'. *J Cell Sci* **111 (Pt 6)**, 769-779 (1998).
219. S. N. Giri *et al.*, Antifibrotic effect of decorin in a bleomycin hamster model of lung fibrosis. *Biochem Pharmacol* **54**, 1205-1216 (1997).
220. Y. Isaka *et al.*, Gene therapy by skeletal muscle expression of decorin prevents fibrotic disease in rat kidney. *Nat Med* **2**, 418-423 (1996).
221. B. M. Deasy, R. J. Jankowski, J. Huard, Muscle-derived stem cells: characterization and potential for cell-mediated therapy. *Blood Cells Mol Dis* **27**, 924-933 (2001).
222. B. Gharaibeh *et al.*, Isolation of a slowly adhering cell fraction containing stem cells from murine skeletal muscle by the preplate technique. *Nat Protoc* **3**, 1501-1509 (2008).
223. S. Ota *et al.*, Intramuscular transplantation of muscle-derived stem cells accelerates skeletal muscle healing after contusion injury via enhancement of angiogenesis. *Am J Sports Med* **39**, 1912-1922 (2011).
224. Y. Tang, J. Xiao, Y. Wang, M. Li, Z. Shi, Effect of adenovirus-mediated TGF-beta1 gene transfer on the function of rabbit articular chondrocytes. *J Orthop Sci* **22**, 149-155 (2017).
225. H. Maruki *et al.*, Effects of a cell-free method using collagen vitrigel incorporating TGF-beta1 on articular cartilage repair in a rabbit osteochondral defect model. *J Biomed Mater Res B Appl Biomater* **105**, 2592-2602 (2017).
226. G. DuRaine *et al.*, Regulation of the friction coefficient of articular cartilage by TGF-beta1 and IL-1beta. *J Orthop Res* **27**, 249-256 (2009).
227. X. M. Meng, D. J. Nikolic-Paterson, H. Y. Lan, TGF-beta: the master regulator of fibrosis. *Nat Rev Nephrol* **12**, 325-338 (2016).
228. M. A. A. Mahdy, Skeletal muscle fibrosis: an overview. *Cell Tissue Res* **375**, 575-588 (2019).

229. J. Xie *et al.*, MicroRNA-regulated, systemically delivered rAAV9: a step closer to CNS-restricted transgene expression. *Mol Ther* **19**, 526-535 (2011).

Curriculum Vitae

Lara Pferdehirt

4242 Laclede Ave, Apt 208
St. Louis, MO 63108
lara.pferdehirt@wustl.edu
(832) 275 - 3642

EDUCATION

Washington University in St. Louis

Ph.D. Biomedical Engineering — August 2016 - present

M.S. Biomedical Engineering GPA: 3.85 — August 2016 - May 2019

Rice University

B.S. Bioengineering — August 2012 - May 2016

AWARDS & ACHIEVEMENTS

iBiology Business Concepts for Life Sciences Certificate	2019
Philip and Sima Needleman Student Fellowship in Regenerative Medicine	2018 - 2019
Just in Time Core Usage Funding Program – Institute of Clinical and Translational Science, Washington University in St. Louis	2018 - 2019
Gene K. Beare Memorial Fellow	2016 - 2017
Distinction in Research & Creative Work	2016
Gulf Coast Undergraduate Research Symposium Participant - Outstanding Presentation	2015
iGEM Gold Medalist and Nominee for Best in Environmental Tract and Best New Part	2015
IBB Poster Symposium Top Poster and Presentation Award	2015

PUBLICATIONS

Pferdehirt L*, Damato A*, Dudek M, Meng QJ, Herzog ED, Guilak F. Synthetic gene circuits for preventing disruption of the circadian clock due to inflammation. PNAS*, in submission.*

Klimak M, Nims RJ, **Pferdehirt L**, Collins K, Harasymowicz N, Setton L, Guilak F. Immunoengineering the Next Generation of Arthritis Therapies. Acta Biomaterialia. 2021.

Nims RJ*, **Pferdehirt L*,** Ho NB, Savadipour A, Lorentz J, Sohi S, Kassab J, Ross AK, O'Conor CJ, Liedtke W, Zhang B, McNulty A, Guilak F. A Synthetic Mechanogenetic Gene Circuit for Autonomous Drug Delivery in Engineered Tissues. Sci Adv. 2021; 7(5):eabd9858

Choi RK, Collins K, Springer L, **Pferdehirt L**, Ross A, Wu CL, Moutos F, Harasymowicz N, Brunger JM, Pham C, Guilak F. A Genome-engineered Bioartificial Implant for Autoregulated Anti-Cytokine Drug Delivery. BioRxiv. 2020.

Guilak F, **Pferdehirt L**, Ross AK, Choi YR, Collins K, Nims RJ, Katz DB, Klimak M, Tabbaa S, Pham CTN. Designer Stem Cells: Genome Engineering and the Next Generation of Cell-Based Therapies. J Orthop Res. 2019; 37(6):1287-1293.

Pferdehirt L, Ross AK, Brunger JM, Guilak F. A Synthetic Gene Circuit for Self-Regulating Delivery of Biologic Drugs in Engineered Tissues. Tissue Eng Part A. 2019; 25(9-10):809-820.

Zhao W, **Pferdehirt L**, Segatori L. Quantitatively Predictable Control of Cellular Protein Levels through Proteasomal Degradation. ACS Synth Biol. 2018; 7(2):540-552.

POSTERS & PRESENTATIONS

Pferdehirt L, Guo P, Lu A, Huard M, Guilak F, Huard J. Genome Engineered Muscle Derived Stem Cells for Autoregulated Anti-Inflammatory and Anti-Fibrotic Activity. Orthopaedic Research Society 67th Annual Meeting; 2021 Feb 12-16. ***Podium Presentation**

Nims RJ, **Pferdehirt L**, Savadipour A, Lorentz J, Sohi S, Kassab J, Guilak F. Mechanogenetic Circuits for Short- and Long-Lived Drug Delivery in Response to Mechanical Loading Protect Engineered Cartilage from Interleukin-1. Orthopaedic Research Society 66th Annual Meeting; 2020 Feb 8-11; Phoenix, AZ.

Pferdehirt L, Nims RJ, Ross AK, Lorentz J, Savadipour A, Guilak F. An Artificial Mechanogenetic Circuit for Targeted Gene Activation. 6th International Mammalian Synthetic Biology Workshop; 2019 May 17-19; Evanston, IL.

Pferdehirt L, Nims RJ, Ross AK, Lorentz J, Savadipour A, Guilak F. An Artificial Mechanogenetic Circuit for Targeted Gene Activation. 4th Annual Regenerative Medicine Symposium; 2019 Mar 12; St. Louis, MO. ***Needleman Fellow Presentation**

Nims RJ, **Pferdehirt L,** Ross AK, Lorentz J, Savadipour A, Guilak F. An Artificial Mechanogenetic Circuit for Targeted Gene Activation in Response to Compressive or Osmotic Loading. Musculoskeletal Research Center Winter Symposium; 2019 Feb 20; St. Louis, MO. ***Podium Presentation**

Nims RJ, **Pferdehirt L**, Ross AK, Lorentz J, Savadipour A, Guilak F. An Artificial Mechanogenetic Circuit for Targeted Gene Activation in Response to Compressive or Osmotic Loading. Orthopaedic Research Society 65th Annual Meeting; 2019 Feb 2-5; Austin, TX. ***New Investigator Recognition Award (NIRA)**

Choi RK, Collins K, Springer L, **Pferdehirt L**, Ross A, Wu CL, Moutos F, Harasymowicz N, Brunger JM, Pham C, Guilak F. A Genome-engineered Bioartificial Implant for Autoregulated Anti-Cytokine Drug Delivery. Orthopaedic Research Society 65th Annual Meeting; 2019 Feb 2-5; Austin, TX.

Ross A, **Pferdehirt L**, Guilak F. MicroRNA-Sequencing Reveals Specific Mediators of Inflammation in Tissue-Engineered Cartilage. Orthopaedic Research Society 65th Annual Meeting; 2019 Feb 2-5; Austin, TX.

Pferdehirt L, Ross AK, Brunger JM, Guilak F. A Synthetic Transcription System Based on NF-kB Signaling for Cartilage Tissue Engineering Using Self Regulating Delivery of Therapeutic Biologic Drugs. Orthopaedic Research Society 64th Annual Meeting; 2018 Mar 9-13; New Orleans, LA. ***Podium Presentation**

Pferdehirt L, Ross AK, Brunger JM, Guilak F**.** A Self-Regulating Synthetic Transcription System for the Attenuation of NF-κB Signaling*,* Orthopedic Research Society Midwest Musculoskeletal Conference, St. Louis, MO (July 2017) ***Finalist for poster award**

Pferdehirt L, Ross AK, Brunger JM, Guilak F. A Self-Regulating Synthetic Transcription System for the Attenuation of NF-κB Signaling, Musculoskeletal Regenerative Medicine and Biology Conference, St. Louis, MO (May 2017)

Pferdehirt L, Brookshier C, Gough V, Stockenbojer E. Next-Gen Aortix: A 4 mm Intra-Aortic Heart Pump, Rice Undergraduate Research Symposium and University Design Showcase, Houston, TX (April 2016)

Pferdehirt L, Zhao W, Segatori L. NanoDeg-Mediated Protein Knockdown*,* Gulf Coast Undergraduate Research Symposium, Houston, TX (Oct 2015)

Rice University and Hong Kong University of Science and Technology, Potassium, Phosphate, and Nitrate Biosensors, iGEM 2015 Jamboree Poster Session and Presentation, Boston, MA (Sept 2015)

Pferdehirt L, Zhao W, Segatori L. NanoDeg-Mediated Protein Knockdown, NSF Bionetworks REU Summer Undergraduate Research Poster Session, Houston, TX (Jul 2015) ***Won best poster and presentation award**

EXPERIENCE

The Biotechnology and Life Sciences (BALSA) Group Spring 2019 – Spring 2021

St. Louis, MO

Advisor, Project Manager, and Consultant

- Serve as a consultant, project manager, and advisor for a nonprofit organization that provides consulting services in St. Louis
- As a project manager, lead a team of 3 consultants on projects focusing on market research, technology assessment, and business strategy
- As an advisor, advised clients and negotiated engagement letters with clients for projects

Flagship Pioneering June 2020 – August 2020

Boston, MA

VentureLabs Fellow

- Worked at a venture capital firm focused on creating and building life sciences companies
- Worked with 3 different teams exploring different scientific topics and focusing on platform company creation
- Pressure tested ideas and created company pitch decks

ClearView Healthcare Partners June 2020

Boston, MA (Virtual)

Connect to Clearview Fellow

- Participated in an internship for advanced degree candidates to better understand company focus and consulting services provided
- Focused on case strategy

Bain & Company May 2020

Houston, TX (Virtual)

Bain ADvantage Intern

- Participated in an internship for advanced degree candidates and worked on a case with a team based in Houston and Seattle for a Telecom company
- Did diligence on a business after a recent acquisition and presenting findings to the partner team

RESEARCH EXPERIENCE

Farshid Guilak Lab Aug 2016 - Present

Washington University, St. Louis, MO

Graduate Research Student

- Working in an orthopaedic and regenerative medicine lab for applications in biomedicine and tissue engineering with research focusing on editing cells that can sense stimuli and respond with therapeutic drugs for arthritis
- Spearheaded a new research area in the lab to solve new problems and learn unique analytical skills
- Collaborating with two labs on projects involving drug delivery and muscle fibrosis

Laura Segatori Lab Jan 2015 – May 2016
Rice University, Houston, TX
Undergraduate Research Assistant

- Worked in a cell and protein engineering lab for applications in biomedicine and bionanotechnology
- Contributed to research involving antibody and protein engineering to develop a universal way to target and degrade proteins. Investigated the controllability of our degradation system through variations in nanobody half-life and in nanobody expression levels
- Investigating the binding affinity of our system to targeted proteins and the universality of our system through different degradation tags
- Gained hands-on experience in protein engineering through wet-lab work and plasmid design, and strengthened my interdisciplinary skills by working in an interdisciplinary lab

Capstone Design Aug 2015 – May 2016
Rice University, Houston, TX
Team Member

- Worked on building a next-generation intra-aortic heart assist device for a medical device company
- Gained hands-on experience in engineering design, brainstorming, computer automated design, 3D printing, prototyping, and all documentation associated with building a medical device
- Served as the Team Facilitator and Liaison, strengthening my ability to work in teams and conflict-resolution

iGEM (International Genetic Engineered Machine) Competition Mar – Sept 2015
Rice University, Houston, TX
Rice – Hong Kong University of Science and Technology (HKUST) Team Member

- Designed genetic circuits to sense nutrient concentrations in the soil. Focused on developing the application of the biosensors in a paper-based, cell-free system and as a biofertilizer, gaining synthetic biology experience
- A primary liaison between the Rice team and the HKUST team and a presenter at the Jamboree, strengthening my leadership, communication, and presentation skills

NSF Bionetworks REU Summer 2015
Rice University, Houston, TX
Research Intern

- Continued research on our system to target and degrade proteins in the **Segatori Lab**
- Along with lab work, the program included journal clubs, mentoring of high school students, biotechnology projects, bioethics classes, and participation in the **2015 IBB Summer Poster Session**

VOLUNTEERING, LEADERSHIP, TEACHING, & MENTORSHIP ACTIVITIES

Director of Marketing, The BALSA Group February 2020-Present

- Networked with current clients and professionals in St. Louis to increase visibility and get new clients
- Organized monthly networking events and professional and career development sessions
- Lead initiatives and work with 7 other officers to run the organization

Orthopaedic Research Society Social Media Committee Member December 2019-Present

- Communicate science advocacy, society events, and orthopaedic research through social media
- Collaborate with other members to organize networking events

Market Strategy Mentor for Sling Health COVID Bootcamp May 2020

- Mentored teams on entrepreneurs focused on building COVID-related companies on market strategy and entry to market

Washington University Biomedical Engineering Student Researchers Mentor October 2016-Present

- Mentored and currently mentoring undergraduate, masters, and PhD students
- Trained students in laboratory techniques for orthopaedic tissue engineering, molecular biology, gene therapy, experimental design, and data collection and analysis

Young Scientist Program Mentor October 2016-May 2020

- Advise and mentor high school kids at a local high school in St. Louis (Soldan) throughout all four years of high school to help prepare them for college and attain their future goals
- Take them on fieldtrips to help determine what their interests are in the STEM field

Teaching Assistant for Molecular Systems Biology Aug 2017-Dec 2017

- Work as a teaching assistant for a graduate level course focused on systems biology
- Hold office hours, assist with project proposals and homework, and lead some lectures
- Improving my mentoring and teaching abilities

Underclassmen Mentor Aug 2015 – May 2016

- Biomedical Engineering Society (BMES) Rice Mentor – advise underclassmen bioengineers on coursework and research, improving my mentoring skills
- Discussed research opportunities with undergraduates at Rice's Research Fair

Youth Soccer Coach Aug 2013 – Aug 2015

- Led and coordinated an all-girl club soccer team, improving my leadership and organizational skills

English Teacher Summers: 2008-2012

- Taught English to young kids (ages 6-8 mostly) at the YMCA Summer Camp in Istanbul, Turkey
- Leadership opportunity that improved my patience and skills to be a good communicator and effective teacher